

MYCOPLASMA PNEUMONIAE

TERMINAL ORGANELLE DEVELOPMENT
AND GLIDING MOTILITY

by

BENJAMIN MICHAEL HASSELBRING

(Under the Direction of Duncan Charles Krause)

ABSTRACT

With a minimal genome containing less than 700 open reading frames and a cell volume < 10% of that of model prokaryotes, *Mycoplasma pneumoniae* is considered among the smallest and simplest organisms capable of self-replication. And yet, this unique wall-less bacterium exhibits a remarkable level of cellular complexity with a dynamic cytoskeleton and a morphological asymmetry highlighted by a polar, membrane-bound terminal organelle containing an elaborate macromolecular core. The *M. pneumoniae* terminal organelle functions in distinct, and seemingly disparate cellular processes that include cytoadherence, cell division, and presumably gliding motility, as individual cells translocate over surfaces with the cell pole harboring the structure engaged as the leading end. While recent years have witnessed a dramatic increase in the knowledge of protein interactions required for core stability and adhesin trafficking, the mechanism of *M. pneumoniae* gliding has not been defined nor have interdependencies between the various terminal organelle functions been assessed. The studies presented in the current volume describe the first genetic and molecular investigations into the location, components, architecture, and regulation of the *M. pneumoniae* gliding machinery. The data indicate that cytoadherence and gliding motility are separable properties, and identify a subset of *M. pneumoniae* proteins contributing directly to the latter process. Characterizations of novel gliding-deficient mutants confirm that the terminal organelle contains the molecular gliding machinery, revealing that with the loss of a single terminal organelle cytoskeletal element, protein P41, terminal organelles detach from the cell body but retain gliding function. The current studies additionally reveal that an intricate balance of transient activation and repression of the gliding machinery is required for normal terminal organelle development and cell division. A second terminal organelle protein, P24, which is normally transcribed with the gene encoding P41, is shown to directly contribute towards this regulation in a P41-dependent manner.

INDEX WORDS: mycoplasma, terminal organelle, gliding motility, cell division, cytoadherence, protein trafficking

MYCOPLASMA PNEUMONIAE
TERMINAL ORGANELLE DEVELOPMENT
AND GLIDING MOTILITY

by

BENJAMIN MICHAEL HASSELBRING

B.S., Indiana University, 2002

A Dissertation Submitted to the Graduate Faculty of The University of Georgia in Partial
Fulfillment of the Requirements for the Degree

DOCTOR OF PHILOSOPHY

ATHENS, GEORGIA

2006

© 2006

Benjamin Michael Hasselbring

All Rights Reserved

MYCOPLASMA PNEUMONIAE
TERMINAL ORGANELLE DEVELOPMENT
AND GLIDING MOTILITY

by

BENJAMIN MICHAEL HASSELBRING

Major Professor: Duncan C. Krause
Committee: Mark A. Farmer
 Lawrence J. Shimkets
 Eric V. Stabb

Electronic Version Approved:

Maureen Grasso
Dean of the Graduate School
The University of Georgia
December 2006

TABLE OF CONTENTS

	Page
LIST OF TABLES	vii
LIST OF FIGURES	viii
INTRODUCTION	1
CHAPTER	
1 Review of the Literature	5
<i>Mollicutes</i> History, Classification, and General Characteristics	5
The <i>Mycoplasmataceae</i>	10
Pathogenesis.....	13
History of <i>Mycoplasma pneumoniae</i>	16
<i>M. pneumoniae</i> Disease.....	17
<i>M. pneumoniae</i> Genetics	20
<i>M. pneumoniae</i> Cellular Biology	22
Terminal Organelle Functions	24
References.....	43
2 Mutant Analysis Reveals a Specific Requirement for Protein P30 in <i>Mycoplasma pneumoniae</i> Gliding Motility <i>The Journal of Bacteriology</i> , 187: 6281-89	59
Abstract.....	60
Introduction.....	60

	Materials and Methods	64
	Results	68
	Discussion.....	76
	Acknowledgements	82
	References.....	82
3	Terminal Organelle Development in the Cell	
	Wall-less Bacterium <i>Mycoplasma pneumoniae</i>	
	<i>Proceedings of the National Academy of Sciences</i> , 103: 16478-83	90
	Abstract.....	91
	Introduction.....	91
	Results	93
	Discussion.....	104
	Materials and Methods	108
	Acknowledgements	110
	References.....	110
	Supplementary Materials and Methods	112
	Supplementary Movie Legends	114
4	Transposon Mutagenesis Identifies Genes Associated	
	with <i>Mycoplasma pneumoniae</i> Gliding Motility	
	<i>The Journal of Bacteriology</i> , 188: 6335-45	116
	Abstract.....	117
	Introduction.....	118
	Materials and Methods	120

	Results	122
	Discussion.....	135
	Acknowledgements	144
	References.....	144
5	Cytoskeletal Protein P41 is Required to Anchor the Terminal Organelle of the Wall-less Prokaryote <i>Mycoplasma pneumoniae</i> <i>Molecular Microbiology</i> , in press	152
	Summary.....	153
	Introduction.....	153
	Results	157
	Discussion.....	166
	Experimental Procedures.....	171
	Acknowledgements	173
	References.....	173
	Supplementary Movie Legends	177
6	Analysis of P41 and P24 Function in <i>Mycoplasma pneumoniae</i> Terminal Organelle Development and Gliding Motility	181
	Abstract.....	182
	Results	182
	References.....	201
7	Dissertation Summary.....	203
	References.....	213

LIST OF TABLES

	Page
Chapter 1	
Table 1: Taxonomy and general characteristics of <i>Mollicutes</i>	9
Table 2: Major <i>Mollicutes</i> pathogens of animals and humans	12
Table 3: Steady-state levels of terminal organelle proteins in <i>M. pneumoniae</i> cytadherence mutants	29
Chapter 2	
Table 1: Mean gliding and corrected gliding velocities and percent time resting for wild-type <i>M. pneumoniae</i> cytadherence mutant and revertant strains, and transformants	71
Table 2: Wild-type and mutant glass-binding under conditions used for quantitation of gliding velocities and frequencies	78
Chapter 4	
Table 1: Protein profiles, gliding capacity, and glass binding by wild-type <i>M. pneumoniae</i> and the indicated cytadherence-negative mutants	124
Table 2: Insertion site identification for <i>M. pneumoniae</i> SGA mutants	128
Table 3: Characterization of cell gliding and glass binding for wild-type <i>M. pneumoniae</i> and selected SGA mutants	132

LIST OF FIGURES

	Page
Chapter 1	
Figure 1: Phylogenetic divergence of <i>Mollicutes</i> from their emergence through the present	8
Figure 2: Cryoelectron tomographic analysis of terminal organelle core architecture.....	25
Figure 3: Schematic illustration of protein interactions required for cytodherence	33
Chapter 2	
Figure 1: Cytodherence-associated protein P30 in wild-type <i>M. pneumoniae</i> , mutants II-3 and II-7, and revertant II-3R.....	63
Figure 2: Analysis of wild-type and mutant <i>M. pneumoniae</i> satellite growth	69
Figure 3: Western immunoblot analysis of P30 and P65 in wild-type, mutant, revertant, and transformant <i>M. pneumoniae</i>	73
Figure 4: Analysis of P30-EYFP in mutant II-3.....	75
Figure 5: Assessment of HA by wild-type <i>M. pneumoniae</i> and P30 mutant, revertant, and transformant strains.....	77
Chapter 3	
Figure 1: Time-lapse phase contrast / fluorescence microscopy of terminal organelle appearance, development and separation during <i>M. pneumoniae</i> growth	95

Figure 2: Time-lapse phase contrast / fluorescence microscopy of terminal organelle development without separation during growth of non-motile <i>M. pneumoniae</i> mutant III-4.....	98
Figure 3: Time-lapse phase contrast / fluorescence microscopy demonstrating the appearance of P41-YFP before cessation of gliding.....	100
Figure 4: Phase contrast / fluorescence microscopy of <i>M. pneumoniae</i> cells producing P30-CFP and P41-YFP.....	101
Figure 5: Quantitation of P30-YFP fluorescence intensity over time	103
Figure 6: Model for <i>M. pneumoniae</i> terminal organelle duplication and growth cycle	107
 Chapter 4	
Figure 1: Analysis of <i>M. pneumoniae</i> cytoadherence mutant satellite growth.....	125
Figure 2: Representative satellite growth patterns of <i>M. pneumoniae</i> SGA mutants.....	126
Figure 3: Western immunoblot analysis of selected SGA transformants.....	131
Figure 4: Analysis of satellite growth formation over time for representative SGA mutant phenotypes.....	133
Figure 5: Schematic diagram of disrupted loci for selected SGA mutants to assess likelihood of polar consequences of transposon insertions	136
 Chapter 5	
Figure 1: Organization of the P65 operon in <i>M. pneumoniae</i>	156
Figure 2: Western immunoblotting of MPN311 mutants	158
Figure 3: Terminal organelle localization in wild-type and MPN311 mutant cells	160

Figure 4: Visualization of wild-type and MPN311 mutant cell gliding	162
Figure 5: Time-lapse analysis of terminal organelle development in MPN311 mutants.....	164
Figure 6: Complementation of MPN311 mutants with recombinant P41 and P24 individually	167

Chapter 6

Figure 1: Recombinant alleles generating P41 and P24 mutants	185
Figure 2: Function of P41 and P24 in <i>M. pneumoniae</i> gliding motility	188
Figure 3: Function of P41 and P24 in <i>M. pneumoniae</i> terminal organelle development	191
Figure 4: Investigation of reciprocal dependency between P41 and P24 for terminal organelle localization	195
Figure 5: Dynamic P24 focal organizations in the absence of P41	198

Chapter 7

Figure 1: Loss of P30 from the trailing filament of gliding MPN309 mutants.....	211
---	-----

INTRODUCTION

With genomes as small as ~580 kbp and cell volumes equally as diminutive at less than 10% of those of model prokaryotes, members of the wall-less bacterial class *Mollicutes* are among the smallest and simplest organisms capable of self-replication. Since their emergence as a distinct phylogenetic lineage over 600 million years ago, the *Mollicutes* have undergone an unprecedented series of genomic reductions culminating most notably in the loss of complete pathways for *de novo* synthesis of nucleotides and amino acids, as well as the known mechanisms for transcriptional regulation and two-component signaling. As a result of their vast genetic streamlining, members of the *Mollicutes* are resigned to obligate dependencies upon specific eukaryotic hosts for survival in nature. Since the majority of the over 200 known species engender little or no host immune response, these unique parasites are commonly dismissed as simple, insignificant organisms. And yet, over 40 members of the genus *Mycoplasma* are vertebrate pathogens of major medical and agricultural significance, with *Mycoplasma pneumoniae* serving as a leading cause of pneumonia in humans and having the capacity to produce fatal extrapulmonary manifestations.

In addition to its medical significance, *M. pneumoniae* is genuinely intriguing from a biological perspective. Despite the absence of a supportive cell wall, individual cells exhibit a distinctive, asymmetrical morphology imparted by a dynamic cytoskeleton and highlighted by a polar, differentiated terminal organelle that harbors an elaborate macromolecular core. The terminal organelle functions in diverse cellular processes that include adherence to host epithelium (cytadherence) and cell division, and the structure also engages as the leading

end of translocation as *M. pneumoniae* cells glide over solid surfaces. While recent studies have begun to establish the hierarchy of protein interactions required for core stability and adhesin trafficking, the molecular components and mechanism of the gliding machinery remain unknown, nor is it clear how the terminal organelle assembles into a functional complex. Moreover, possible interdependencies between the various terminal organelle functions have not been assessed.

The current volume is divided into seven chapters beginning with a review of several aspects of *Mycoplasma* biology pertinent to the research presented subsequently. Chapter two introduces the reader to *M. pneumoniae* gliding motility and describes the development of two distinct motility assays designed to allow the facile identification of *M. pneumoniae* mutants defective in gliding motility and to determine, quantitatively, specific gliding defects at the cellular level. Using each approach, gliding capabilities of *M. pneumoniae* mutants lacking or producing altered derivatives of the terminal organelle protein P30 are characterized. Via the reintroduction of altered P30 alleles onto a P30⁻ mutant, this surface protein is definitively placed as the first *M. pneumoniae* protein for which genetic evidence backs a specific requirement in cell gliding. Significantly, chapter two introduces the concept that gliding motility and cytoadherence are separable properties for *M. pneumoniae*, and also describes the construction and functionality of a yellow fluorescence protein (YFP) fusion to P30, a visual reporter of terminal organelle location and assembly paramount for the studies presented in subsequent chapters.

Chapter three provides novel insights into the relationship between *M. pneumoniae* gliding motility and cell division, findings that present themselves through analyses of the spatial, temporal, and kinetic properties of wild-type terminal organelle development. Using P30-YFP in conjunction with additional reporter fusions, the trafficking of specific *M. pneumoniae* proteins to assembling terminal organelles is visualized. Using various

combinations of cyan fluorescence protein (CFP) and YFP fusions to these terminal organelle proteins, the relative chronology of their incorporation is deduced. Quantification of fluctuations in fluorescence emissions, combined with analyses of terminal organelle development under conditions inducing translational arrest, investigate the kinetics of terminal organelle assembly, and examination of cell gliding behaviors during terminal organelle development and cell division elucidate the relationships between these processes.

With the knowledge that gliding motility and cytoadherence are separable properties for *M. pneumoniae*, with the former appearing to be intricately associated with cell division, the studies presented in chapter four seek to identify proteins specifically associated with *M. pneumoniae* gliding so that the component identities of the gliding motor and a mechanism for its function may begin to be elucidated. In screening over 3500 individual transposon mutants for gliding defects, approximately 50 gliding-deficient strains are identified. Inactivated genes are found commonly to encode components of various metabolic pathways, as expected, but several others are putatively involved in DNA and protein modification and could possibly function in regulatory capacities, for example, to modulate motor activation during cell division. The majority of the identified gliding-associated genes, however, are found to encode *Mycoplasma*-specific proteins of unknown function, several of which are *M. pneumoniae* cytoskeletal elements and / or known components of the terminal organelle. Specific motility defects of mutants from each class are characterized, and the stabilities of known terminal organelle components are assessed for each. The data suggest a specific requirement for each gliding-associated gene for wild-type levels of motility.

Chapters five and six focus solely on two cytoadherence-positive *M. pneumoniae* gliding mutants with distinct transposon insertions in gene MPN311 encoding protein P41, a

cytoskeletal component of the terminal organelle. Insertional inactivation of MPN311 is found to result in the loss of both P41 and P24, the latter being a product of the ORF immediately downstream. In their absence, terminal organelle development is poorly coordinated spatially and temporally with gliding during cell division. Furthermore, loss of P41 and P24 is accompanied by separation of the terminal organelle from the *M. pneumoniae* cell body. Detached terminal organelles retain gliding capacity, demonstrating definitively that this structure constitutes the *M. pneumoniae* gliding motor. The construction and characterization of recombinant strains solely lacking P41 or P24 identify a structural role for P41 in anchoring the terminal organelle to the *M. pneumoniae* cell body, and show that P24 is dependent upon P41 for its localization at the terminal organelle, where it normally contributes to the initiation of nascent terminal organelle assembly and regulation of the gliding motor.

The dissertation concludes with a summary of the content and significance of these studies concentrating on their relatedness and on their impact on our understanding of cellular engineering in this minimal microbe. Directions for future research are presented, as are additional data from studies currently in progress. After reviewing this work, I hope the reader comes away with a new respect for *M. pneumoniae* and will from here forth argue against its stigma as a simplistic microorganism.

CHAPTER 1

REVIEW OF THE LITERATURE

***Mollicutes* History, Classification, and General Characteristics**

In the closing years of the 19th century, research at the Pasteur institute included investigations by Edward Nocard and Pierre Roux into the causative nature of contagious bovine pleuropneumonia (CBPP), a respiratory disease of cattle still incurring devastating production loss in endemic areas worldwide. Using standard techniques of the day, initial attempts to identify a causative agent proved unsuccessful until pulmonary fluid from an infected animal was introduced into a semi-permeable pouch of sterile medium and placed into the peritoneal cavity of a live rabbit (Nocard E. and Roux P., 1898). After three weeks of incubation, liquid from the recovered pouch presented an opacity absent from uninoculated controls and routinely engendered CBPP symptoms when administered to healthy cattle (Nocard E. and Roux P., 1898). Although the significance of their research was not appreciated at the time, Nocard and Roux had successfully, but unwittingly, cultivated the first member of a unique class of cell wall-less eubacteria currently comprised of over 200 obligately-parasitic species.

By the 1910s, Nocard and Roux's CBPP agent had proven capable of growth in cell-free media containing mammalian serum. Combined with direct microscopic visualization

(Bordet, 1910), this ability to self-replicate verified its bacterial status. And yet, the minimal replicative units of the CBPP organism were capable of passing through filter pores of 150 nm (Elford, 1929), a property later found to derive from its lack of a supportive cell wall. Over the next two decades, such baseline characterization established for Nocard and Roux's CBPP agent facilitated the association of additional filterable, wall-less bacteria with severe mucosal, rheumatic, and neurological diseases of domesticated mammals (Bridre and Donetien, 1923; Findlay *et al.*, 1938; Sabin, 1938; Shoetensack, 1936); the connotation pleuropneumonia-like organisms (PPLO) was adopted in reference to these novel bacteria. By 1937 the first PPLO of human origin, the urogenital tract pathogen presently known as *Mycoplasma hominis*, had been identified (Dienes and Edsall, 1937).

During the next quarter century, the medical and agricultural importance of many PPLOs saw their extensive cataloging by culture and serology. The existing PPLO connotation was replaced with the general term "mycoplasma" referring to all species of filterable bacteria lacking a defining cell wall and requiring the presence of serum for growth *in vitro*. The next quarter century witnessed a considerable influx in mycoplasma research. Efforts underway in the field of biophysics to define the lower limit of life, i.e., the smallest self-replicating organisms, inevitably drew considerable attention to these minute microbial oddities. Furthermore, mycoplasmas became the preferable organisms for basic studies of membrane biology as their small volume meant a high surface-to-volume ratio, the absence of a cell wall facilitated membrane preparation, and the lipid composition of their membranes could be manipulated simply by varying media conditions. Elsewhere in the clinical and veterinary fields, advances in diagnostics combined with an increasing understanding of their biochemical and metabolic properties, saw a significant boom in the isolation of novel mycoplasma species.

The advent of genetic-based taxonomy in the 1980's revealed a need to refine the evolutionary relationships of the wall-less organisms. The term "mycoplasma" was discarded in taxonomic circles, and members of the group were compiled into the new bacterial class *Mollicutes* (Latin: "mollis" = soft and "cutes" = skin) with *Mycoplasma* one of eight genera. Consisting of 4 orders and 5 families (Figure 1.1), mollicutes group within the phylum *Firmicutes*, sharing ancestry with Streptococcal and Clostridial lineages of the low G+C Gram-positive eubacteria. Extensive characterization of the class by 16s rRNA sequencing has allowed their evolution to be traced along the context of major paleontological changes during the Earth's history (Maniloff, 2002). Thus, approximately 600 million years ago (mya), coinciding with the Cambrian explosion of multicellular marine animals, the spontaneous loss of peptidoglycan biosynthetic capability spawned the emergence of the *Mollicutes* lineage (Fig. 1.1), the ancestral species of which is thought to be most similar to the modern *Acholeplasma* (refer to table 1.1 for an overview of taxonomy and characteristics of *Mollicutes* genera). Over the next 100 million years, as its eukaryotic counterparts developed more and more complex arrangements of multicellularity, the ancestral mollicute underwent rapid genomic reduction therein losing aerobic metabolic pathways and cytochromes, several rRNA genes, as well as amino and nucleic acid biosynthetic capability. Thus, from its early stages, the lineage appeared destined for an obligately-parasitic existence. The emergence of land plants 470 mya coincided with the first internal branching of the *Mollicutes* to produce a second lineage similar to the modern *Mesoplasma/Entomoplasma*. Approximately 50 million years later, major expansion of marine life and the appearance of the first land animals (the Silurian - Devonian boundary) saw both branches undergoing additional differentiation. Although the selective pressures are not understood, from the ancestral Mesoplasmas emerged a lineage similar to the

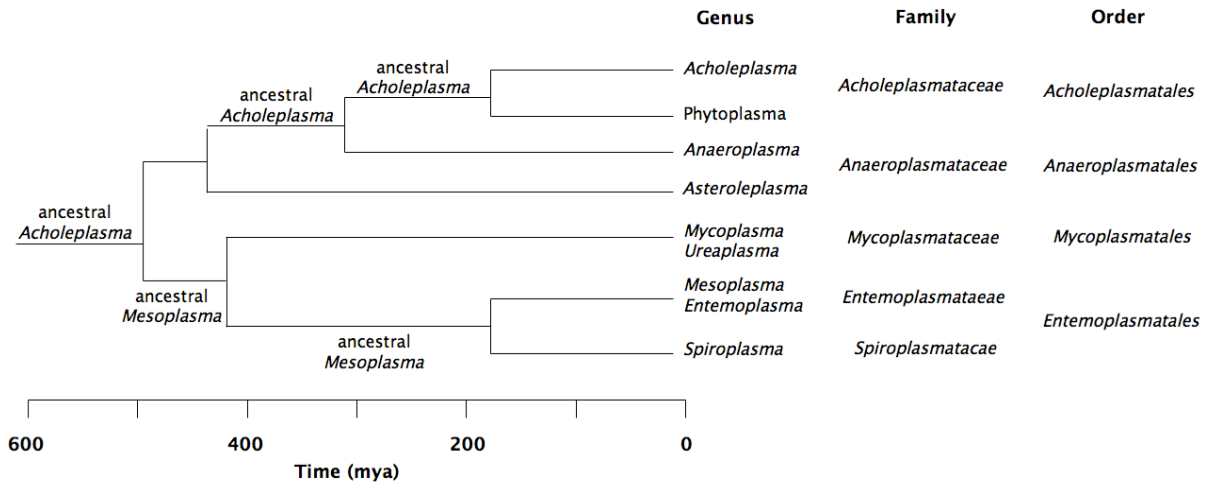


Fig. 1.1. Phylogenetic divergence of *Mollicutes* from their emergence through the present.

Modified from (Maniloff, 2002)

Table 1.1. Taxonomy and general characteristics of *Mollicutes*

Family	Genus	No. of Taxa	Phenotypic Characteristics	Habitat
<i>Mycoplasmataceae</i>	<i>Mycoplasma</i>	107	opt. growth 37°C	Humans, animals
	<i>Ureaplasma</i>	7	Urease positive	Humans, animals
<i>Entomoplasmataceae</i>	<i>Entomoplasma</i>	6	Opt. growth 30 °C	Insects, plants
	<i>Mesoplasma</i>	12	Opt. growth 30 °C	Insects, plants
<i>Spiroplasmataceae</i>	<i>Spiroplasma</i>	34	Helical morphology	Insects, plants
<i>Acholeplasmataceae</i>	<i>Acholeplasma</i>	14	Opt. growth 30–37 °C	Animals, plant surfaces
	<i>Phytoplasma</i>	6	Uncultured in vitro	Insects, plants
<i>Anaeroplasmataceae</i>	<i>Anaeroplasma</i>	4	Obligate anaerobes	Dig. tract of ruminant mammals
	<i>Asteroleplasma</i>	1	Obligate anaerobes	Dig. tract of ruminant mammals

Modified from ref. (Johansson and Pettersson, 2002)

modern *Mycoplasma* and *Ureaplasma* genera, which currently contain over 100 species of obligate vertebrate parasites. In parallel, from the ancestral *Acholeplasmas* emerged a branch similar to modern *Asteroloplasmas*. While the new *Asteroloplasma* and *Mycoplasma* *Ureaplasma* lineages would remain relatively stable, branching only internally to optimize their parasitism of emerging hosts, approximately 270 mya, and again for reasons unknown, from the *Acholeplasma* lineage emerged the obligately anaerobic *Aneroplasmas*. The appearance of flowering plants in the Middle Jurassic period spawned the final significant branchings within the group, with *Spiroplasma* deriving from the *Mesoplasma* and the presently-uncultured *Phytoplasma* emerging from *Acholeplasma*.

The *Mycoplasmataceae*

Over half of the current 200 *Mollicutes* species reside within the family *Mycoplasmataceae*. Consisting of two genera, *Mycoplasma* and *Ureaplasma*, the elevated percentage of mollicutes grouping within this single lineage likely reflects an increased occurrence of isolation due to their medical and agricultural significance (see below). As an aside, it should be noted that via 16s rRNA typing, the genus *Ureaplasma* should rightfully be dissolved and its seven species reassigned into the genus *Mycoplasma* (Maniloff, 2002), as ureaplasmas are basically mycoplasmas with urease activity. Moreover, several *Mycoplasma* species, including the type species *Mycoplasma mycoides*, should be withdrawn from the genus as they are more closely related to other *Mollicute* lineages. However the inevitable confusion such reorganizations would cause in the medical and veterinary fields will likely preserve the current nomenclature.

Rightful members of the *Mycoplasmataceae* arrange in two major phylogenetic clusters, the *pneumoniae* group and the *hominis* group. Most preferentially colonize mucosal interfaces of the respiratory or urogenital tract of a specific vertebrate host. Over 40 cause disease in humans and domesticated animals. Of the sixteen species isolated from humans, approximately half are commensals, with *Mycoplasma salivarium*, *Mycoplasma orale*, *Mycoplasma faucium*, and others commonly colonizing the oropharynx, and some, including *Mycoplasma primatum* and *Mycoplasma spermatophilum*, typically residing in the urogenital tract. Four species, *Mycoplasma pneumoniae*, *Mycoplasma hominis*, *Mycoplasma genitalium*, and *Ureaplasma* spp. are established pathogens of the urogenital or respiratory tract by the fulfillment of Koch's postulates (the latter is a heterogeneous species consisting of two biovars, *U. urealyticum* and *U. parvum*, which will be considered together here). Three additional species, *Mycoplasma fermentans*, *Mycoplasma penetrans*, and *Mycoplasma amphoriforme* are likely associated with human disease, although a direct correlation in non-immunocompromised individuals has not been demonstrated for either (Lo *et al.*, 1992; Pitcher *et al.*, 2005; Williams *et al.*, 1970). An overview of animal and human *Mycoplasmataceae* pathogens and their disease characteristics is presented in table 1.2. For an in-depth review the reader is directed to the following references (Blanchard, 2002; Frey, 2002). Disease characteristics of the established human pathogens of the *Mycoplasmataceae* family are described *in brevia* below.

M. genitalium is the leading cause of nonchlamydial-nongonococcal urethritis (NCNGU) in males, accounting for up to 25% of acute cases (Bjornelius *et al.*, 2000; Gambini *et al.*, 2000; Totten *et al.*, 2001). More recently, *M. genitalium* has been associated with chronic NCNGU with detection both by PCR and by direct isolation from men with recurrent disease symptoms following antibiotic treatment and resolution of the acute stage

Table 1.2. Major *Mollicute* pathogens of animals and humans

Host/Mollicute species	Disease
Bovine	
<i>M. bovis</i>	mastitis, pneumonia, polyarthritis, abortion, sterility
<i>M. dispar</i>	pneumonia
<i>M. californicum</i>	mastitis
<i>M. canadense</i>	mastitis
<i>M. bovigenitalium</i>	mastitis and genital disease
<i>M. bovocculi</i>	conjunctivitis
<i>Ureaplasma diversum</i>	metritis, sterility, abortion
Sheep and Goat	
<i>M. capricolum</i> subsp. <i>capripneumoniae</i>	contagious caprine pleuropneumoniae
<i>M. capricolum</i> subsp. <i>capricolum</i>	mastitis, arthritis
<i>M. mycoides</i> subsp. <i>capri</i>	pneumonia, mastitis, arthritis, septicemia
<i>M. mycoides</i> subsp. <i>mycoides</i> LC	pneumonia, mastitis, arthritis, septicemia
<i>M. agalactiae</i>	infectious agalactia
<i>M. ovipneumoniae</i>	pneumonia
<i>M. conjunctivae</i>	infectious keratoconjunctivitis
Poultry	
<i>M. gallisepticum</i>	sinusitis, chronic respiratory disease
<i>M. synoviae</i>	air sacculitis, arthritis, tendosynovitis
<i>M. meleagridis</i>	air sacculitis, sinusitis, arthritis
<i>M. anseris</i>	respiratory tract infections
Swine	
<i>M. hyopneumoniae</i>	enzootic pneumonia
<i>M. hyorhinis</i>	pneumonia, arthritis
<i>M. hyosynoviae</i>	arthritis
Dog and Cat	
<i>M. cynos</i>	pneumonia
<i>M. felis</i>	conjunctivitis, pneumonia
<i>Haemoplasma canis</i>	anemia
<i>Haemoplasma felis</i>	anemia
Rodents	
<i>M. arthritidis</i>	arthritis
<i>M. pulmonis</i>	respiratory and genital tract infections
Humans	
<i>M. genitalium</i>	urethritis (men)
<i>M. pneumoniae</i>	pneumonia, bronchitis
<i>M. hominis</i>	PID, sterility (women) meningitis, pneumonia (neonates)
<i>Ureaplasma</i> spp.	PID, sterility (women) meningitis, pneumonia (neonates)
<i>M. fermentans</i>	unknown
<i>M. penetrans</i>	unknown

Modified from (Blanchard, 2002) and (Frey, 2002)

(Horner *et al.*, 2001). Definitive correlations between *M. genitalium* infection and urogenital disease of women have not been established. In contrast, *M. hominis* and ureaplasmas present significant health risks to women, although their correlations with urogenital diseases in men are lacking. *M. hominis* and Ureaplasma proliferate in women with bacterial vaginosis (BV) (Keane *et al.*, 2000; Rosenstein *et al.*, 1996) and have been isolated from the endometrium and fallopian tubes of women with pelvic inflammatory disease (Taylor-Robinson, 1996). However, the specific contributions of either in these multi-etiological diseases remain unclear. A stronger pool of data specifically incriminates *M. hominis* and ureaplasmas in neonatal and post-partum infections where up to 50% of newborns may become inoculated during birth when the mother is a carrier. Both typically colonize the respiratory tract of such neonates, causing pneumonia, although rarely, *M. hominis* and Ureaplasma have been recovered from the cerebrospinal fluid of newborns with meningoencephalitis (Alonso-Vega *et al.*, 1997; Waites *et al.*, 1988).

Only one member of the *Mycoplasmataceae*, *M. pneumoniae*, exists in nature as an obligate pathogen of the human respiratory tract. *M. pneumoniae* infections are generally mild and self-limiting with the most common clinical manifestations occurring as tracheobronchitis and atypical “walking” pneumonia (Waites and Talkington, 2004). Rarely, however, fatal extrapulmonary manifestations occur in non-immunocompromised individuals, reflecting a capacity for the organism to spread systemically. A more comprehensive review of *M. pneumoniae* disease will be discussed later in this chapter.

Pathogenesis

Persistence and resurgence of mycoplasma infections following initial antibiotic clearance is a common theme. This apparent ability to evade adaptive host immune

responses stems largely from phenotypic plasticities by which many pathogenic mycoplasmas are capable of altering the expression and structure of specific surface proteins. In the absence of signal transduction pathways and means for transcriptional regulation, such modulations are achieved by an array of genetic manipulations that include site-specific promoter and gene inversions (*Mycoplasma pulmonis*), poly A strand slippage (*Mycoplasma hyorhinis*, *M. hominis*, *M. fermentans*), homologous recombination (*Mycoplasma bovis*), and intragenomic recombination producing chimeric genes from multiple repetitive elements (*M. pneumoniae*, *M. genitalium*) (Yogev *et al.*, 2002). Still, the molecular basis of Mycoplasma pathogenicity remains largely elusive. While membrane fusion with, or outright invasion into transformed cell lines has been documented for several species, including *M. gallisepticum*, *M. genitalium*, *M. fermentans*, and *M. pneumoniae*, only *M. penetrans* has been shown to reside and multiply within normal cell types (although *M. penetrans* has only been isolated from immunocompromised patients) (Lo *et al.*, 1993). Furthermore, although an array of hydrolytic enzymes has been identified in mycoplasmas, including phospholipases, proteases, and nucleases (Bendjennat *et al.*, 1997; Moriguchi *et al.*, 1989; Razin *et al.*, 1998), evidence for direct contribution of such proteins in mycoplasma pathogenesis remains largely speculative. Rather, all *Mycoplasmataceae* produce hydrogen peroxide as a metabolic byproduct, and thus a common denominator in their pathogenicity may stem from oxidative damage to the host cell and subsequent cytological damage from the host immune and inflammatory responses (Almagor *et al.*, 1984; Arai *et al.*, 1983; Cole *et al.*, 1968; Sobeslavsky and Chanock, 1968).

Regardless of their precise virulence mechanism(s), for every pathogenic mycoplasma, host colonization and subsequent disease progression is absolutely dependent upon their ability to reside and propagate within the host epithelial surface. As such, the mechanisms and proteins utilized for cytoadherence have been the subject of

intense investigation and have focused primarily on a subset of *Mycoplasmataceae* (*M. pneumoniae*, *M. genitalium*, *M. gallisepticum*, and *Mycoplasma mobile*) which produce a polar, membrane-bound extension of their cell bodies mediating this process (Kirchhoff *et al.*, 1984). For each of these morphologically-differentiated species so far examined, cytoadherence-associated proteins typically localize predominantly or exclusively to these polar structures (Baseman *et al.*, 1987; Hu *et al.*, 1982; Kusumoto *et al.*, 2004; Uenoyama *et al.*, 2004). Still, it is unlikely that cytoadherence alone can be considered a virulence factor as each of the other 200 species of non-differentiated *Mollicutes*, commensals and pathogens alike, also exhibits the ability to bind to host epithelial surfaces as a necessity for its obligately-parasitic existence. Along these same lines, the previous adage that mycoplasma pathogenicity stems largely from oxidative damage to the host cell may not fit either, as all *Mollicutes* examined to date, exhibit this same feature.

Interestingly, of the pathogenic *Mycoplasmataceae* producing differentiated polar structures, gliding motility has been observed for each species examined (Kirchhoff, 1992). Unfortunately, due to technical difficulties, for none of these gliding species has motility on normal epithelial surfaces been examined. Still, it is tempting to hypothesize that this small, unique group of differentiated mycoplasmas has evolved to utilize gliding as an adaptive advantage within the host environment, perhaps allowing migration to areas of lower cell density to minimize competition for receptor binding or nutrients. Alternatively, gliding may facilitate host colonization prior to receptor binding by facilitating penetration of the epithelial mucosal layer. Alas, the contribution of gliding motility towards the pathogenicity of these differentiated species is only speculative, for no gliding mycoplasmas do mutants currently exist with motility defects that retain the capacity to bind to host tissues at wild-type levels. The separation of these two phenotypes is a necessity for defining the relationship between mycoplasma gliding and virulence.

The remainder of this chapter, as well as the research presented in subsequent sections, focuses on the gliding human pathogen, *M. pneumoniae*. While *M. pneumoniae* is the most extensively characterized of the *Mollicutes*, previous studies have focused primarily on its attachment to host epithelia and have not attempted to explore other intriguing aspects of its cell biology such as the relationships between cytoadherence and motility, the mechanism(s) and proteins employed for cell gliding, or the characteristics of *M. pneumoniae* cell division and the possible role of gliding motility in that process. Each will be addressed in subsequent chapters.

History of *Mycoplasma pneumoniae*

While *M. hominis* carries the distinction of being the first-described mycoplasma of human origin (Dienes and Edsall, 1937), preliminary characterizations of another had begun several years earlier, although its identity as such would not be realized for over a quarter-century. By the 1930's, the medical field had become increasingly aware of an atypical type of pneumonia with generally mild, flu-like symptoms that were often disproportionate to the lung infiltrations observed by X-ray. The coming of the Second World War saw increasing occurrences of these symptoms as the crowded conditions of military barracks enhanced its incidence of transmission. Coined primary atypical pneumonia (PAP) in medical circles or "walking" pneumonia in military jargon, its distinctive disease characteristics prompted studies by Eaton *et al.* in the early 1940's to identify a causative agent. Using sputum from symptomatic individuals, Eaton and colleagues were able to propagate a biological agent in chicken embryos, however, no definitive organism was detected by the high magnification light microscopy available to the researchers. As the agent was capable of passing through

filters that excluded typical bacteria, was resistant to penicillin and sulfonamides, and was not successfully cultivated *in vitro* on standard PPLO media of the day, Eaton's agent, as it came to be called, was considered to have a viral classification (Eaton *et al.*, 1945). However, continued characterization of Eaton's agent through the 1950's revealed its susceptibility to new antimicrobial compounds combative against PPLOs, and thus many researchers began to doubt the fidelity of its viral classification (Marmion and Goodburn, 1961). In 1962, Chanock *et al.* successfully cultivated the organism in cell-free medium and definitively demonstrated its status as a PPLO (Chanock *et al.*, 1962). Eaton's agent was officially named *Mycoplasma pneumoniae* the following year (Chanock *et al.*, 1963) and over the last four decades has become the most extensively characterized member of the *Mollicutes*.

***M. pneumoniae* Disease**

M. pneumoniae is the leading cause of pneumonia in children and young adults and accounts for up to 20-30% of all pneumonia requiring hospitalization (Alexander *et al.*, 1966; Block *et al.*, 1995; CDC, 2002; Clyde and Denny, 1967; Foy, 1993; Ruuskanen *et al.*, 1992). The species is prevalent across all reaches of the globe and infections may occur at any time during the year, however higher incidences are observed in temperate climates and during the summer and fall elsewhere (Joosting *et al.*, 1976; Suhs and Feldman, 1966). Infections can result in permanent lung damage, and rarely, *M. pneumoniae* has been observed to disseminate systemically to cause fatal extrapulmonary manifestations (Chryssanthopoulos *et al.*, 2001; Ieven *et al.*, 1998; Maisel *et al.*, 1967; Tjhie *et al.*, 1997; Waites and Talkington, 2004). Classically, however, due to its typically mild symptoms and

difficulty in culture and diagnosis, the incidence and significance of *M. pneumoniae* infection has been underappreciated and often attributed to viral etiologies. This has led to the misconception that *M. pneumoniae* is an obscure pathogen. In recent years, however, reports from the medical field have increasingly described *M. pneumoniae* infections in the young and elderly (Dorigo-Zetsma *et al.*, 2001; Ferwerda *et al.*, 2001; Heiskanen-Kosma *et al.*, 1998). This apparent heightened awareness within the medical community likely stems from a combination of increased rates of transmission due to elevated numbers of elderly and the very young interacting in the close proximity of health-care, retirement, and child-care facilities, together with more accurate diagnosis via the use of molecular detection tools.

Whereas classic pneumococcal pneumonia is characterized by an acute onset with high fever and the production of mucopurulent sputum, the atypical pneumonia produced by *M. pneumoniae* is distinct in its slow onset and generally chronic nature (Clyde, 1971; Luby, 1991). Thus, after inhalation, *M. pneumoniae* generally requires an incubation period of 2-3 weeks before the onset of disease. Predominant early symptoms including fever and sore throat generally last for less than two weeks, although dry cough, malaise, and headache typically exist as well during early stages and generally persist for several additional weeks (Ferwerda *et al.*, 2001; Luby, 1991; Stevens *et al.*, 1978; Waites and Talkington, 2004).

Because a virus was originally suspected as the causative agent of primary atypical pneumonia, early diagnostic measures focused predominately on serological testing. In particular, complement fixation assays have been the classical method of diagnosis, although recent years have seen the abandonment of this technique. Rather, the diagnostic means of choice currently utilize include PCR amplification of the 16s ribosomal RNA gene or, more commonly, the gene encoding the major *M. pneumoniae* adhesin P1 (Ferwerda *et*

al., 2001). Typically, samples from nasopharyngeal aspirates or pharyngeal swabs offer sufficient template for these diagnostics.

While *M. pneumoniae* symptoms generally resolve on their own in less than a month, antibiotic treatment is commonly prescribed to shorten the acute phase. While all mycoplasmas are naturally resistant to β -lactams, polymyxins, sulfonamides, naladixic acid, and rifampicin, *M. pneumoniae* is susceptible to tetracyclines and macrolides, with clarithromycin and azithromycin being the current antimicrobials of choice for treating *M. pneumoniae* infection (Cassell *et al.*, 1991; Harris *et al.*, 1998; Waites and Talkington, 2004; Wubbel *et al.*, 1999). Rather than incurring direct cytopathic effects, these bacteriostatic agents are thought to simply aid in the clearance and eradication of the organisms by the natural host immune responses.

In healthy individuals, *M. pneumoniae* infections typically generate a strong immune response with an increase in reactive antibodies of the IgM type within the first two weeks, followed by antibodies of the IgG type and of the secretory IgA class in the following three to eight weeks (Biberfeld, 1968, 1971; Hu *et al.*, 1983). Anti-*M. pneumoniae* antibodies generally target the bacterial lipids, polysaccharides, and several surface proteins necessary for virulence, especially the major adhesin protein P1 (Allen and Prescott, 1978; Leith *et al.*, 1983). Most pathogenic mycoplasmas usually induce a strong cytokine response (Razin *et al.*, 1998). *M. pneumoniae* infections in particular are marked by increases in IL-1 β , IL-6, TNF- α , and INF- γ resulting in localized inflammation and the recruitment of professional phagocytes (Kita *et al.*, 1992). While these responses are crucial to *M. pneumoniae* clearance, they also contribute to the disease symptoms.

A growing body of evidence supports correlations between *M. pneumoniae* infections and the development or exacerbation of chronic asthma, suggesting an immunopathological

basis to its disease spectrum (Biscardi *et al.*, 2004; Johnston *et al.*, 2005; Szczpanik *et al.*, 2004; Teig *et al.*, 2005; (Waites and Talkington, 2004). These findings are consistent with longstanding data whereby *M. pneumoniae* infection is frequently associated with autoimmune responses, particularly the development of hemagglutinins, IgM antibodies directed against *M. pneumoniae* surface proteins but which also target the I antigen of host erythrocytes (Janney *et al.*, 1978). The extent to which autoimmune responses contribute to the variety of extrapulmonary manifestations observed with *M. pneumoniae* disease is uncertain. Extrapulmonary consequences are reported for roughly 25% of *M. pneumoniae* infections and typically manifest as inflammations of the dermal, cardiac, hepatic, renal, synovial joint, and central nervous tissues (Chryssanthopoulos *et al.*, 2001; Ieven *et al.*, 1998; Maisel *et al.*, 1967; Tjhie *et al.*, 1997; Waites and Talkington, 2004). *M. pneumoniae* has been cultured directly from each tissue in the cases of these extrapulmonary sequelae, reflecting a capacity to spread systemically. While the routes and mechanisms of its spread remain undetermined, *M. pneumoniae* is capable of invading and persisting for extended periods in tissue culture cells *in vitro* (Dallo and Baseman, 2000; Yavlovich *et al.*, 2004), and thus it is tempting to speculate that intracellular invasion *in vivo* may facilitate spreading. However, to date, internalized *M. pneumoniae* have not been recovered from any type of host cell nor has invasion been documented in differentiated, primary cell lines *in vitro*.

***M. pneumoniae* Genetics**

As mentioned previously, *M. pneumoniae* groups within the *Mycoplasmataceae* family of *Mollicutes*, members of which are confined to obligately-parasitic relationships with specific vertebrate hosts for survival in nature. Such host dependencies stem largely from

the loss of vast amounts of genomic information including pathways required for *de novo* synthesis of purines and pyrimidines, amino acids, fatty acids, and metabolic cofactors (Dandekar *et al.*, 2000; Himmelreich *et al.*, 1996). The *M. pneumoniae* genome consists of a single chromosome of a mere 816 kbp encoding 42 RNA genes and less than 700 putative open reading frames, approximately 50-100 of which are pseudogenes encoding only fragmented or truncated products and which may likely be discarded in the future (Dandekar *et al.*, 2000; Himmelreich *et al.*, 1996). In addition to its minimal metabolic complement, the *M. pneumoniae* genome is strikingly devoid of means of typical transcriptional regulation and two-component signaling, as well as known mechanisms for protein secretion and cell motility. In addition, *M. pneumoniae* lacks homologs for many of the conserved cell division proteins and cytoskeletal elements characteristic of model organisms including MinC/D, ParB, and MreB; moreover, of the conserved Fts genes, *M. pneumoniae* contains only FtsH and FtsZ. Its genome additionally lacks few complete systems required to repair errors incurred during chromosome replication or from damage due to oxidative stress; most notably the *mut* genes for mismatch repair are completely absent and many genes of the SOS pathway have likewise been lost including the main response-regulator *lexA*. The absence of these seemingly essential systems is an intriguing finding considering that *M. pneumoniae* produces H₂O₂ as a metabolic by-product (Cohen and Somerson, 1967). The lack of such systems may contribute to the elevated rates of genetic mutation observed for *M. pneumoniae* and fellow Mollicutes relative to model prokaryotes (Matic *et al.*, 1995).

Apart from the technical difficulties of working with *M. pneumoniae* due to its fastidious nature and genetic instability, a multitude of other obstacles exist. *M. pneumoniae*, like all *Mollicutes*, has evolved to use the codon UGA to encode the amino acid tryptophan rather than as the normal opal stop codon. Thus, overexpression and purification of *M. pneumoniae* proteins in *Escherichia coli*, *Bacillus subtilis*, or other genetically tractable

organisms is somewhat problematic. While opal suppressor strains exist for *E. coli*, and *B. subtilis*, such systems generally offer only leaky translation at best and are often not suitable when the expression of genes with several UGA codons is required. In addition, *M. pneumoniae* has no known phages and carries no natural plasmids, nor have attempts at the propagation of plasmids for the expression of genes in *M. pneumoniae* been successful. Furthermore, despite the independent efforts of several groups, homologous recombination for targeted gene knockout has not been reported. Thus, the inability to construct *M. pneumoniae* knockout mutants deems that protein function may only be assessed after the serendipitous isolation of mutants exhibiting a desired phenotype. Although no naturally occurring transposable elements are evident in the genome, the *Staphylococcus aureus* transposon Tn4001 (Byrne *et al.*, 1989) does function in *M. pneumoniae* and inserts at random genetic loci (Hutchison *et al.*, 1999). By default then, Tn4001 is the tool of choice for mutagenesis and genetic complementation experiments and has been used successfully for both (Fisseha *et al.*, 1999; Hedreyda *et al.*, 1993; Hutchison *et al.*, 1999; Waldo *et al.*, 2005).

***M. pneumoniae* Cellular Biology**

In addition to its medical significance, and starkly contrasting its minimal genetic complement, *M. pneumoniae* exhibits a remarkable level of morphological and ultrastructural complexity. Despite the lack of a supportive cell wall, *M. pneumoniae* cells display a filamentous morphology averaging approximately 2.0 μm in length and a mere 0.2 μm in diameter (Muse *et al.*, 1976), dimensions which confer a cell volume less than 10% of that of model prokaryotes. Its minute body is highlighted by a differentiated, membrane-bound appendage protruding from a single cell pole. This unique terminal organelle harbors an

elaborate core complex, oriented longitudinally, and often described as “electron-dense” due to its observed opacity in transmission electron micrographs after fixation and staining (Biberfeld and Biberfeld, 1970; Wilson and Collier, 1976). The core of the *M. pneumoniae* terminal organelle stands pronounced as a major component of a larger cytoskeletal framework, which, after Triton X-100 detergent-treatment of intact cells, appears as thin, helical filaments approximately 5 nm in diameter emerging from the base of the terminal organelle core to follow the general contours of the cell body (Gobel *et al.*, 1981; Meng and Pfister, 1980). Based upon their biochemical and structural properties, these cytoskeletal filaments were originally hypothesized to be a prokaryotic equivalent to actin microfilaments (Neimark, 1977). However, subsequent efforts to identify the analogous protein subunits were unsuccessful; completion of the genome sequence likewise verified the lack of such genes. The molecular makeup and functions of this larger cytoskeletal network remain undefined as, to date, no *M. pneumoniae* mutants have been assessed microscopically for the absence or structural abnormalities in these filamentous elements.

Recent characterizations of the *M. pneumoniae* cytoskeleton have focused primarily on the structure of the terminal organelle core. Several independent studies originally described the core as being composed predominantly of two parallel rods exhibiting periodic striations and enlarging to form a terminal “button” abutting the cell membrane at the distal end of the organelle (Biberfeld and Biberfeld, 1970; Wilson and Collier, 1976). The advent of cryoelectron microscopy has significantly reduced the occurrence of fixation artifacts and has led to a major refining of the core architecture (Hegermann *et al.*, 2002; Henderson and Jensen, 2006; Seybert *et al.*, 2006). The terminal button region is now known to be comprised of at least three subunits. At its most distal end, an arch of globular proteins appears to contact an inner layer of peripheral membrane proteins (Fig. 1.2a, arrows c and b, respectively). Behind this layer, the terminal button is composed of two distinct units (Fig.

1.2b, arrows D and E) separated by a gap perpendicular to the axis of the core (Fig. 1.2b). Proceeding proximally, the classical rod-like structures appear, although data now indicate that they are compositionally distinct and of different lengths and thicknesses, with only the longer and thicker of the two rods making contact with the terminal button (Fig. 1.2c and d). Both rods, although clearly parallel, exhibit a jointed, multisubunit architecture (Fig 1.2c, individual subunits denoted with arrows F-J). Each is bent approximately 150° just proximal to its midpoint, with the thinner rod following the inner curvature of the thicker. Distal to the bend, each is discretely segmented, appearing similar to a vertebral column, while proximal to the bend the rods become continuous. Interestingly, the distal segmented regions appear to be conformationally flexible; the gap distance between them varies, as does the conformation of the segments themselves, although at any one time, all are either uniformly straight, convex, or concave relative to the core axis (Fig. 1.2d). Finally, at the base of the terminal organelle core, a convex, bowl-like complex appears (Fig. 1.2c, subunit K) and is more or less perpendicular to the core rods although the distance and the angle between these structures varies considerably (Fig 1.2d). Interestingly, the bowl complex is not always apparent, suggesting that it may be constructed subsequent to other components during the process of core assembly.

While advances in structural imaging have clearly enhanced our understanding of terminal organelle architecture, molecular identities of the core subunits remain undefined.

Terminal Organelle Functions

The *M. pneumoniae* terminal organelle is implicated to function in several distinct and seemingly disparate cellular processes including cytoadherence, gliding motility, and cell

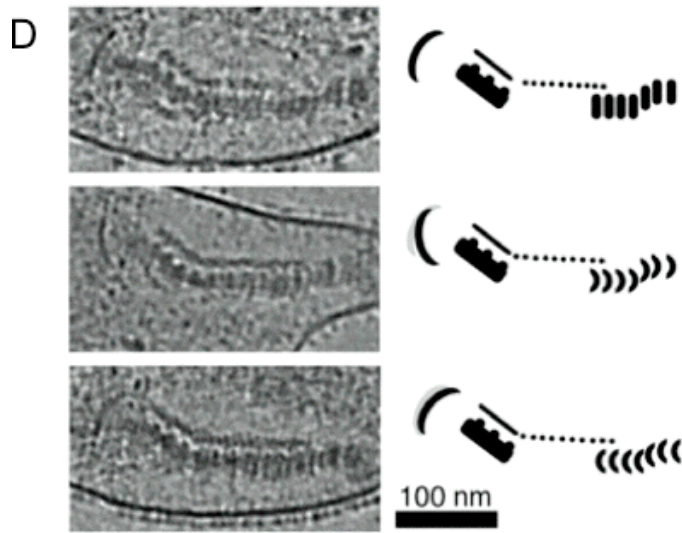
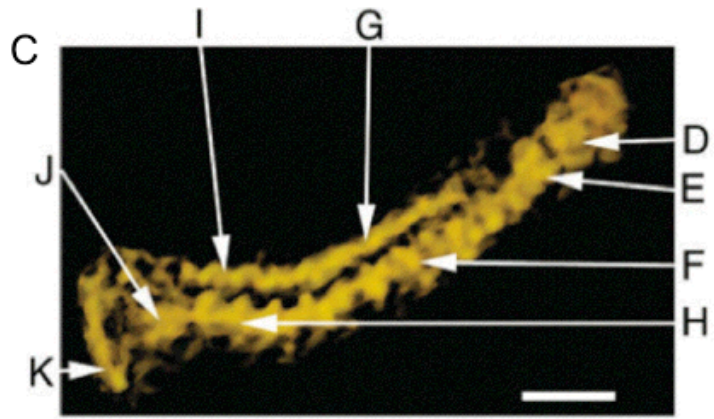
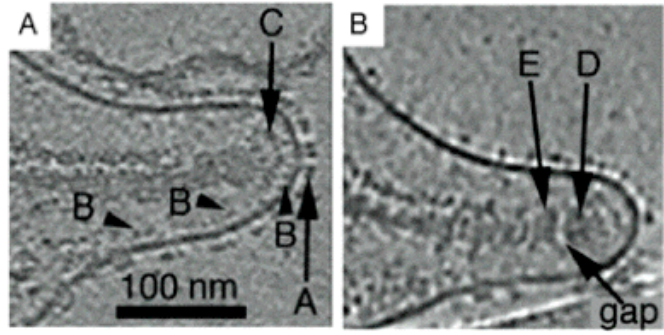


Fig. 1.2. Cryoelectron tomographic analysis of terminal organelle core architecture.

The terminal organelle core is comprised of at least 10 distinct subunits. Panels A-C: The terminal button (subunits C, D, and E) abuts peripheral membrane proteins (subunit B) at the distal end of the terminal organelle. Panel C: Subunit E of the terminal button connects to the longer and thicker of the two central rods, which have a jointed architecture composed of conformationally-flexible subunits (G and F, and panel D) proximal to a 150 ° bend at their midpoint. Behind this bend, the rod subunits (I and H) assume a more continuous composition, merging with a bowl-like complex (subunit K) at the base of the core. Panel D: The distances and angles between the bowl-like complex and core rods vary considerably. Adapted with permission from Henderson and Jensen (2006).

division. Assembly of the terminal organelle is hypothesized to occur via a specific sequence of events whereby certain proteins interact early to form the foundation for subsequent assembly of the terminal organelle core and proper incorporation and anchoring of adhesins into the terminal organelle membrane. The process coincides with chromosome replication with nascent terminal organelles developing adjacent to an existing structure, but the means by which these processes are temporally and spatially regulated is unknown. Via analysis of mutants deficient in cytodherence, several proteins have been implicated to function in the hierarchy of interactions required for these events to take place. The current understanding of terminal organelle development and function is discussed.

Cytadherence: The ability to attach to host tissue is a crucial aspect of *M. pneumoniae* colonization and has been the study of intense and ongoing investigation for over three decades. Early electron micrographs of *M. pneumoniae*-infected respiratory epithelium revealed an intimate association between the terminal organelle and the host epithelial surface (Collier and Clyde, 1974). Subsequent investigations demonstrated that pretreatment of host tissue with neuraminidase significantly reduced *M. pneumoniae* cytodherence capability to suggest sialoglycoconjugates as a primary host receptor (Powell *et al.*, 1976).

Protein P1: In the opposite approach to neuraminidase treatment of host epithelium as a means to identify host receptors, treatment of *M. pneumoniae* cells themselves with proteases was found to markedly reduce their cytodherence capacity. Specifically, trypsinized cells, over time, could regain cytodherence capability after reincubation in fresh, trypsin-free medium, unless erythromycin was present to prevent protein synthesis (Hu *et al.*, 1977). Subsequent comparison of SDS-PAGE profiles of trypsinized versus non-

trypsinized cells revealed that cleavage of a single 170 kDa protein, designated protein P1, correlated with the observed reductions in cytodherence (Hu *et al.*, 1977). Shortly thereafter, immunolocalization studies demonstrated P1 to localize predominantly to the terminal organelle (Baseman *et al.*, 1982; Feldner *et al.*, 1982; Hu *et al.*, 1982). These studies likewise showed P1 to be a major antigen in natural human infections. Additionally, the work further supported the function of P1 as a major surface adhesin as the same monoclonal antibodies employed to assess its localization were likewise capable of inhibiting cytodherence. Definitive evidence to place P1 as a true cytoadhesin came a year later, when Krause *et al.* ruled out the possibility of steric and metabolic side-effects on the previous outcome by demonstrating that anti-P1 Fab fragments alone inhibited cytodherence but not metabolism (Krause and Baseman, 1983).

In parallel to these early characterizations of adhesin P1, ongoing studies were seeking to identify additional cytodherence-related proteins. While *M. pneumoniae* typically does not encounter host erythrocytes during the course of normal infections, a system was developed to exploit its capacity to bind red blood cells (hemadsorption, HA) as a convenient indicator of cytodherence capability. Using this approach, seven distinct classes of HA-negative mutants have been identified over the last three decades. Their analyses have revealed that in addition to P1, at least six other proteins function either directly for receptor binding or in other aspects of terminal organelle structure necessary for the proper incorporation and conformation of adhesin proteins. For reference, an overview of the protein profiles of each class of cytodherence mutants is presented below in table 1.3.

Proteins A, B, and C: Class IV HA mutants lack a total of four identifiable proteins: the major adhesin P1, the 72 kDa protein A, and 90 and 40 kDa proteins B and C, respectively

Table 1.3. Steady-state levels of terminal organelle proteins in *M. pneumoniae* cytdherence mutants

Mutant class	cytdherence-associated proteins						
	P1	B/C	P30	HMW1	HMW2	HMW3	P65
I-2	+++	+++	++	+	-	+	+
II-3	+++	+++	-	+++	+++	+++	++
II-7	+++	+++	++Δ	+++	+++	+++	++
III-4	+++	-	+++	+++	+++	+++	+++
IV-22	-	-	+++	+++	+++	+++	+++
M6	+++	+++	++Δ	-	+	+	+
<i>hmw3-</i>	+++	+++	+++	+++	+++	-	++

Modified from (Balish and Krause, 2002). +++ indicates wild-type levels, ++ indicates intermediate levels, + indicates low levels, - indicates none detected, Δ indicates a truncated P30.

(Krause *et al.*, 1982). Proteins A, B, and C are likewise absent in class III mutants, although P1 remains present at wild-type levels (Krause *et al.*, 1982). Thus, A, B and C were first hypothesized to contribute directly to cytodherence and virulence, possibly in a P1-independent manner. While the localization of protein A has not been determined, crosslinking studies have revealed proteins B and C to reside within a 12 Å proximity to P1, suggesting B and C may complex with P1 at the cell surface to perhaps facilitate its binding to host receptors (Layh-Schmitt and Herrmann, 1994). In further support of this possible association, proteins B and C were identified as cleavage products of MPN142, the gene immediately downstream of MPN141, which encodes P1 (Layh-Schmitt and Herrmann, 1992), with the B/C precursor being translationally-coupled to P1 (Waldo and Krause, 2006). Their loss in the class III mutant stems from a frameshift mutation near the N-terminus of MPN142 (Waldo *et al.*, 2005). Similarly, the mutation in class IV leading to the loss of P1, B, and C results from a frameshift in MPN141, encoding P1 (Krause *et al.*, 1982; Waldo and Krause, 2006). The molecular identity of protein A has not been determined. Significantly, complementation of class III but not class IV mutants with MPN142 restores cytodherence capacity. Likewise, reintroduction of B and C alone into class IV mutants is not sufficient to restore cytodherence (Waldo and Krause, 2006). Thus the data strongly suggest that P1, B, and C indeed function as a heterologous adhesin complex.

High molecular weight cytodherence-associated proteins: In addition to P1, B, and C, three high molecular weight (HMW) cytoskeletal proteins are required for cytodherence. HA mutants I-2, M6, and 201G lack proteins HMW1, HMW2, and HMW3, respectively, and are unable to cluster adhesin P1 into a discrete focus (Baseman *et al.*, 1982; Hahn *et al.*, 1998; Krause *et al.*, 1982; Willby and Krause, 2002). HMW1-HMW3 normally localize to the terminal organelle of wild-type cells, and, while specific components of the terminal

organelle core corresponding to these proteins have not been identified, their absence confers significant deleterious effects on core stability and structure, making these proteins likely candidates for having a direct role in core architecture (Krause and Balish, 2004).

HMW2 is a 216-kDa protein consisting of proline-rich regions at its N- and C-termini with the central 1600 amino acids of its entire 1818 residues predicted to consist almost entirely of coiled-coils. These coiled regions are interrupted briefly at many sites, raising the possibility that the HMW2 tertiary structure is conformationally flexible. The loss of HMW2 in mutant I-2 confers detrimental downstream effects on the stability of several additional terminal organelle proteins including proteins HMW1 and HMW3 (Popham *et al.*, 1997). For HMW1 and HMW2 this dependency is reciprocal. Thus, with the loss of HMW1 in mutant M6, HMW2 is subjected to rapid proteolytic turnover. Likewise with the absence of HMW2 in mutant I-2, HMW1 rapidly degrades after translation due to its inability to associate with the cytoskeleton (Balish *et al.*, 2001; Willby *et al.*, 2004). As neither mutant is capable of assembling terminal organelle cores, HMW1 and HMW2 are thought to cooperate early in the core assembly sequence.

Unlike the relationship between HMW1 and HMW2, loss of HMW3 in mutant 201G does not affect the stabilities of HMW1 and HMW2 (Willby and Krause, 2002). This observation suggests that HMW3 is incorporated into developing terminal organelles subsequent to HMW1 and HMW2 (Krause and Balish, 2004). Electron micrographs support this notion, as terminal organelle cores are indeed present in HMW3 mutant 201G. Interestingly, however, in the absence of HMW3, 201G cores are occasionally observed separated at their proximal end (Willby and Krause, 2002), suggesting that HMW3 may stabilize connections between the central rods, perhaps facilitating their association with the bowl-like complex at the base of the terminal organelle.

Complementation of mutants I-2 and M6 with various derivatives of HMW1 and HMW2 has identified specific regions of each protein required for their reciprocal dependencies and for HMW3 stability (refer to figure 1.3 below for a current model of protein interactions required for terminal organelle development). Delivery of full-length recombinant HMW2 into mutant I-2 restores the stability of HMW1 and HMW3, conferring proper core architecture, and results in the reacquisition of P1 at the terminal organelle (Balish *et al.*, 2003a). Interestingly, delivery of an altered HMW2 allele, lacking 80% of its central portion but expressing the N and C-termini together as a stable 38 kDa protein, is likewise capable of restoring HMW3 stability, but HMW1 remains unstable and P1 is unable to traffic to the terminal organelle (Balish *et al.*, 2003a). Complementation studies of mutant M6 further support an association between HMW1 and P1, and implicate the HMW1 C-terminus to be essential for P1 localization and HMW2-3 stability. Thus, while delivery of full-length HMW1 into mutant M6 allows for proper P1 clustering and stabilizes HMW2 and therefore HMW3, an altered HMW1 allele lacking the C-terminal 112 residues is unable to restore these phenotypes. And yet, an HMW1 allele truncated by only 41 amino acids is sufficient to restore HMW2, and HMW3 stability, but remains insufficient for P1 localization at the terminal organelle (Willby *et al.*, 2004). The data suggest that interactions between residues in the C-termini of HMW1 and HMW2 are essential for core formation. Provided these stabilizing associations, core assembly progresses and allows for the incorporation of HMW3. It also appears that P1, although not dependent on the HMW1/HMW2 pathway for its stability, requires the presence of the extreme C-terminus of HMW1 for proper incorporation into the terminal organelle membrane. However, as P1 also fails to consistently localize to the terminal organelle of mutant 201G (Willby and Krause, 2002), HMW3 may be required indirectly for P1 localization through its stabilizing effects on core architecture.

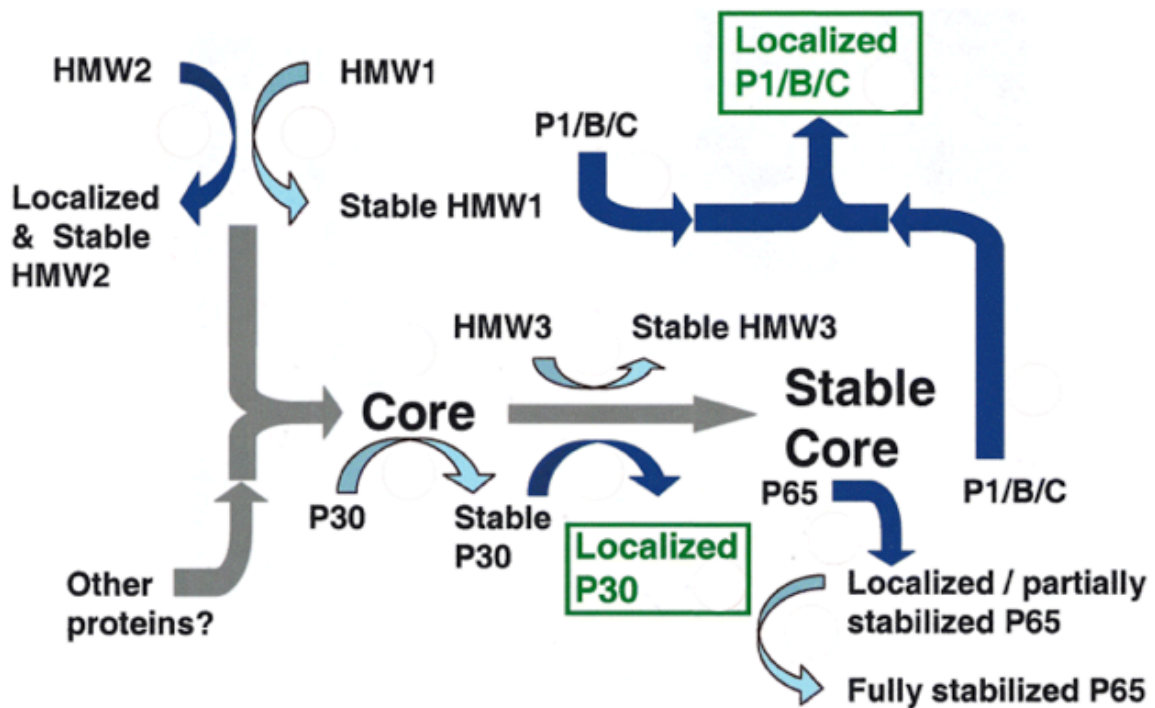


Figure 1.3. Schematic illustration of protein interactions required for cytodherence. Light blue arrows indicate steps involving the stabilization of a given component protein. Dark blue arrows reflect steps at which protein localization is affected. Grey arrows indicate steps at which no such distinction can be made. Modified from (Krause and Balish, 2004).

It stands to be mentioned here that the C-terminus of HMW2 is produced in wild-type *M. pneumoniae* cells as a second, stable protein in addition to the full-length copy of HMW2. Rather than deriving from the proteolytic cleavage of a portion of HMW2 monomers, this smaller, 28-kDa form (protein P28) arises from internal translation initiation near the C-terminus of the gene encoding HMW2, MPN310 (Fisseha *et al.*, 1999). P28 includes most of the proline rich sequences at the HMW2 C-terminus as well as several coiled-coil regions. These features may suggest a structural role for P28 in the bundling of HMW2 monomers and facilitating interactions between HMW2 and other members of the cytoskeleton. And yet, a definitive function has not been determined for P28. Mutant C1R1 contains an in-frame deletion of a small portion of HMW2 encompassing the internal translation initiation codon required for its expression. Yet, C1R1 is HA positive, produces terminal organelle cores, expresses HMW1 and HMW3 at wild-type levels, and is likewise capable of localizing P1 properly at the terminal organelle (Balish *et al.*, 2003a). The effects that loss of P28 may confer on other aspects of *M. pneumoniae* cell biology including cell division or gliding motility have not been assessed.

Proteins P65 and P30: Like proteins HMW1, HMW2, and HMW3, proteins P65 and P30 localize to the terminal organelle of wild-type cells (Baseman *et al.*, 1987). Transcribed with HMW2 or HMW3, respectively, steady state levels of P65 and P30 are markedly reduced in mutants I-2 and M6, but also in mutant 201G (Krause and Balish, 2004), indicating they require HMW3 for stability and are incorporated relatively late in the terminal organelle assembly sequence. Characterizations of two distinct classes of P30 mutants suggest that P30 is directly involved in receptor binding and that *M. pneumoniae* cytoadherence requires the combined contribution of both P30 and P1 at the terminal organelle surface. Thus, mutants II-3 and II-7, which produce no P30 due to a frameshift mutation, or a truncated

copy of the protein due to an internal in-frame deletion of 144 bp near the C-terminus, respectively (Dallo *et al.*, 1996; Romero-Arroyo *et al.*, 1999), are HA negative and avirulent, although P1 stability and localization are not affected, nor are there any obvious abnormalities in core architecture. Antibodies targeting the C-terminus of P30 inhibit HA by wild-type *M. pneumoniae* (Baseman *et al.*, 1987). Moreover, the reduced HA capacity of mutant II-3 is restored to wild-type levels by the delivery of a wild-type P30 allele (Romero-Arroyo *et al.*, 1999); the possibilities of secondary mutations in mutant II-7 have not been assessed. While the identity of specific host receptors bound by P30 has not been determined, for mutant II-3, unlike wild-type, pretreatment of respiratory epithelium with neuraminidase does not reduce cytoadherence capacity (Krause *et al.*, 1982) (although the binding capacity of mutant II-3 to untreated respiratory tissue is significantly below wild-type levels), a finding which suggests that P30 binds receptors other than sialic acid.

The function of P65 is unknown due to a lack of appropriate mutants. However, as P65 levels are reduced in P30⁻ mutant II-3 (Jordan *et al.*, 2001), which expresses the HMW proteins at wild-type levels, current data suggest that P65 incorporation into the terminal organelle is dependent upon the prior localization of P30, the latter occurring after HMW3 incorporation (Fig. 1.3). The dependency scheme, along with structural and biochemical features of each, suggest that P65 and P30 may function cooperatively. P65 is peripherally associated with the terminal organelle membrane and is an exclusive component of the Triton X- insoluble cytoskeleton (Proft *et al.*, 1995). In contrast, P30 is only weakly associated with the cytoskeleton and is an integral membrane protein possessing only one predicted membrane-spanning segment, with the majority of the protein surface-exposed (Layh-Schmitt *et al.*, 1997). It is tempting to speculate that, subsequent to P30 incorporation into the membrane, P65 associates with P30 and assumes a scaffolding function in

connecting P30 to the *M. pneumoniae* cytoskeleton. Isolation of mutants lacking P65 will be required to substantiate this hypothesis.

Additional and suspected cytodherence-associated proteins: In addition to the eight aforementioned cytodherence-associated proteins, three additional proteins, P200, P41, and P24, are known to localize to the terminal organelle of wild-type cells. For protein P200, a mutant exists and has recently been characterized (Jordan *et al.*, 2006). Interestingly, this large cytoskeletal element is dispensable for HA but partially required for binding to normal human bronchial epithelium. As P200 appears surface-exposed due to its sensitivity to protease V8 treatment of whole cells (unpublished data), it is feasible that P200 may facilitate the binding of receptor molecules absent from the surface of red blood cells but expressed on normal respiratory tissue. However, the P200 mutant also exhibits reduced gliding motility, which may account for its limited capacity to colonize ciliated, mucosal epithelium (see below).

While *M. pneumoniae* mutants lacking P41 or P24 have not been identified, their genomic and cellular location suggests that they may also function in cytodherence. P41 and P24 are the third and fourth genes of the four gene operon that encodes P65 and HMW2 (Krause *et al.*, 1997). Relative to P30 and P65, which occupy the extreme distal portion of the terminal organelle, P41 and P24 localize to the base of the terminal organelle (Kenri *et al.*, 2004), presumably near the bowl-like complex. While P24 is not a component of the Triton X-100 insoluble fraction, P41 is a cytoskeletal protein with predicted coiled-coiled domains (Kenri *et al.*, 2004; Krause *et al.*, 1997), suggesting it may confer a possible structural role in terminal organelle architecture.

Gliding Motility: In addition to its well-documented function in cytodherence, the *M. pneumoniae* terminal organelle is implicated to function in gliding motility. Hence, individual cells glide over solid surfaces intermittently at velocities averaging 0.3 $\mu\text{m}/\text{sec}$ (Radestock and Bredt, 1977) with the cell pole harboring the terminal organelle always engaged as the leading end (Kenri *et al.*, 2004).

Although the least characterized form of eubacterial motility, gliding is exhibited by bacteria from many branches of the phylogenetic tree (McBride, 2001). It is particularly common and has been extensively studied in the Myxobacteria, Cyanobacteria, and the *Cytophaga-Flavobacterium* group. For the *Mollicutes*, gliding motility was first described sixty years ago for low-passage strains of *M. pulmonis* (Andrewes, 1946). And yet, of the over 200 known species, gliding motility has subsequently been described for only six: *M. pneumoniae*, *M. genitalium*, *M. pulmonis*, *M. gallisepticum*, *M. amphoriforme* and *M. mobile* (Andrewes, 1946; Bredt, 1968; Hatchel *et al.*, 2006; Kirchhoff, 1992). Each possesses a differentiated terminal structure, implicating these appendages to harbor the molecular gliding machinery (Kirchhoff *et al.*, 1984). For each of the gliding mycoplasmas, motility is temperature dependent with the highest velocities and shortest resting periods occurring at each species' optimum growth temperature (Bredt, 1979; Hatchel *et al.*, 2006; Kirchhoff, 1992).

Gliding capabilities of the current bank of *M. pneumoniae* cytodherence mutants have not been assessed. In fact, *M. mobile* is the sole mycoplasma species for which the mechanism of gliding has been investigated. UV irradiation of wild-type populations and subsequent screening for strains exhibiting atypical satellite growth (active gliding of individual cells from the periphery of microcolonies) has allowed the isolation of several *M. mobile* mutants with combined gliding, HA, and glass-binding deficiencies (Miyata *et al.*, 2000). The defects of each mutant map to distinct point mutations in a single *gli* operon

encoding four proteins of 123, 349, 521, and 42 kDa which cooperatively assemble into a motor complex within the *M. mobile* membrane at the base of its polar structure (Seto *et al.*, 2005b; Uenoyama *et al.*, 2004; Uenoyama and Miyata, 2005b). The current model of *M. mobile* gliding suggests that Gli123 functions early in the assembly of the membrane motor complex, associating with internal cytoskeletal elements and serving as a binding partner for the large, integral membrane protein Gli521, which in turn anchors a “leg”-like protein, Gli349, to the cell surface (Adan-Kubo *et al.*, 2006; Seto *et al.*, 2005b; Uenoyama *et al.*, 2004; Uenoyama and Miyata, 2005b). Although a role for the 42-kDa protein has not presented in the literature, it is speculated to act as an ATPase, transferring bond energy through Gli521 which in turn causes a conformational “twitch” in the Gli349 leg (M. Miyata, personal communication). The combined cytodherence gliding, and glass-binding defects of the *gli* mutants reflect the role of Gli349 as the major *M. mobile* cytodhesin, which binds sialoglycoconjugates similar to *M. pneumoniae* (Nagai and Miyata, 2006).

It remains uncertain whether any parallels can be drawn between the mechanism of *M. mobile* gliding and the means by which *M. pneumoniae* achieves this process. Other than the P200 mutant described above, no spontaneously-arising or transposon-induced *M. pneumoniae* strains with gliding defects have been isolated. Furthermore, inspection of the 816-kbp *M. pneumoniae* genome reveals no orthologs of proteins that function in bacterial motility of any type in walled species. Likewise, the known components of the *M. mobile* gliding machinery are not present in *M. pneumoniae*. Thus, even if homologous recombination were possible in *M. pneumoniae*, a lack of identifiable gene targets would hinder the construction of gliding mutants. Besides P200, adhesin P1 is the sole *M. pneumoniae* protein for which a role in gliding has been implicated. Hence, the addition of P1-specific antibodies to cultures of wild-type *M. pneumoniae* inhibits gliding motility (Feldner *et al.*, 1982; Seto *et al.*, 2005a), although cells treated as such have also been

reported to lose their capacity to bind inert surfaces, an absolute prerequisite for this form of motility (Seto *et al.*, 2005a).

While the energetics of *M. pneumoniae* gliding have not been investigated, gliding of *M. mobile* is thought to be powered solely by ATP (Jaffe *et al.*, 2004; Uenoyama and Miyata, 2005a). Remarkably, even after Triton X -100 treatment of wild-type *M. mobile* cells, the remaining cytoskeleton is capable of reanimation and gliding at velocities of viable cells when ATP is reintroduced (Uenoyama and Miyata, 2005a). While the data seem to contradict the role of the *M. mobile* membrane gliding motor complex, they nevertheless disclose a remarkable direct contribution of the *M. mobile* cytoskeleton in cell gliding. Because of major differences in cytoskeletal structure between *M. mobile* and *M. pneumoniae*, i.e. *M. mobile* does not produce any identifiable core complex within its terminal structure, it is difficult to extrapolate the *M. mobile* data to derive a similar model as to the contribution of the *M. pneumoniae* cytoskeleton in cell gliding. However, in light of the recent electron cryotomography data demonstrating that the *M. pneumoniae* terminal organelle core is conformationally flexible (Henderson and Jensen, 2006), it is conceivable that alternating contractions and extensions of the core may drive *M. pneumoniae* gliding by an inchworm-like process, provided that surface adhesins are physically connected to the core as proposed by Henderson and Jensen (Henderson and Jensen, 2006).

Due to an absence of *M. pneumoniae* mutants with gliding deficiencies but retaining wild-type cytoadherence, the role of gliding motility in *M. pneumoniae* pathogenesis remains undetermined. And yet, it is tempting to speculate that gliding motility may play a decisive role in *M. pneumoniae* virulence. Hence, after inhalation, *M. pneumoniae* must immediately overcome innate host defenses represented most notably by the formidable mucocilliary escalator. Overlying the pericilliary fluid, this highly viscous mucosal blanket is synthesized by isolated pockets of mucous glands and mucin-secreting goblet cells interspersed

between ciliated epithelial cells (Widdicombe *et al.*, 1997). Beating in unison over 20 times per second, the cilia extend into the mucus layer propelling its contents upwards at rates of approximately 70 - 400 $\mu\text{m}/\text{sec}$ (Samet and Cheng, 1994; Widdicombe *et al.*, 1997). These *in vivo* conditions can be reproduced *in vitro* with a normal human bronchial epithelial (NHBE) cell model system which has recently been used successfully to investigate the early interactions between *M. pneumoniae* cells and human respiratory epithelium (Jordan *et al.*, 2006). The data reveal that wild-type *M. pneumoniae* colonizes the NHBE surface in a time-dependent manner, initially localizing predominantly to the tips of ciliary shafts and later to the base of the cilia at the epithelial surface. As *M. pneumoniae* cells are not observed at early time-points on the surface of non-ciliated cells, the data suggest that gliding motility is employed early in host colonization whereby cells quickly contact and glide down the ciliary shaft to escape the mucociliary escalator. Furthermore, these recent studies reveal that, while initially colonizing only ciliated cells, over the ensuing six hours individual mycoplasmas appeared to spread laterally over the adjacent surfaces of both ciliated and non-ciliated cells. Thus, gliding motility may be employed subsequent to initial colonization allowing cells to disperse to areas of lower cell density to avoid competition with neighboring cells for nutrients or host receptors.

Cell division: In a significant 2001 study, Seto *et al.* demonstrated that the polar assembly of nascent terminal organelles coincides temporally with the initiation of chromosome replication (Seto *et al.*, 2001). Log-phase cultures of wild-type *M. pneumoniae* were fixed and labeled with DAPI to highlight the nucleoid and also with anti-P1 antibodies to enumerate and localize terminal organelles via immunofluorescence. By quantifying nucleoid intensities relative to the number and location of terminal organelles in fixed cells, Seto *et al.* showed that as DAPI intensity increases from 1 to 1.5 chromosome equivalents,

two discrete P1 foci become evident adjacent to each other at the cell pole. Cells progressing through chromosome replication with 1.5-2 chromosome equivalents typically exhibit separation of the P1 foci, with one remaining polar and the second assuming a lateral position. Upon the completion of chromosome replication, P1 foci occupy opposite poles of the *M. pneumoniae* cell. Additionally, the nucleoids themselves become distinctly separated, occupying opposite regions of the lengthened cell body and appearing to abut each P1 focus. The data suggest not only that terminal organelle duplication coincides temporally with the initiation of chromosome replication, but also that the migration of one terminal organelle to the opposite cell pole proceeds concurrently with the progression of chromosome replication, and that terminal organelle migration may facilitate chromosome segregation.

As the techniques employed by Seto *et al.* required cell fixation, the data were unable to address cell gliding behaviors during these progressions. In fact, descriptions of *M. pneumoniae* cell division in viable cultures are limited to just a few studies conducted almost 40 years ago (Bredt, 1968; Furness *et al.*, 1968). While these early studies were unable to definitively discern terminal organelle location, they suggest that gliding motility may be intricately associated with cell division. Hence, in Bredt's characterizations of *M. pneumoniae* gliding in the 1960's (Bredt, 1968), he observed that while individual cells commonly engage in transient resting periods during their motility tracks, such gliding cessation occasionally coincided with the appearance of a second polar knob-like protrusion adjacent to the first, which had been the leading end during motility. Over an average of three hours, one of the protrusions became displaced to the opposite cell pole. Cytokinesis was observed to follow with the resumption of motility by both daughter cells.

While Seto and Bredt's data seem to correlate, with the latter study additionally suggesting that regulation of *M. pneumoniae* gliding is as intricate component of cell

division, the mechanism of terminal organelle duplication remains enigmatic. The current hypothesis derives from the original architectural data suggesting the core to be composed of two parallel rods of identical structure and suggests that terminal organelle duplication occurs in a semi-conservative manner. Thus, separation of the core rods allows for each to serve as a template for the assembly of its pair (Boatman, 1979). Provided the core is a functional component of the *M. pneumoniae* gliding motor, such a mechanism could account for Bredt's observations that gliding motility ceases during what appeared to be the formation and an adjacent, polar terminal organelle. However, in light of recent electron tomographic imaging, the current hypothesis may need to be refined, as the distinct composition of each core rod would intrinsically complicate a semi-conservative mechanism of core duplication (Henderson and Jensen, 2006).

Definitive evidence to define the mechanism of terminal organelle duplication and the function of gliding motility in cell division, will require, at the least, the ability to track the incorporation of individual proteins into developing terminal organelles of viable, gliding-competent *M. pneumoniae* cells. GFP-based reporter systems seem to be the most promising tools for such investigations. Already, fluorescent protein fusions have been utilized to verify the terminal organelle localization of numerous proteins including HMW2, P41, P24, and P65 (Balish *et al.*, 2003b; Kenri *et al.*, 2004). While time-lapse analyses of the incorporation of such fusion proteins into developing organelles have not been described, the use of combined phase-contrast and fluorescence time-lapse imaging seems feasible not only to document the appearance and development of nascent terminal organelles but also to analyze cell gliding behaviors during the assembly process. Perhaps time-lapse visualization of terminal organelle assembly via the use of such viable reporter systems will likewise elucidate more clearly the mechanism and kinetics of terminal organelle development.

References

- Adan-Kubo, J., Uenoyama, A., Arata, T., and Miyata, M. (2006) Morphology of isolated Gli349, a leg protein responsible for *Mycoplasma mobile* gliding via glass binding, revealed by rotary shadowing electron microscopy. *J Bacteriol* **188**: 2821-2828.
- Alexander, E.R., Foy, H.M., Kenny, G.E., Kronmal, R.A., McMahan, R., Clarke, E.R., MacColl, W.A., and Grayston, J.T. (1966) Pneumonia due to *Mycoplasma pneumoniae*. Its incidence in the membership of a co-operative medical group. *N Engl J Med* **275**: 131-136.
- Allen, P.Z., and Prescott, B. (1978) Immunochemical studies on a *Mycoplasma pneumoniae* polysaccharide fraction: cross-reactions with type 23 and 32 antipneumococcal rabbit sera. *Infect Immun* **20**: 421-429.
- Almagor, M., Kahane, I., and Yatziv, S. (1984) Role of superoxide anion in host cell injury induced by *Mycoplasma pneumoniae* infection. A study in normal and trisomy 21 cells. *J Clin Invest* **73**: 842-847.
- Alonso-Vega, C., Wauters, N., Vermeylen, D., Muller, M.F., and Serruys, E. (1997) A fatal case of *Mycoplasma hominis* meningoencephalitis in a full-term newborn. *J Clin Microbiol* **35**: 286-287.
- Andrewes, C.H. (1946) A motile organism of the pleuropneumoniae group. *Journal of Pathological Bacteriology* **58**: 578-580.
- Arai, S., Munakata, T., and Kuwano, K. (1983) Mycoplasma interaction with lymphocytes and phagocytes: role of hydrogen peroxide released from *M. pneumoniae*. *Yale J Biol Med* **56**: 631-638.

- Balish, M.F., Hahn, T.W., Popham, P.L., and Krause, D.C. (2001) Stability of *Mycoplasma pneumoniae* cytoadherence-accessory protein HMW1 correlates with its association with the triton shell. *J Bacteriol* **183**: 3680-3688.
- Balish, M.F., and Krause, D.C. (2002) Cytoadherence and the Cytoskeleton. In *Molecular Biology and Pathogenicity of Mycoplasmas*. Razin, S. and Herrmann, R. (eds). New York: Kluwer Academic/Plenum Publishers, pp. 491-518.
- Balish, M.F., Ross, S.M., Fisseha, M., and Krause, D.C. (2003a) Deletion analysis identifies key functional domains of the cytoadherence-associated protein HMW2 of *Mycoplasma pneumoniae*. *Mol Microbiol* **50**: 1507-1516.
- Balish, M.F., Santurri, R.T., Ricci, A.M., Lee, K.K., and Krause, D.C. (2003b) Localization of *Mycoplasma pneumoniae* cytoadherence-associated protein HMW2 by fusion with green fluorescent protein: implications for attachment organelle structure. *Mol Microbiol* **47**: 49-60.
- Baseman, J.B., Cole, R.M., Krause, D.C., and Leith, D.K. (1982) Molecular basis for cytoadsorption of *Mycoplasma pneumoniae*. *J Bacteriol* **151**: 1514-1522.
- Baseman, J.B., Morrison-Plummer, J., Drouillard, D., Puleo-Schepke, B., Tryon, V.V., and Holt, S.C. (1987) Identification of a 32-kilodalton protein of *Mycoplasma pneumoniae* associated with hemadsorption. *Isr J Med Sci* **23**: 474-479.
- Bendjennat, M., Blanchard, A., Loutfi, M., Montagnier, L., and Bahraoui, E. (1997) Purification and characterization of *Mycoplasma penetrans* Ca²⁺/Mg²⁺-dependent endonuclease. *J Bacteriol* **179**: 2210-2220.
- Biberfeld, G. (1968) Distribution of antibodies within 19 S and 7 S immunoglobulins following infection with *Mycoplasma pneumoniae*. *J Immunol* **100**: 338-347.
- Biberfeld, G., and Biberfeld, P. (1970) Ultrastructural features of *Mycoplasma pneumoniae*. *J Bacteriol* **102**: 855-861.

- Biberfeld, G. (1971) Antibodies to brain and other tissues in cases of *Mycoplasma pneumoniae* infection. *Clin Exp Immunol* **8**: 319-333.
- Bjornelius, E., Lidbrink, P., and Jensen, J.S. (2000) *Mycoplasma genitalium* in non-gonococcal urethritis--a study in Swedish male STD patients. *Int J STD AIDS* **11**: 292-296.
- Blanchard, A. (2002) Mycoplasmas of Humans. In *Molecular Biology and Pathogenicity of Mycoplasmas*. Razin, S. and Herrmann, R. (eds). New York: Kluwer Academic/Plenum, pp. 45-71.
- Block, S., Hedrick, J., Hammerschlag, M.R., Cassell, G.H., and Craft, J.C. (1995) *Mycoplasma pneumoniae* and *Chlamydia pneumoniae* in pediatric community-acquired pneumonia: comparative efficacy and safety of clarithromycin vs. erythromycin ethylsuccinate. *Pediatr Infect Dis J* **14**: 471-477.
- Boatman, E.S. (1979) Morphology and Ultrastructure of the *Mycoplasmatales*. In *The Mycoplasmas: Cell Biology*. Vol. 1. Barile, M.F. and Razin, S. (eds): Academic Press, pp. 63-102.
- Bordet, J. (1910) La morphologie du microbe de la peripneumonie des bovines. *Ann. Inst. Pasteur* **24**: 168-179.
- Bredt, W. (1968) Motility and multiplication of *Mycoplasma pneumoniae*. A phase contrast study. *Pathol Microbiol (Basel)* **32**: 321-326.
- Bredt, W. (1979) Motility. In *The Mycoplasmas*. Vol. 1: Academic Press.
- Bridre, J., and Donetien, A. (1923) Le microbe de l'agalaxie contagieuse et sa culture in vitro. *Compt. Rend.* **177**: 841-843.
- Byrne, M.E., Rouch, D.A., and Skurray, R.A. (1989) Nucleotide sequence analysis of IS256 from the *Staphylococcus aureus* gentamicin-tobramycin-kanamycin-resistance transposon Tn4001. *Gene* **81**: 361-367.

- Cassell, G.H., Drnec, J., Waites, K.B., Pate, M.S., Duffy, L.B., Watson, H.L., and McIntosh, J.C. (1991) Efficacy of clarithromycin against *Mycoplasma pneumoniae*. *J Antimicrob Chemother* **27 Suppl A**: 47-59.
- CDC (2002) *Mycoplasma pneumoniae* disease information. Centers for Disease Control and Prevention.
- Chanock, R.M., Hayflick, L., and Barile, M.F. (1962) Growth on artificial medium of an agent associated with atypical pneumonia and its identification as a PPLO. *Proc Natl Acad Sci U S A* **48**: 41-49.
- Chanock, R.M., Mufson, M.A., Somerson, N.L., and Couch, R.B. (1963) Role of Mycoplasma (Pplo) in Human Respiratory Disease. *Am Rev Respir Dis* **88**: SUPPL 218-239.
- Chryssanthopoulos, C., Eboriadou, M., Monti, K., Soubassi, V., and Sava, K. (2001) Fatal disseminated intravascular coagulation caused by *Mycoplasma pneumoniae*. *Pediatr Infect Dis J* **20**: 634-635.
- Clyde, W.A., Jr., and Denny, F.W. (1967) Mycoplasma infections in childhood. *Pediatrics* **40**: 669-684.
- Clyde, W.A., Jr. (1971) *Mycoplasma pneumoniae* pneumonia. *Mil Med* **136**: 20-22.
- Cohen, G., and Somerson, N.L. (1967) *Mycoplasma pneumoniae*: hydrogen peroxide secretion and its possible role in virulence. *Ann N Y Acad Sci* **143**: 85-87.
- Cole, B.C., Ward, J.R., and Martin, C.H. (1968) Hemolysin and peroxide activity of *Mycoplasma* species. *J Bacteriol* **95**: 2022-2030.
- Collier, A.M., and Clyde, W.A., Jr. (1974) Appearance of *Mycoplasma pneumoniae* in lungs of experimentally infected hamsters and sputum from patients with natural disease. *Am Rev Respir Dis* **110**: 765-773.
- Dallo, S.F., Lazzell, A.L., Chavoya, A., Reddy, S.P., and Baseman, J.B. (1996) Biofunctional domains of the *Mycoplasma pneumoniae* P30 adhesin. *Infect Immun* **64**: 2595-2601.

- Dallo, S.F., and Baseman, J.B. (2000) Intracellular DNA replication and long-term survival of pathogenic mycoplasmas. *Microb Pathog* **29**: 301-309.
- Dandekar, T., Huynen, M., Regula, J.T., Ueberle, B., Zimmermann, C.U., Andrade, M.A., Doerks, T., Sanchez-Pulido, L., Snel, B., Suyama, M., Yuan, Y.P., Herrmann, R., and Bork, P. (2000) Re-annotating the *Mycoplasma pneumoniae* genome sequence: adding value, function and reading frames. *Nucleic Acids Res* **28**: 3278-3288.
- Dienes, L., and Edsall, G. (1937) Observations on the L-organism of Klieneberger. *Proc. Soc. Exptl. Biol. Med.* **36**: 740-744.
- Dorigo-Zetsma, J.W., Wilbrink, B., van der Nat, H., Bartelds, A.I., Heijnen, M.L., and Dankert, J. (2001) Results of molecular detection of *Mycoplasma pneumoniae* among patients with acute respiratory infection and in their household contacts reveals children as human reservoirs. *J Infect Dis* **183**: 675-678.
- Eaton, M.D., G., M., W., v.H., and M., C. (1945) Studies on the etiology of primary atypical pneumonia. II. Properties of the virus isolated and propagated in chick embryos. *J Exp Med* **82**: 317-328.
- Elford, W.J. (1929) Ultra-filtration methods and their application in bacteriological and pathological studies. *Brit. J. Exptl. Path.* **10**: 126-144.
- Feldner, J., Gobel, U., and Bredt, W. (1982) *Mycoplasma pneumoniae* adhesin localized to tip structure by monoclonal antibody. *Nature* **298**: 765-767.
- Ferwerda, A., Moll, H.A., and de Groot, R. (2001) Respiratory tract infections by *Mycoplasma pneumoniae* in children: a review of diagnostic and therapeutic measures. *Eur J Pediatr* **160**: 483-491.
- Findlay, G.M., Klieneberger, E., MacCallum, F.O., and Mackenzie, R.D. (1938) Rolling Disease. New syndrome in mice associated with a pleuropneumonia-like organism. *Lancet* **235**: 1511-1513.

- Fisseha, M., Gohlmann, H.W., Herrmann, R., and Krause, D.C. (1999) Identification and complementation of frameshift mutations associated with loss of cytoadherence in *Mycoplasma pneumoniae*. *J Bacteriol* **181**: 4404-4410.
- Foy, H.M. (1993) Infections caused by *Mycoplasma pneumoniae* and possible carrier state in different populations of patients. *Clin Infect Dis* **17 Suppl 1**: S37-46.
- Frey, J. (2002) Mycoplasmas of Animals. In *Molecular Biology and Pathogenicity of Mycoplasmas*. Razin, S. and Herrmann, R. (eds). New York: Kluwer Academic/Plenum, pp. 73-90.
- Furness, G., Pipes, F.J., and McMurtrey, M.J. (1968) Analysis of the life cycle of *Mycoplasma pneumoniae* by synchronized division and by ultraviolet and x irradiations. *J Infect Dis* **118**: 7-13.
- Gambini, D., Decleva, I., Lupica, L., Ghislanzoni, M., Cusini, M., and Alessi, E. (2000) *Mycoplasma genitalium* in males with nongonococcal urethritis: prevalence and clinical efficacy of eradication. *Sex Transm Dis* **27**: 226-229.
- Gobel, U., Speth, V., and Bredt, W. (1981) Filamentous structures in adherent *Mycoplasma pneumoniae* cells treated with nonionic detergents. *J Cell Biol* **91**: 537-543.
- Hahn, T.W., Willby, M.J., and Krause, D.C. (1998) HMW1 is required for cytoadhesin P1 trafficking to the attachment organelle in *Mycoplasma pneumoniae*. *J Bacteriol* **180**: 1270-1276.
- Harris, J.A., Kolokathis, A., Campbell, M., Cassell, G.H., and Hammerschlag, M.R. (1998) Safety and efficacy of azithromycin in the treatment of community-acquired pneumonia in children. *Pediatr Infect Dis J* **17**: 865-871.
- Hatchel, J.M., Balish, R.S., Duley, M.L., and Balish, M.F. (2006) Ultrastructure and gliding motility of *Mycoplasma amphoriforme*, a possible human respiratory pathogen. *Microbiology* **152**: 2181-2189.

- Hedreyda, C.T., Lee, K.K., and Krause, D.C. (1993) Transformation of *Mycoplasma pneumoniae* with Tn4001 by electroporation. *Plasmid* **30**: 170-175.
- Hegermann, J., Herrmann, R., and Mayer, F. (2002) Cytoskeletal elements in the bacterium *Mycoplasma pneumoniae*. *Naturwissenschaften* **89**: 453-458.
- Heiskanen-Kosma, T., Korppi, M., Jokinen, C., Kurki, S., Heiskanen, L., Juvonen, H., Kallinen, S., Sten, M., Tarkiainen, A., Ronnberg, P.R., Kleemola, M., Makela, P.H., and Leinonen, M. (1998) Etiology of childhood pneumonia: serologic results of a prospective, population-based study. *Pediatr Infect Dis J* **17**: 986-991.
- Henderson, G.P., and Jensen, G.J. (2006) Three-dimensional structure of *Mycoplasma pneumoniae's* attachment organelle and a model for its role in gliding motility. *Mol Microbiol* **60**: 376-385.
- Himmelreich, R., Hilbert, H., Plagens, H., Pirkl, E., Li, B.C., and Herrmann, R. (1996) Complete sequence analysis of the genome of the bacterium *Mycoplasma pneumoniae*. *Nucleic Acids Res* **24**: 4420-4449.
- Horner, P., Thomas, B., Gilroy, C.B., Egger, M., and Taylor-Robinson, D. (2001) Role of *Mycoplasma genitalium* and *Ureaplasma urealyticum* in acute and chronic nongonococcal urethritis. *Clin Infect Dis* **32**: 995-1003.
- Hu, P.C., Collier, A.M., and Baseman, J.B. (1977) Surface parasitism by *Mycoplasma pneumoniae* of respiratory epithelium. *J Exp Med* **145**: 1328-1343.
- Hu, P.C., Cole, R.M., Huang, Y.S., Graham, J.A., Gardner, D.E., Collier, A.M., and Clyde, W.A., Jr. (1982) *Mycoplasma pneumoniae* infection: role of a surface protein in the attachment organelle. *Science* **216**: 313-315.
- Hu, P.C., Huang, C.H., Collier, A.M., and Clyde, W.A., Jr. (1983) Demonstration of antibodies to *Mycoplasma pneumoniae* attachment protein in human sera and respiratory secretions. *Infect Immun* **41**: 437-439.

- Hutchison, C.A., Peterson, S.N., Gill, S.R., Cline, R.T., White, O., Fraser, C.M., Smith, H.O., and Venter, J.C. (1999) Global transposon mutagenesis and a minimal *Mycoplasma* genome. *Science* **286**: 2165-2169.
- Ieven, M., Demey, H., Ursi, D., Van Goethem, G., Cras, P., and Goossens, H. (1998) Fatal encephalitis caused by *Mycoplasma pneumoniae* diagnosed by the polymerase chain reaction. *Clin Infect Dis* **27**: 1552-1553.
- Jaffe, J.D., Miyata, M., and Berg, H.C. (2004) Energetics of gliding motility in *Mycoplasma mobile*. *J Bacteriol* **186**: 4254-4261.
- Janney, F.A., Lee, L.T., and Howe, C. (1978) Cold hemagglutinin cross-reactivity with *Mycoplasma pneumoniae*. *Infect Immun* **22**: 29-33.
- Johansson, K.E., and Pettersson, B. (2002) Taxonomy of Mollicutes. In *Molecular Biology and Pathogenicity of Mycoplasmas*. Razin, S. and Herrmann, R. (eds). New York: Kluwer Academic/Plenum, pp. 1-29.
- Joosting, A.C., Harwin, R.M., Coppin, A., Battaglia, P., and van der Hoef, P. (1976) A serological investigation of *Mycoplasma pneumoniae* infection on the Witwatersrand. *S Afr Med J* **50**: 2134-2135.
- Jordan, J.L., Berry, K.M., Balish, M.F., and Krause, D.C. (2001) Stability and subcellular localization of cytoadherence-associated protein P65 in *Mycoplasma pneumoniae*. *J Bacteriol* **183**: 7387-7391.
- Jordan, J.L., Chang, H.Y., Balish, M.F., Holt, L.S., Bose, S.R., Hasselbring, B.M., Waldo, R.H., 3rd, Krunkosky, T.M., and Krause, D.C. (2006) Protein P200 is Dispensable for *Mycoplasma pneumoniae* Hemadsorption but not Gliding Motility or Colonization of Differentiated Bronchial Epithelium. *Infect Immun*.
- Keane, F.E., Thomas, B.J., Gilroy, C.B., Renton, A., and Taylor-Robinson, D. (2000) The association of *Mycoplasma hominis*, *Ureaplasma urealyticum* and *Mycoplasma*

- genitalium* with bacterial vaginosis: observations on heterosexual women and their male partners. *Int J STD AIDS* **11**: 356-360.
- Kenri, T., Seto, S., Horino, A., Sasaki, Y., Sasaki, T., and Miyata, M. (2004) Use of fluorescent-protein tagging to determine the subcellular localization of *Mycoplasma pneumoniae* proteins encoded by the cytoadherence regulatory locus. *J Bacteriol* **186**: 6944-6955.
- Kirchhoff, H., Rosengarten, R., Lotz, W., Fischer, M., and Lopatta, D. (1984) Flask-shaped mycoplasmas: properties and pathogenicity for man and animals. *Isr J Med Sci* **20**: 848-853.
- Kirchhoff, H. (1992) Motility. In *Mycoplasmas- Molecular Biology and Pathogenesis*. J. Maniloff, R.N.M., L. R. Finch & J. B. Baseman. (ed). Washington, D.C.: American Society for Microbiology, pp. 289-306.
- Kita, M., Ohmoto, Y., Hirai, Y., Yamaguchi, N., and Imanishi, J. (1992) Induction of cytokines in human peripheral blood mononuclear cells by mycoplasmas. *Microbiol Immunol* **36**: 507-516.
- Krause, D.C., Leith, D.K., Wilson, R.M., and Baseman, J.B. (1982) Identification of *Mycoplasma pneumoniae* proteins associated with hemadsorption and virulence. *Infect Immun* **35**: 809-817.
- Krause, D.C., and Baseman, J.B. (1983) Inhibition of *Mycoplasma pneumoniae* hemadsorption and adherence to respiratory epithelium by antibodies to a membrane protein. *Infect Immun* **39**: 1180-1186.
- Krause, D.C., Proft, T., Hedreyda, C.T., Hilbert, H., Plagens, H., and Herrmann, R. (1997) Transposon mutagenesis reinforces the correlation between *Mycoplasma pneumoniae* cytoskeletal protein HMW2 and cytoadherence. *J Bacteriol* **179**: 2668-2677.

- Krause, D.C., and Balish, M.F. (2004) Cellular engineering in a minimal microbe: structure and assembly of the terminal organelle of *Mycoplasma pneumoniae*. *Mol Microbiol* **51**: 917-924.
- Kusumoto, A., Seto, S., Jaffe, J.D., and Miyata, M. (2004) Cell surface differentiation of *Mycoplasma mobile* visualized by surface protein localization. *Microbiology* **150**: 4001-4008.
- Layh-Schmitt, G., and Herrmann, R. (1992) Localization and biochemical characterization of the ORF6 gene product of the *Mycoplasma pneumoniae* P1 operon. *Infect Immun* **60**: 2906-2913.
- Layh-Schmitt, G., and Herrmann, R. (1994) Spatial arrangement of gene products of the P1 operon in the membrane of *Mycoplasma pneumoniae*. *Infect Immun* **62**: 974-979.
- Layh-Schmitt, G., Himmelreich, R., and Leibfried, U. (1997) The adhesin related 30-kDa protein of *Mycoplasma pneumoniae* exhibits size and antigen variability. *FEMS Microbiol Lett* **152**: 101-108.
- Leith, D.K., Trevino, L.B., Tully, J.G., Senterfit, L.B., and Baseman, J.B. (1983) Host discrimination of *Mycoplasma pneumoniae* proteinaceous immunogens. *J Exp Med* **157**: 502-514.
- Lo, S., Kotani, H., and Hu, W.S. (1993) Molecular and cell biology of opportunistic infections in AIDS. *Mycoplasmas and AIDS. Mol Cell Biol Hum Dis Ser* **2**: 229-256.
- Lo, S.C., Hayes, M.M., Tully, J.G., Wang, R.Y., Kotani, H., Pierce, P.F., Rose, D.L., and Shih, J.W. (1992) *Mycoplasma penetrans* sp. nov., from the urogenital tract of patients with AIDS. *Int J Syst Bacteriol* **42**: 357-364.
- Luby, J.P. (1991) Pneumonia Caused by *Mycoplasma pneumoniae* Infection. In *Clinics in Chest Medicine: Atypical Pneumonia Syndromes*. Vol. 12(2). Winterbauer, R.H. (ed). Philadelphia: W.B. Saunders Company, pp. 237-244.

- Maisel, J.C., Babbitt, L.H., and John, T.J. (1967) Fatal *Mycoplasma pneumoniae* infection with isolation of organisms from lung. *Jama* **202**: 287-290.
- Maniloff, J. (2002) Phylogeny and Evolution. In *Molecular Biology and Pathogenicity of Mycoplasmas*. Razin, S. and Herrmann, R. (eds). New York: Kluwer Academic/Plenum, pp. 31-43.
- Marmion, B.P., and Goodburn, G.M. (1961) Effect of an organic gold salt on Eaton's primary atypical pneumonia agent and other observations. *Nature* **189**: 247-248.
- Matic, I., Rayssiguier, C., and Radman, M. (1995) Interspecies gene exchange in bacteria: the role of SOS and mismatch repair systems in evolution of species. *Cell* **80**: 507-515.
- McBride, M.J. (2001) Bacterial Gliding Motility: Multiple Mechanisms for Cell Movement over Surfaces. *Annu Rev Microbiol* **55**: 49-75.
- Meng, K.E., and Pfister, R.M. (1980) Intracellular structures of *Mycoplasma pneumoniae* revealed after membrane removal. *J Bacteriol* **144**: 390-399.
- Miyata, M., Yamamoto, H., Shimizu, T., Uenoyama, A., Citti, C., and Rosengarten, R. (2000) Gliding mutants of *Mycoplasma mobile*: relationships between motility and cell morphology, cell adhesion and microcolony formation. *Microbiology* **146**: 1311-1320.
- Moriguchi, K., Hirai, K., and Shike, S. (1989) Stimulated intraphagosomal release of eosinophil peroxidase and acid phosphatase in the rats spontaneously infected with *Mycoplasma pulmonis*: a cytochemical study. *Exp Mol Pathol* **51**: 220-230.
- Muse, K.E., Powell, D.A., and Collier, A.M. (1976) *Mycoplasma pneumoniae* in hamster tracheal organ culture studied by scanning electron microscopy. *Infect Immun* **13**: 229-237.

- Nagai, R., and Miyata, M. (2006) Gliding motility of *Mycoplasma mobile* can occur by repeated binding to N-acetylneuraminylactose (sialyllactose) fixed on solid surfaces. *J Bacteriol* **188**: 6469-6475.
- Neimark, H.C. (1977) Extraction of an actin-like protein from the prokaryote *Mycoplasma pneumoniae*. *Proc Natl Acad Sci U S A* **74**: 4041-4045.
- Nocard E., and Roux P. (1898) Le microbe de la peripneumonie. *Ann. Inst. Pasteur* **12**: 240-262.
- Pitcher, D.G., Windsor, D., Windsor, H., Bradbury, J.M., Yavari, C., Jensen, J.S., Ling, C., and Webster, D. (2005) *Mycoplasma amphoriforme* sp. nov., isolated from a patient with chronic bronchopneumonia. *Int J Syst Evol Microbiol* **55**: 2589-2594.
- Popham, P.L., Hahn, T.W., Krebs, K.A., and Krause, D.C. (1997) Loss of HMW1 and HMW3 in noncytadhering mutants of *Mycoplasma pneumoniae* occurs post-translationally. *Proc Natl Acad Sci U S A* **94**: 13979-13984.
- Powell, D.A., Hu, P.C., Wilson, M., Collier, A.M., and Baseman, J.B. (1976) Attachment of *Mycoplasma pneumoniae* to respiratory epithelium. *Infect Immun* **13**: 959-966.
- Proft, T., Hilbert, H., Layh-Schmitt, G., and Herrmann, R. (1995) The proline-rich P65 protein of *Mycoplasma pneumoniae* is a component of the Triton X-100-insoluble fraction and exhibits size polymorphism in the strains M129 and FH. *J Bacteriol* **177**: 3370-3378.
- Radestock, U., and Bredt, W. (1977) Motility of *Mycoplasma pneumoniae*. *J Bacteriol* **129**: 1495-1501.
- Razin, S., Yogev, D., and Naot, Y. (1998) Molecular biology and pathogenicity of mycoplasmas. *Microbiol Mol Biol Rev* **62**: 1094-1156.

- Romero-Arroyo, C.E., Jordan, J., Peacock, S.J., Willby, M.J., Farmer, M.A., and Krause, D.C. (1999) *Mycoplasma pneumoniae* protein P30 is required for cytoadherence and associated with proper cell development. *J Bacteriol* **181**: 1079-1087.
- Rosenstein, I.J., Morgan, D.J., Sheehan, M., Lamont, R.F., and Taylor-Robinson, D. (1996) Bacterial vaginosis in pregnancy: distribution of bacterial species in different gram-stain categories of the vaginal flora. *J Med Microbiol* **45**: 120-126.
- Ruuskanen, O., Nohynek, H., Ziegler, T., Capeding, R., Rikalainen, H., Huovinen, P., and Leinonen, M. (1992) Pneumonia in childhood: etiology and response to antimicrobial therapy. *Eur J Clin Microbiol Infect Dis* **11**: 217-223.
- Sabin, A.B. (1938) Identification of the filtrable, transmissible neurolytic agent isolated from Toxoplasma-infected tissue as a new pleuro-pneumonia-like microbe. *Science* **88**: 575-576.
- Samet, J.M., and Cheng, P.W. (1994) The role of airway mucus in pulmonary toxicology. *Environ Health Perspect* **102 Suppl 2**: 89-103.
- Seto, S., Layh-Schmitt, G., Kenri, T., and Miyata, M. (2001) Visualization of the attachment organelle and cytoadherence proteins of *Mycoplasma pneumoniae* by immunofluorescence microscopy. *J Bacteriol* **183**: 1621-1630.
- Seto, S., Kenri, T., Tomiyama, T., and Miyata, M. (2005a) Involvement of P1 adhesin in gliding motility of *Mycoplasma pneumoniae* as revealed by the inhibitory effects of antibody under optimized gliding conditions. *J Bacteriol* **187**: 1875-1877.
- Seto, S., Uenoyama, A., and Miyata, M. (2005b) Identification of a 521-kilodalton protein (Gli521) involved in force generation or force transmission for *Mycoplasma mobile* gliding. *J Bacteriol* **187**: 3502-3510.
- Seybert, A., Herrmann, R., and Frangakis, A.S. (2006) Structural analysis of *Mycoplasma pneumoniae* by cryo-electron tomography. *J Struct Biol*.

- Shoetensack, H.M. (1936) Pure cultivation of filtrable virus isolated from canine distemper. *Kitasato Arch. Exptl. Med.* **13**: 175-184.
- Sobeslavsky, O., and Chanock, R.M. (1968) Peroxide formation by mycoplasmas which infect man. *Proc Soc Exp Biol Med* **129**: 531-535.
- Stevens, D., Swift, P.G., Johnston, P.G., Kearney, P.J., Corner, B.D., and Burman, D. (1978) *Mycoplasma pneumoniae* infections in children. *Arch Dis Child* **53**: 38-42.
- Suhs, R.H., and Feldman, H.A. (1966) Serologic epidemiologic studies with *M. pneumoniae*. II. Prevalence of antibodies in several populations. *Am J Epidemiol* **83**: 357-365.
- Taylor-Robinson, D. (1996) Infections due to species of *Mycoplasma* and *Ureaplasma*: an update. *Clin Infect Dis* **23**: 671-682; quiz 683-674.
- Tjhie, J.H., van de Putte, E.M., Haasnoot, K., van den Brule, A.J., and Vandenbroucke-Grauls, C.M. (1997) Fatal encephalitis caused by *Mycoplasma pneumoniae* in a 9-year-old girl. *Scand J Infect Dis* **29**: 424-425.
- Totten, P.A., Schwartz, M.A., Sjostrom, K.E., Kenny, G.E., Handsfield, H.H., Weiss, J.B., and Whittington, W.L. (2001) Association of *Mycoplasma genitalium* with nongonococcal urethritis in heterosexual men. *J Infect Dis* **183**: 269-276.
- Uenoyama, A., Kusumoto, A., and Miyata, M. (2004) Identification of a 349-kilodalton protein (Gli349) responsible for cytoadherence and glass binding during gliding of *Mycoplasma mobile*. *J Bacteriol* **186**: 1537-1545.
- Uenoyama, A., and Miyata, M. (2005a) Gliding ghosts of *Mycoplasma mobile*. *Proc Natl Acad Sci U S A* **102**: 12754-12758.
- Uenoyama, A., and Miyata, M. (2005b) Identification of a 123-kilodalton protein (Gli123) involved in machinery for gliding motility of *Mycoplasma mobile*. *J Bacteriol* **187**: 5578-5584.

- Waites, K.B., Rudd, P.T., Crouse, D.T., Canupp, K.C., Nelson, K.G., Ramsey, C., and Cassell, G.H. (1988) Chronic *Ureaplasma urealyticum* and *Mycoplasma hominis* infections of central nervous system in preterm infants. *Lancet* **1**: 17-21.
- Waites, K.B., and Talkington, D.F. (2004) *Mycoplasma pneumoniae* and its role as a human pathogen. *Clin Microbiol Rev* **17**: 697-728.
- Waldo, R.H., 3rd, Jordan, J.L., and Krause, D.C. (2005) Identification and complementation of a mutation associated with loss of *Mycoplasma pneumoniae* virulence-specific proteins B and C. *J Bacteriol* **187**: 747-751.
- Waldo, R.H., 3rd, and Krause, D.C. (2006) Synthesis, stability, and function of cytoadhesin P1 and accessory protein B/C complex of *Mycoplasma pneumoniae*. *J Bacteriol* **188**: 569-575.
- Widdicombe, J.H., Bastacky, S.J., Wu, D.X., and Lee, C.Y. (1997) Regulation of depth and composition of airway surface liquid. *Eur Respir J* **10**: 2892-2897.
- Willby, M.J., and Krause, D.C. (2002) Characterization of a *Mycoplasma pneumoniae* hmw3 mutant: implications for attachment organelle assembly. *J Bacteriol* **184**: 3061-3068.
- Willby, M.J., Balish, M.F., Ross, S.M., Lee, K.K., Jordan, J.L., and Krause, D.C. (2004) HMW1 is required for stability and localization of HMW2 to the attachment organelle of *Mycoplasma pneumoniae*. *J Bacteriol* **186**: 8221-8228.
- Williams, M.H., Brostoff, J., and Roitt, I.M. (1970) Possible role of *Mycoplasma fermentans* in pathogenesis of rheumatoid arthritis. *Lancet* **2**: 277-280.
- Wilson, M.H., and Collier, A.M. (1976) Ultrastructural study of *Mycoplasma pneumoniae* in organ culture. *J Bacteriol* **125**: 332-339.
- Wubbel, L., Muniz, L., Ahmed, A., Trujillo, M., Carubelli, C., McCoig, C., Abramo, T., Leinonen, M., and McCracken, G.H., Jr. (1999) Etiology and treatment of community-acquired pneumonia in ambulatory children. *Pediatr Infect Dis J* **18**: 98-104.

Yavlovich, A., Tarshis, M., and Rottem, S. (2004) Internalization and intracellular survival of *Mycoplasma pneumoniae* by non-phagocytic cells. *FEMS Microbiol Lett* **233**: 241-246.

Yogev, D., Browning, G.F., and Wise, K.S. (2002) Genetic mechanisms of surface variation. In *Molecular Biology and Pathogenicity of Mycoplasmas*. Razin, S. and Herrmann, R. (eds). New York: Kluwer Academic/Plenum, pp. 417-443.

CHAPTER 2

MUTANT ANALYSIS REVEALS A SPECIFIC REQUIREMENT FOR PROTEIN P30 IN *MYCOPLASMA PNEUMONIAE* GLIDING MOTILITY¹

¹ Hasselbring *et al.* 2005. *The Journal of Bacteriology*. 187: 6281-89
Reprinted here with permission of publisher.

ABSTRACT

The cell wall-less prokaryote *Mycoplasma pneumoniae*, long considered among the smallest and simplest cells capable of self-replication, has a distinct cellular polarity characterized by the presence of a differentiated terminal organelle which functions in adherence to human respiratory epithelium, gliding motility, and cell division. Characterization of hemadsorption (HA)-negative mutants has resulted in identification of several terminal organelle proteins including P30, the loss of which results in developmental defects and decreased adherence to host cells, but their impact on *M. pneumoniae* gliding has not been investigated. Here we examined the contribution of P30 to gliding motility on the basis of satellite growth and cell gliding velocity and frequency. *M. pneumoniae* HA mutant II-3 lacking P30 was non-motile, but HA mutant II-7 producing a truncated P30 was motile, albeit at a velocity 50-fold less than that of wild-type. HA⁺ revertant II-3R producing an altered P30 was unexpectedly not fully wild-type with respect to gliding. Complementation of mutant II-3 with recombinant wild-type and mutant alleles confirmed the correlation between gliding defect and loss or alteration in P30. Surprisingly, fusion of yellow fluorescent protein to the C-terminus of P30 had little impact on cell gliding velocity and significantly enhanced HA. Finally, while quantitative examination of HA revealed clear distinctions among these mutant strains, gliding defects did not correlate strictly with the HA phenotype, and all strains attached to glass at wild-type levels. Taken together, these findings suggest a role for P30 in gliding motility that is distinct from its requirement in adherence.

Mycoplasmas are cell wall-less prokaryotes with minimal genomes and limited biosynthetic capabilities, dictating a strict dependence on host species for survival in nature

(43). *Mycoplasma pneumoniae* is a human pathogen primarily colonizing the respiratory tract. While the most common clinical manifestations of infection are tracheobronchitis and atypical or “walking” pneumonia (7, 12, 14, 30), recent studies indicate a strong correlation with asthma (5, 24, 38), and extrapulmonary complications are not uncommon (53). Adherence of *M. pneumoniae* cells to host respiratory epithelium (cytadherence) is required for colonization and pathogenesis (20) and is mediated largely by a differentiated terminal organelle (9, 39). This well-defined apical structure is a membrane-bound extension of the mycoplasma cell distinguished ultrastructurally by an electron-dense core (4), which is a major constituent of the *M. pneumoniae* cytoskeleton (17, 35).

M. pneumoniae cells exhibit gliding motility, with the terminal organelle always the leading end (6), but details regarding the biological significance and the mechanism of gliding are largely unknown. Although the *M. pneumoniae* genome has been sequenced and twice annotated (11, 19), close inspection reveals no homology to proteins known to be involved in bacterial motility of any type in walled bacteria. Furthermore, while gliding motility has been described for several mycoplasma species, even within the genus *Mycoplasma* there appear to be distinct gliding mechanisms, as proteins thought to function in *M. mobile* gliding are absent from the genomes of the gliding mycoplasmas *M. genitalium*, *M. gallisepticum*, and *M. pneumoniae* (15, 23, 37, 46, 49, 56).

Analysis of *M. pneumoniae* hemadsorption (HA)-negative mutants has resulted in identification of a number of proteins associated with cytadherence (2, 27, 47, 48), including the putative adhesin P30, a membrane protein localizing primarily to the terminal organelle (3) and which is predicted to orient with a cytoplasmic N-terminus and the C-terminus exposed on the cell surface (Fig. 2.1A; 10, 32). *M. pneumoniae* HA mutant II-3 lacks detectable P30 due to a frameshift in the corresponding gene (MPN453; Fig. 2.1A) (44). A second-site mutation in HA revertant II-3R restores the wild-type reading frame for all but 17

residues (Fig. 2.1A and 2.1B; 44). HA mutant II-7 has an in-frame deletion of residues 207–254 in a C-terminal pro-rich-repeat region (Fig. 2.1A; 10), resulting in an internally truncated P30 derivative. Mutants II-3 and II-7 also exhibit reduced levels of the peripheral membrane protein P65, normally found on the mycoplasma cell surface at the attachment organelle (25, 41). The function of P65 is unknown, and it remains undetermined if the cytoadherence defects in strains II-3 and II-7 are due directly to the loss / alteration in P30 or are an indirect result of reduced levels of P65.

Possible consequences of the defects in mutants II-3 and II-7 on cell motility have not been investigated. In the current study we assessed gliding motility on the basis of satellite growth around microcolonies and by digital microcinematography for wild-type *M. pneumoniae*, HA mutants II-3 and II-7, and revertant II-3R, noting a correlation between the rate of satellite growth and cell gliding velocities. Complete loss of P30 was accompanied by failure to glide, while alterations in P30 resulted in reduced gliding velocity and frequency. Complementation studies with recombinant wild-type and mutant P30 alleles confirmed a specific requirement for P30 in gliding motility and established that a gliding defect does not correlate with reduced steady-state levels of P65. Attachment to a substrate is a strict prerequisite for gliding motility, but reduced gliding velocity and frequency for II-7 and II-3R was not a function of substrate-binding capability, suggesting a direct defect in the gliding mechanism resulting from the loss or alteration of P30. Finally, in contrast to the markedly reduced gliding speeds and frequencies that resulted from the changes in P30 in II-7 and II-3R, the fusion of enhanced yellow fluorescent protein (EYFP) at the C-terminus of P30, nearly doubling its size, had little effect on P30 function in gliding and HA.

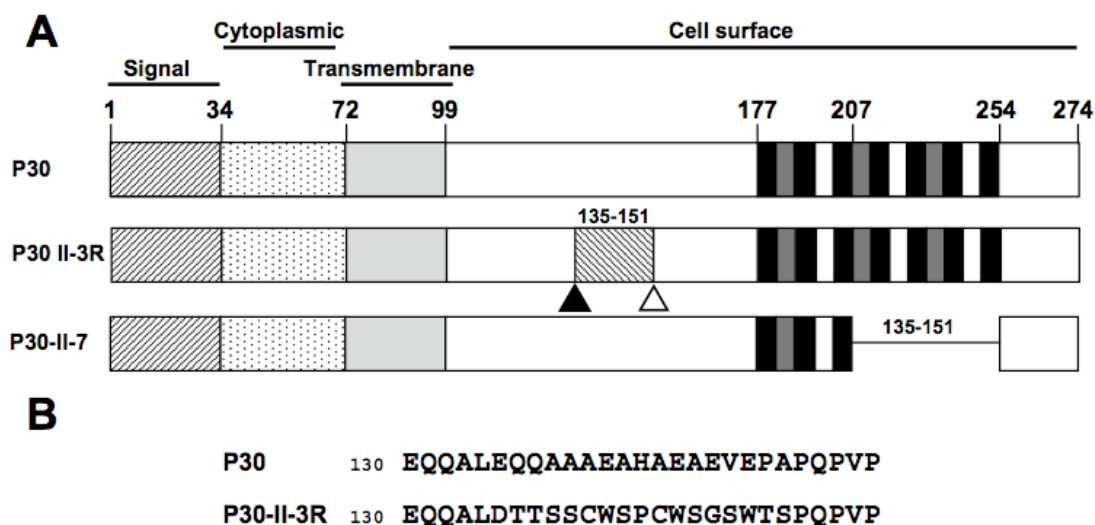


FIG. 2.1. Cytoadherence-associated protein P30 in wild-type *M. pneumoniae*, mutants II-3 and II-7, and revertant II-3R. (A) Wild-type P30 is predicted to have a single transmembrane domain. Experimental data (10, 32) suggest an orientation with the C-terminus on the cell surface. P30-II-3R: a frameshift (open triangle) resulted in mutant II-3 with no detectable P30. A second-site mutation (solid triangle) in revertant II-3R restored P30 except for residues 135-151 (see B below). P30-II-7: P30 derivative resulting from in-frame deletion of residues 207-254 in mutant II-7. (B) Amino acid sequence for P30 from wild-type and II-3R *M. pneumoniae* for the indicated residues.

MATERIALS AND METHODS

Mycoplasma strains. Wild-type *M. pneumoniae* strain M129 (33) was used at the 18th broth passage. Spontaneously arising HA mutants II-3 and II-7 (29), and HA revertant II-3R (44), all derived from M129, were described previously.

Recombinant P30 derivatives and *M. pneumoniae* transformation. Resident alleles for P30 from wild-type, mutant II-7, and revertant II-3R, together with upstream MPN454 (*p21*) and its corresponding promoter (57), were amplified by PCR, engineering an *EcoRI* site in 5' primer EcoRlp21pos (5'-GTAGCTTCATGAATTCGGTCT-3'), which was used with the 3' primer hmw3neg (5'-CAAAGCTAATTGGTTCATCACTGTC-3'). The resulting PCR products were cloned using standard protocols (45) into Tn4001.2062 within plasmid pKV74 (18) using the *EcoRI* site in the upstream primer and a *BamHI* site downstream of MPN453, then transformed into *Escherichia coli*, and subsequently purified and sequenced (Integrated Biotechnology Laboratories, University of Georgia, Athens, GA). Mycoplasma transformation was achieved as described previously (18); multiple transformants were isolated from each transformation and expanded as described previously (18, 52).

Western immunoblotting. Samples were prepared for sodium dodecylsulfate polyacrylamide gel electrophoresis (31) and Western immunoblotting (54) as follows. After blocking in 5% skim-milk in Tris-buffered saline (TBS; 0.2 M Tris-HCl, 0.85% NaCl, pH 8.2), membranes were incubated with primary antibody for 2 h at room temperature, washed 5 x 5 min in TTBS (TBS with 0.05% Tween-20), probed with secondary AP-conjugated antibody (Bio-Rad, Hercules, CA, or Promega; Madison, WI) for 1 h at room temperature, and washed again 5 x 5 min in TTBS. Monoclonal P30-specific antibody (44) was used at 1:750, rabbit anti-P65 serum (40) was used at 1:3000, anti-P1 serum (28) was used at 1:1000, and anti-GFP (Clontech; Palo Alto, CA) was used at 1:1000.

Generation of a P30-EYFP fusion. The gene for wild-type P30 was amplified by PCR using 5' primer BamHlp21pos (5'-GTAGCTGGATCCACTTGGTCT-3') and 3' primer Ncolp30neg (5'-AAGCACCATGGAGCGTTTTGGTGGGA-3'), generating *Bam*HI and *Nco*I sites near the 5' and 3' ends of the product, respectively, and replacing the stop codon with ATG of the *Nco*I recognition sequence. The resulting product was digested with *Bam*HI and *Nco*I (Promega) and ligated into the corresponding sites of pEYFP (Clontech). The resulting plasmid was digested with *Bam*HI and *Eco*R1 to liberate *p30-eyfp*, which was cloned into the corresponding sites in the Tn4001 derivative in plasmid pMT85 (E. Pirkl and R. Herrmann, manuscript in preparation), then transformed into *E. coli* DH5 α . The resulting plasmid was sequenced and electroporated into *M. pneumoniae* as described previously (18). Genomic DNA from mycoplasma transformants was digested with *Hind*III (Promega), re-ligated, and transformed into *E. coli*. Plasmid DNA from kanamycin-resistant transformants was sequenced to determine the transposon junction using pMT85-specific primer pMT85seq (5'-CCGCGCGTTGGCCGATTCATTAATGCACGC-3'). An intergenic insertion was identified for two of eight transformants sequenced, one of which is described here in subsequent studies (insertion at nucleotide 372,735, between MPN312 and MPN313).

EYFP Fluorescence microscopy. Mycoplasma cultures were inoculated directly into 600 μ l SP-4 medium (55) in 4-well borosilicate-glass chambers (Nalge/Nunc, Naperville, IL) and incubated overnight at 37°C. Phase and fluorescence images captured on a Leica DM IRB inverted microscope (Leica Microsystems, Wetzlar, Germany) at an exposure of 0.4 sec using phase-contrast optics (100X oil-immersion objective, 1.4 numerical aperture) through a Chroma EYFP filter set (Chroma, Rockingham, VT) were recorded and digitized with a Hamamatsu Orca ER CCD camera (Hamamatsu Photonics, Hamamatsu City, Japan)

using the computer program Openlab v3.0-4.0 (Improvision, Lexington, MA). Images were merged using Openlab or Adobe Photoshop v6.0-7.0 (Adobe Systems, Inc., San Jose, CA).

Analysis of satellite growth. Motility stocks of each strain (see below) were diluted serially 10^{-2} - 10^{-5} in SP-4 medium / 3% (w/v) gelatin and inoculated into adjacent wells of 4-well borosilicate-glass chambers. At 12 h intervals post-inoculation the appearance of satellite motility around colonies was recorded digitally with phase-contrast optics (40X) as described above.

Microcinematography and quantitation of cell gliding. In order to quantitate gliding velocities for individual cells we modified a microcinematographic approach described over 30 years ago for *M. pneumoniae* (6) to take advantage of new technologies. Mycoplasmas grown in SP-4 medium in tissue-culture flasks for 72 h, until approximately mid-logarithmic growth phase, were harvested by centrifugation at 17,000 x *g* for 25 min at 4°C, suspended in 2.5 ml fresh SP-4 medium supplemented with gelatin (3% w/v) by passage through a 25-gauge needle 7X, divided into motility stocks, and stored at -80°C. Motility stocks were thawed, mixed with 500 μ l of fresh SP-4 / 3%-gelatin / 0.05M HEPES (pH 7.2), passed through a 25-gauge needle 5X to disperse cell aggregates, and inoculated into 4-well borosilicate glass chambers, which were placed onto the observation stage of a Leica DM IRB microscope enclosed within an incubation chamber (Solent Scientific Limited, Portsmouth, U.K.) pre-heated to 37°C. After 10 min at 37°C images were recorded and digitized at automated frame intervals as described above. The number of cells per field at the start of image capture was 30-60, with gliding velocities measured for a minimum of 200 cells per strain from no less than five separate studies, varying motility stocks and media batches for control purposes. Gliding was quantitated using the Openlab measurements module v3.51-4.0 (Improvision). Briefly, digitally recorded images of each frame were compiled into an image stack, with motility quantitated by recording the XY coordinates of

the leading edge of each motile cell in the observation field for each frame. An intrinsic time stamp was assigned per frame during capture, and the gliding velocity of each cell was calculated by dividing the distance covered (change in XY coordinates) by the absolute time between frames. A cell resting period was assigned when there was no net cell movement greater than 1 pixel (0.0645 μm) between sequentially captured frames. Corrected gliding velocities were calculated as the total distance traveled by a cell divided by total time of the field interval minus the amount of time spent in resting periods.

Analysis of HA and attachment to glass. HA is a convenient indicator for *M. pneumoniae* cytoadherence (50). Qualitative assessment of HA to mycoplasma colonies was performed as described previously (29) using sheep or chicken blood. HA was measured quantitatively with [^3H]-thymidine-labeled mycoplasmas (13), using SP-4 rather than Hayflick medium. For quantitation of attachment to glass, frozen stocks of radiolabeled mycoplasma cultures were thawed and centrifuged for 5 min at 123 x *g* to remove cellular aggregates, and 150- μl aliquots of the resulting suspension were added to 500 μl of HEPES-buffered SP-4 medium / 3.9%-gelatin, pH 7.2 (final gelatin concentration 3.0%). Suspensions were inoculated in triplicate onto sterile glass coverslips in 24-well plates and incubated 30 min at 37°C. Coverslips were then washed 3X in PBS and analyzed by liquid scintillation spectrometry. Experiments were repeated four times per strain per condition tested.

Statistical Analyses. Quantitative motility, HA, and glass-binding data were assessed for statistical significance. Differences between strains were considered significant if comparison by a two-tailed Student's *t* test had a *P* value of < 0.05.

RESULTS

Evaluation of gliding motility by satellite growth. Several bacterial species manifest gliding motility as satellite growth or colony spreading over time. Although there are exceptions, satellite growth usually correlates with a gliding-competent phenotype (34, 51). The known gliding mycoplasma species are unique among gliding prokaryotes in that their motility requires a solid-liquid interface (1, 6, 26), but we were unable to observe satellite growth around wild-type microcolonies at an agar/broth interface with agar concentrations ranging from 0.5 – 12.5%, or with embedding in soft agar as described for *M. mobile* (36). However, satellite growth was evident on polystyrene overlaid with agar concentrations <0.5% or on polystyrene or glass when 3% gelatin was included in broth medium to increase viscosity. Using the latter approach we compared satellite growth for wild-type and P30 mutant *M. pneumoniae*.

Wild-type satellite growth was most clearly observed after 48-72 h using stocks diluted sufficiently to allow unimpeded spreading (Fig. 2.2). HA mutant II-3 exhibited no satellite growth for up to 120 h post-inoculation but rather formed microcolonies having a smooth leading edge (Fig. 2.2). In contrast, HA mutant II-7 and revertant II-3R exhibited limited satellite growth by 48 h, albeit much less dense than for wild-type (Fig. 2.2C and 2.2D, respectively). Satellite growth increased by 72 h but remained considerably less abundant than for wild-type *M. pneumoniae* cultured for the same time period. By 96-120 h satellite growth for both II-7 and II-3R approximated that seen at 72 h for wild-type (data not shown). The extended time-scale required for wild-type satellite growth for these two strains suggested lower gliding velocities and/or gliding frequencies than wild type.

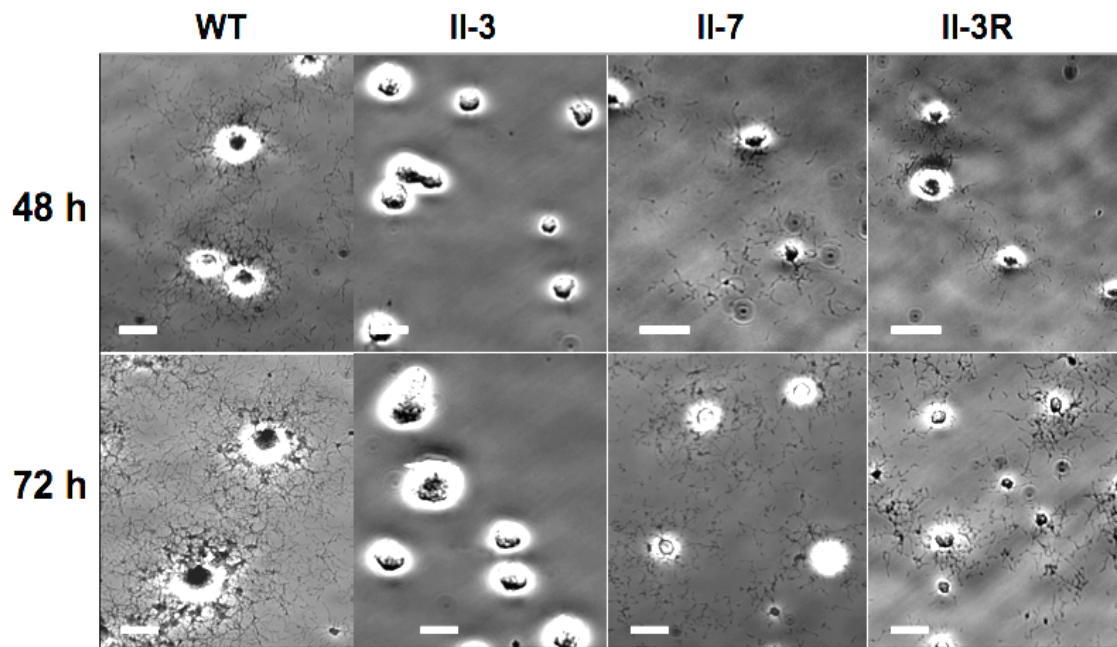


FIG. 2.2. Analysis of wild-type and mutant *M. pneumoniae* satellite growth. Colony morphology of wild-type, mutant II-3, mutant II-7, and revertant II-3R cultured on glass in SP-4 medium + 3% gelatin. Images were captured at 48h and 72h post-inoculation as indicated. Scale bar: 30 μ m.

Quantitation of cellular gliding. Wild-type stocks prepared without centrifugation exhibited a mean gliding velocity of $0.29 \pm 0.0069 \mu\text{m}/\text{sec}$ with a mean corrected velocity of $0.36 \pm .0082 \mu\text{m}/\text{sec}$, consistent with data published previously (42). However, wild-type stocks prepared with a centrifugation step exhibited significantly lower mean gliding and corrected gliding velocities of $0.18 \pm 0.0079 \mu\text{m}/\text{sec}$ and $0.26 \pm 0.0068 \mu\text{m}/\text{sec}$, respectively (Table 2.1). Jaffe et al. likewise noted that centrifugation during mycoplasma stock preparation affected gliding by *M. mobile* (22). However, as stock preparation for *M. pneumoniae* HA mutants required centrifugation, motility stock cultures for all strains in subsequent studies here were prepared in that manner.

Wild-type cellular gliding was recorded at 1 frame-per-sec over 30-sec intervals, but no motility was observed for mutant II-7 or revertant II-3R by these parameters (motility being defined as the translocation of at least 1 μm per field interval). However, cellular motility was evident for II-7 and II-3R with image capture at 1 frame-per-min and field intervals of 20 min, with velocities approximately 20-50-fold slower than wild type (Table 2.1). Wild-type controls exhibited no reduction in motility after 20 min and remained steady over 3 h (data not shown). Mutant II-3 exhibited no motility even when observed over 3 h field intervals and was deemed non-motile under these conditions.

Wild-type *M. pneumoniae* cells commonly exhibit resting periods of varying lengths and frequencies during their motility tracks (6, 42). Because reduced satellite growth could result from increased resting frequencies rather than or in addition to reduced gliding velocities, we also examined the percentage of time that individual cells spent in intermittent resting periods during their motility tracks (% time resting). The slower-gliding II-3R and II-7 strains also exhibited significantly higher % time resting values than did wild-type *M. pneumoniae*, reflecting longer and/or more frequent resting periods (Table 2.1).

Table 2.1. Mean gliding and corrected gliding velocities and percent time resting for wild-type *M. pneumoniae*, cytoadherence mutant and revertant strains, and transformants.

Mycoplasma strain	Mean Gliding Velocity ($\mu\text{m}/\text{sec}$)	Mean Corrected Gliding Velocity ($\mu\text{m}/\text{sec}$)	Percent Time Resting
Wild-type M129	0.18 ± 0.0079	0.26 ± 0.0068	34.6
Mutant II-3	0	0	NA
Transformant II-3 + P30-WT	0.21 ± 0.028	0.29 ± 0.019	31.9
Transformant II-3 + P30-EYFP	0.10 ± 0.025	0.19 ± 0.020	50.3
Revertant II-3R	0.0058 ± 0.00091	0.012 ± 0.0023	47.8
Transformant II-3 + P30-II-3R	0.011 ± 0.0049	0.018 ± 0.0051	48.3
Mutant II-7	0.0035 ± 0.0011	0.0059 ± 0.00093	48.8
Transformant II-3 + P30-II-7	0.0056 ± 0.0028	0.011 ± 0.0081	54.7

Analysis of recombinant P30 derivatives. To confirm that loss or alteration in P30 was directly responsible for the observed motility defects, mutant II-3 transformants with recombinant P30 alleles introduced via transposon delivery were generated and analyzed. Multiple transformants were examined for each construct to control for the site of recombinant transposon insertion, and representative steady-state levels for each are shown by Western immunoblotting in Fig. 2.3. As expected, no P30 was detected in mutant II-3 while the truncated P30 in II-7 migrated faster than wild-type P30 (Fig. 2.3A; 10, 44). Unexpectedly, the truncated P30 in II-7 was consistently less abundant than its wild-type counterpart. Similar results were observed using an antibody specific for the N-terminus of P30, indicating that epitope loss was not responsible for the reduced band intensity (data not shown). The 17-residue change in P30-II-3R increased its electrophoretic mobility to approximately 28,000, compared to 32,000 for wild-type P30 (Fig. 2.3A), while minor species were also observed at approximately 56,000 and 114,000 (Fig. 2.3B), corresponding to dimeric and tetrameric forms. Recombinant P30 levels in mutant II-3 transformants with the wild-type (II-3 + P30-WT), the II-7 (II-3 + P30-II-7), or the II-3R allele (II-3 + P30-II-3R) were generally comparable to that in the corresponding strains from which each was derived. Thus, P30 was produced at wild-type levels in II-3 + P30-WT and near-wild-type levels in II-3R and II-3 + P30-II-3R, and the truncated P30 was observed at similarly reduced levels in II-7 and II-3 + P30-II-7 (Fig. 2.3A).

The II-3 transformants producing recombinant P30 were evaluated for satellite growth and cellular gliding phenotypes. Satellite growth for wild-type *M. pneumoniae* and II-3 + P30-WT was indistinguishable over the same time-frame; likewise, II-3 + P30-II-7 and II-3 + P30-II-3R exhibited limited levels of satellite growth comparable to their II-7 and II-3R counterparts (data not shown). In addition, gliding velocities and resting frequencies for

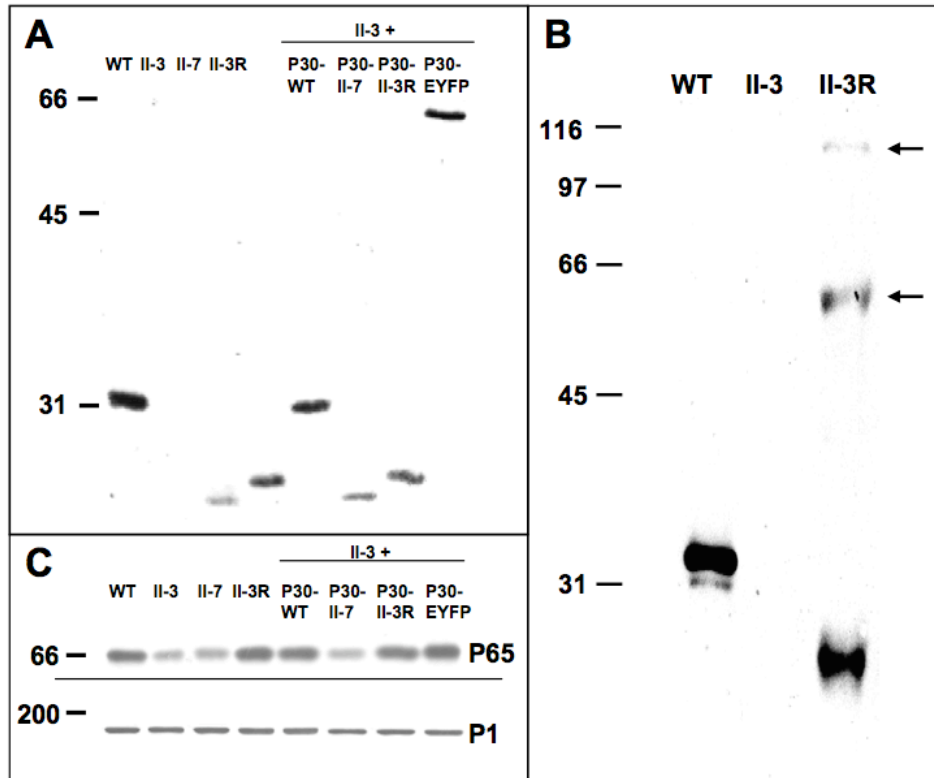


FIG 2.3. Western immunoblot analysis of P30 and P65 in wild-type, mutant, revertant, and transformant *M. pneumoniae*. (A & B) Western immunoblot analysis of the indicated strains probed with P30-specific antibodies; II-3 + P30: mutant II-3 transformed with the indicated recombinant P30 allele by transposon delivery. (B) Samples processed to allow resolution of the multimeric forms of P30 from II-3R (arrows). (C) Western immunoblot analysis of parallel samples from (A) using P65-specific antibodies (top) or P1-specific antibodies as an internal control (bottom).

transformants with P30-WT, P30-II-7, and P30-II-3R were comparable to those in wild-type, II-7, or II-3R *M. pneumoniae*, respectively (Table 2.1). Thus, the defects in gliding correlated specifically with loss or alteration in P30.

Analysis of P30-EYFP. The P30-EYFP fusion of the predicted size (approximately 60,000) was produced in mutant II-3 transformants at levels near that of wild-type P30 and reacted with antibodies to both P30 (Fig. 2.2A) and GFP (data not shown). Like P30 (3; data not shown), the P30-EYFP fusion was observed by fluorescence microscopy to localize predominantly at a single cell pole (Fig. 2.4A), which by time-lapse microcinematography was shown to be the leading end of motile cells (data not shown). Many non-motile cells exhibited two P30 foci (Fig. 2.4A, arrows), probably reflecting attachment organelle duplication, which is thought to precede cell division (47). Satellite growth for II-3 transformants with P30-EYFP was indistinguishable from wild-type (Fig. 2.4B). Although nearly double the size of wild-type P30, the P30-EYFP fusion only reduced gliding velocity slightly (to 65-73% of wild-type), compared to the reduction to 2-5% of wild-type with the P30 defects in II-7 and II-3R (Table 2.1).

P65 stability. P65 is found at reduced steady-state levels in mutants II-3 and II-7 (25). The reversion in II-3 to yield II-3R restored P65 to wild-type levels (Fig. 2.3C), as did the recombinant wild-type, II-3R, and P30-EYFP alleles but not the II-7 allele when introduced into mutant II-3. Thus, II-3R was gliding-defective despite the presence of P65 at wild-type levels.

Analysis of HA and glass binding. HA provides a convenient indicator for adherence to respiratory epithelium (50). As expected (29), when examined qualitatively the HA mutants II-3 and II-7 failed to adsorb sheep erythrocytes, while revertant II-3R (44) was clearly HA+, although not at the high erythrocyte density of wild-type (Fig. 2.5A). A similar pattern was

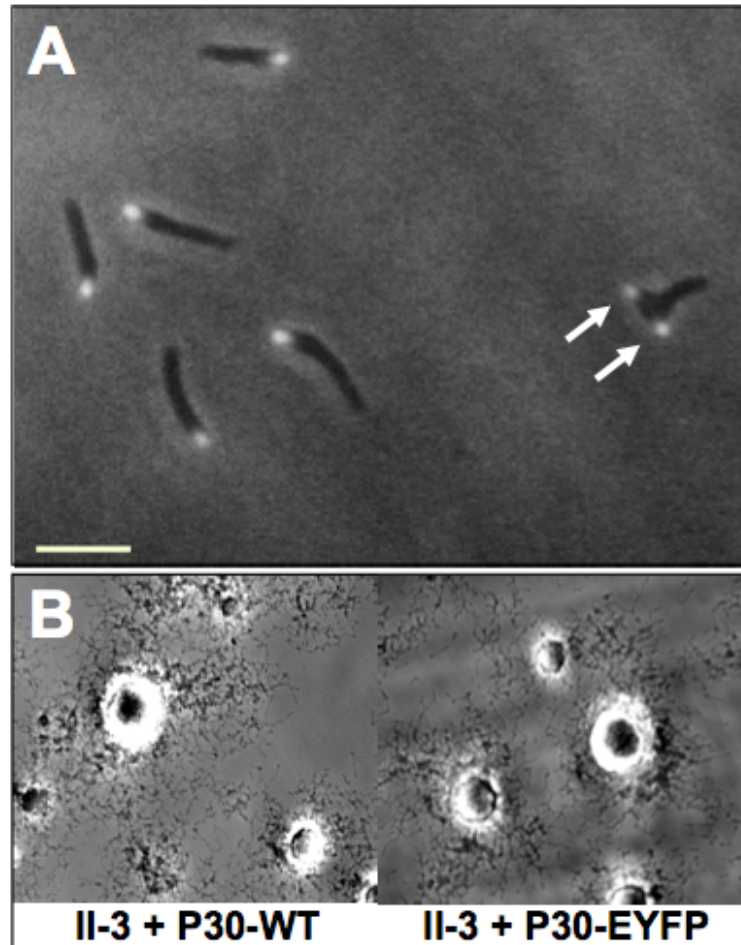


FIG 2.4. Analysis of P30-EYFP in mutant II-3. (A) Fluorescence / phase contrast microscopy established that the P30-EYFP fusion localizes to the terminal organelle, and cells with a second fluorescent focus were apparent (arrows). Scale bar: 2 μm . (B) Satellite growth in mutant II-3 + recombinant P30-EYFP was indistinguishable from mutant II-3 + recombinant wild-type P30. Scale bar: 30 μm .

observed with chicken erythrocytes (data not shown). The quantitative HA assay reinforced in part the qualitative observations but also revealed a difference between II-3 and II-7 (Fig. 2.5B). While mutant II-3 bound to erythrocytes minimally (5% of wild-type), HA by mutant II-7 was significantly higher than that of mutant II-3, at approximately 35% of wild-type. Revertant II-3R HA was substantially higher than II-7 but still only approximately 60% of wild-type. The contribution of P30 in the HA phenotype of each was reinforced by the quantitative HA data using transformants producing recombinant P30 (Fig. 2.5B). Somewhat surprisingly, however, the recombinant P30-EYFP fusion restored HA in mutant II-3 to a level significantly higher than in wild-type or II-3 + P30-WT.

By definition, attachment to a surface is a prerequisite for gliding motility. Given the variability in HA and gliding motility with the loss or alteration in P30, we examined glass binding of each under conditions identical to those used to assess cellular gliding velocities and frequencies. Unlike the HA data, all strains including the non-motile mutant II-3 exhibited levels of glass attachment that were statistically comparable to wild-type (Table 2.2). Thus, under the conditions used here to measure *M. pneumoniae* cell motility, the gliding deficiencies were not simply a function of glass-binding ability.

DISCUSSION

Mycoplasmas are considered to be among the smallest and simplest known cells capable of self-replication, and yet *M. pneumoniae* and related species exhibit distinct cellular polarity characterized by the presence of a complex terminal organelle that is the leading end of gliding cells and initiates mycoplasma binding to host cell receptors. However, the mechanism by which *M. pneumoniae* glides is unknown, and its genome contains no homologs of known motility proteins of any type in walled bacteria or other mycoplasmas. Furthermore, very little is known about specific terminal organelle

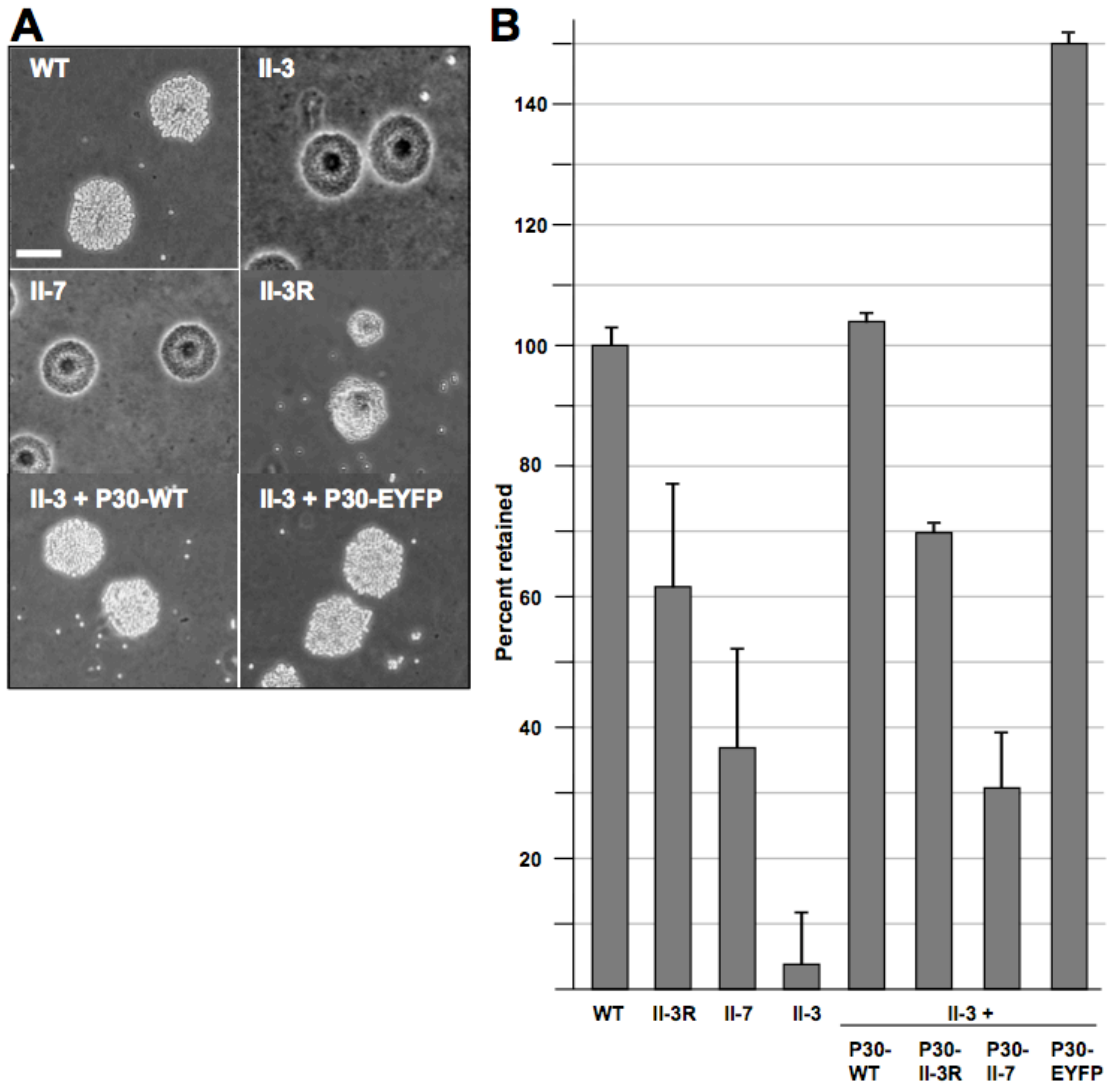


FIG 2.5. Assessment of HA by wild-type *M. pneumoniae* and P30 mutant, revertant, and transformant strains. (A) Qualitative HA by the indicated strains. Scale bar: 60 μm . (B) Quantitative HA by the indicated strains normalized to wild-type binding. Error bars: standard error of the mean.

Table 2.2. Wild-type and mutant glass-binding under conditions used for quantitation of gliding velocities and frequencies. All strains exhibited levels of binding that were indistinguishable from wild-type ($P > 0.05$). Attachment data shown normalized to wild type. Error bars: standard error of the mean.

Strain	% retained \pm SEM
Wild-type	100 \pm 10
HA mutant II-3	84 \pm 10
HA mutant II-7	93 \pm 7
HA revertant II-3R	87 \pm 8
II-3 + P30-WT	90 \pm 7
II-3 + P30-II-7	93 \pm 20
II-3 + P30R	97 \pm 6
II-3 + P30-EYFP	102 \pm 7

components with respect to their function in adherence and gliding (46). In the current study we examined *M. pneumoniae* satellite growth around microcolonies as a possible indicator of gliding motility. Attempts to promote satellite growth using soft agar as described for gliding walled bacteria (34, 51), *Mycoplasma mobile* (36), and *Spiroplasma citri* (21) were unsuccessful, but satellite growth was apparent when *M. pneumoniae* was cultured on plastic or glass in growth medium containing gelatin. At the concentrations examined gelatin is visibly less viscous than soft agar and hence probably requires less force for gliding to be achieved. The inability to observe *M. pneumoniae* satellite growth in soft agar $\geq 0.5\%$ may therefore reflect a lower force-generating capacity than for other gliding species. Regardless, our finding that HA mutant II-7 but not HA mutant II-3 exhibited satellite growth, albeit much slower than wild-type, was unexpected. Likewise was the finding that satellite growth by the HA+ revertant II-3R was not like wild-type. A requirement for P30 in cytoadherence was established previously (3, 29); the current studies indicate an additional role for P30 in gliding motility.

We modified existing microscopy protocols (6) to take advantage of digital technology and measure mycoplasma gliding on the cellular level. Gliding velocities for wild-type strain M129 were comparable to those reported previously (42) for the wild-type FH strain (data not shown) and 20- to 50-fold faster than mutant II-7 and revertant II-3R, while mutant II-3 was non-motile. Thus, the cell velocities and gliding frequencies for wild-type *M. pneumoniae*, mutants II-3 and II-7, and revertant II-3R correlated directly with their satellite growth phenotypes, demonstrating that satellite growth is a good indicator for identifying potential gliding-defective mutants in this species.

Transformation of mutant II-3, having no detectable P30, with recombinant wild-type, mutant, or revertant alleles for P30 by transposon delivery, yielded motility phenotypes that were comparable to those of the strains from which each recombinant allele originated

(Table 2.1). Therefore, it was possible to correlate the specific defects in P30 with the altered motility phenotypes, underscoring a role for P30 in *M. pneumoniae* gliding motility. Our results from complementation analysis also confirmed that the stability of cytoadherence-associated protein P65 is affected specifically by the loss or alteration of P30. However, as gliding remained deficient despite restoration of P65 to wild-type levels in II-3R and mutant II-3 producing recombinant P30-II-3R, the motility defects in P30 mutants cannot be attributed to an effect on P65 levels.

For mutant II-7 and revertant II-3R the reduced gliding velocities correlated specifically with a 48-residue deletion and a 17-residue substitution, respectively, in the putative cell surface domain of P30 (Fig. 2.1). The latter was associated with the formation of multimers that were stable to detergent denaturation (Fig. 2.3B). Wild-type P30 has a single cys residue located in the predicted transmembrane domain, while the substitution in P30R introduced two additional cys residues (Fig. 2.1B). P30 is predicted to assume a coiled-coil conformation from residues 90-150 (data not shown), which includes the region encompassed by the substitution in P30R. Additional cys residues in this region might promote multimerization in the oxidizing environment of the cell exterior. However, the P30R multimers were resistant to reducing agents dithiothreitol and β -mercaptoethanol, with and without alkylation with iodoacetamide (data not shown), suggesting that non-disulfide covalent or strong hydrophobic interactions may contribute to multimerization. Somewhat surprisingly, while the relatively minor substitution in II-3R reduced gliding velocity markedly, fusion of EYFP to P30, which approximately doubled its size, impaired P30 function very little and actually increased HA by 50%. The reason for enhanced HA with this fusion is not clear, but the fact that gliding was not similarly enhanced reinforces the dual but distinct functions of P30 in cytoadherence and cell gliding.

The observation that HA mutants II-3 and II-7 differed with respect to gliding motility prompted a closer examination of their HA phenotypes. As expected, both were indistinguishable by qualitative screening, whereby mycoplasma colonies adsorb erythrocytes (Fig. 2.4A). However, by the more sensitive measure of attachment of radiolabeled mycoplasmas to erythrocytes in suspension, mutant II-7 adherence was 6-7-fold higher than that of mutant II-3. Furthermore, closer inspection of revertant II-3R revealed intermediate levels of HA by both qualitative and quantitative techniques (Fig. 2.4). The relative levels of HA actually paralleled the gliding velocities, with wild-type >> revertant II-3R > mutant II-7 >> mutant II-3, raising the possibility that the gliding defect might actually be an extension of the HA deficiency. However, this conclusion was not supported by the observation that under the conditions used to assess cell gliding, all strains attached to glass at comparable levels.

The role of P30 in gliding motility is not clear. The major adhesin protein P1 localizes to the terminal organelle in wild-type *M. pneumoniae* and in P30 mutants but is non-functional in the latter, raising the possibility that P30 is required to stabilize the adhesin in the appropriate conformation in the mycoplasma membrane (44). Antibodies to P1 cause gliding mycoplasmas to detach from the glass surface (46), but detachment was not pronounced in our studies with P30 mutants. Taken together, these observations suggest that P30 may contribute to the linkage between surface-binding moieties and the force-generating mechanism of *M. pneumoniae*.

Finally, individual cells of mutants II-3 and II-7 (44) and revertant II-3R (data not shown) exhibit a branched morphology rather than the filamentous spindle-like morphology of wild-type *M. pneumoniae* after attaching to plastic or glass. Whereas the non-motile mutant II-3 retains this branched morphology, mutant II-7 (44) and revertant II-3R (data not shown), for which the gliding machinery is indeed active though less efficient, eventually

assume a filamentous shape over time. Thus, based on the current study the filamentous, extended morphology of wild-type cells is likely a function of cell gliding, in which case the filamentous appearance of *M. pneumoniae* cells on ciliated respiratory epithelium (8, 16) suggests that gliding indeed occurs on the surface of host cells as well.

In summary, the current study provides the first genetic evidence linking a specific protein to gliding motility by *M. pneumoniae*. Furthermore, specific domains of P30 thought to be oriented on the mycoplasma cell surface were implicated in gliding function. Surprisingly, fusion of EYFP to the C-terminus of P30 had little impact on gliding and actually enhanced HA. Additional studies including structural analysis of the surface domain of P30 will be required to establish in more detail how P30 functions in both gliding and cytodherence.

ACKNOWLEDGEMENTS

We thank R. Herrman for providing P65-specific antisera, as well as transposon pMT85 prior to publication, J. Baseman for providing P30 antibody, and E. Sheppard and R. Krause for their technical contributions to data analysis.

This work was supported by Public Health Service grant AI49194 from the National Institute of Allergy and Infectious Diseases to D.C.K.

REFERENCES

1. **Andrewes, C. H.** 1946. A motile organism of the pleuropneumoniae group. *J. Path. Bacteriol.* **58**:578-580.
2. **Balish, M. F., and D. C. Krause.** 2002. Cytadherence and the Cytoskeleton, p. 491-518. *In* S. Razin and R. Herrmann (ed.), *Molecular Biology and Pathogenicity of Mycoplasmas*. Kluwer Academic/Plenum Publishers, New York.

3. **Baseman, J. B., J. Morrison-Plummer, D. Drouillard, B. Puleo-Schepke, V. V. Tryon, and S. C. Holt.** 1987. Identification of a 32-kilodalton protein of *Mycoplasma pneumoniae* associated with hemadsorption. *Isr. J. Med. Sci.* **23**:474-479.
4. **Biberfeld, G., and P. Biberfeld.** 1970. Ultrastructural Features of *Mycoplasma pneumoniae*. *J. Bacteriol.* **102**:855-861.
5. **Biscardi, S., M. Lorrot, E. Marc, F. Moulin, B. Boutonnat-Faucher, C. Heilbronner, J. L. Iniguez, M. Chaussain, E. Nicand, J. Raymond, and D. Gendrel.** 2004. *Mycoplasma pneumoniae* and asthma in children. *Clin. Infect. Dis.* **38**:1341-1346.
6. **Bredt, W.** 1968. Motility and multiplication of *Mycoplasma pneumoniae*. A phase contrast study. *Pathol. Microbiol.* **32**:321-6.
7. **Clyde, W. A., Jr., and F. W. Denny.** 1967. Mycoplasma infections in childhood. *Pediatrics* **40**:669-684.
8. **Collier, A. M., and W. A. Clyde, Jr.** 1974. Appearance of *Mycoplasma pneumoniae* in lungs of experimentally infected hamsters and sputum from patients with natural disease. *Am. Rev. Respir. Dis.* **110**:765-773.
9. **Collier, A. M., W. A. Clyde, Jr., and F. W. Denny.** 1971. *Mycoplasma pneumoniae* in hamster tracheal organ culture: immunofluorescent and electron microscopic studies. *Proc. Soc. Exp. Biol. Med.* **136**:569-573.
10. **Dallo, S. F., A. L. Lazzell, A. Chavoya, S. P. Reddy, and J. B. Baseman.** 1996. Biofunctional domains of the *Mycoplasma pneumoniae* P30 adhesin. *Infect. Immun.* **64**:2595-2601.
11. **Dandekar, T., M. Huynen, J. T. Regula, B. Ueberle, C. U. Zimmermann, M. A. Andrade, T. Doerks, L. Sanchez-Pulido, B. Snel, M. Suyama, Y. P. Yuan, R. Herrmann, and P. Bork.** 2000. Re-annotating the *Mycoplasma pneumoniae*

- genome sequence: adding value, function and reading frames. *Nucleic Acids Res.* **28**:3278-3288.
12. **Denny, F. W., W. A. Clyde, Jr., and W. P. Glezen.** 1971. *Mycoplasma pneumoniae* disease: clinical spectrum, pathophysiology, epidemiology, and control. *J. Infect. Dis.* **123**:74-92.
 13. **Fisseha, M., H. W. Gohlmann, R. Herrmann, and D. C. Krause.** 1999. Identification and complementation of frameshift mutations associated with loss of cytoadherence in *Mycoplasma pneumoniae*. *J. Bacteriol.* **181**:4404-4410.
 14. **Foy, H. M.** 1999. *Mycoplasma pneumoniae* pneumonia: current perspectives. *Clin. Infect. Dis.* **28**:237.
 15. **Fraser, C. M., J. D. Gocayne, O. White, M. D. Adams, R. A. Clayton, R. D. Fleischmann, C. J. Bult, A. R. Kerlavage, G. Sutton, J. M. Kelley, R.D. Fritchman, J.F. Weidman, K.V. Small, M. Sandusky, J. Fuhrmann, D. Nguyen, T.R. Utterback, D.M. Saudek, C.A. Phillips, J.M. Merrick, J.F. Tomb, B.A. Dougherty, K.F. Bott, P.C. Hu, T.S. Lucier, S.N. Peterson, H.O. Smith, C.A. Hutchison III, and J.C. Venter.** 1995. The minimal gene complement of *Mycoplasma genitalium*. *Science* **270**:397-403.
 16. **Gabridge, M. G., M. J. Bright, and H. R. Richards.** 1982. Scanning electron microscopy of *Mycoplasma pneumoniae* on the membrane of individual ciliated tracheal cells. *In Vitro* **18**:55-62.
 17. **Gobel, U., V. Speth, and W. Bredt.** 1981. Filamentous structures in adherent *Mycoplasma pneumoniae* cells treated with nonionic detergents. *J. Cell. Biol.* **91**:537-543.
 18. **Hedreyda, C. T., K. K. Lee, and D. C. Krause.** 1993. Transformation of *Mycoplasma pneumoniae* with Tn4001 by electroporation. *Plasmid* **30**:170-175.

19. **Himmelreich, R., H. Hilbert, H. Plagens, E. Pirkl, B. C. Li, and R. Herrmann.** 1996. Complete sequence analysis of the genome of the bacterium *Mycoplasma pneumoniae*. *Nucleic Acids Res.* **24**:4420-4449.
20. **Hu, P. C., A. M. Collier, and J. B. Baseman.** 1976. Interaction of virulent *Mycoplasma pneumoniae* with hamster tracheal organ cultures. *Infect. Immun.* **14**:217-224.
21. **Jacob, C., F. Nouzieres, S. Duret, J. M. Bove, and J. Renaudin.** 1997. Isolation, characterization, and complementation of a motility mutant of *Spiroplasma citri*. *J. Bacteriol.* **179**:4802-4810.
22. **Jaffe, J. D., M. Miyata, and H. C. Berg.** 2004. Energetics of gliding motility in *Mycoplasma mobile*. *J. Bacteriol.* **186**:4254-4261.
23. **Jaffe, J. D., N. Stange-Thomann, C. Smith, D. DeCaprio, S. Fisher, J. Butler, S. Calvo, T. Elkins, M. G. FitzGerald, N. Hafez, C. D. Kodira, J. Major, S. Wang, J. Wilkinson, R. Nicol, C. Nusbaum, B. Birren, H. C. Berg, and G. M. Church.** 2004. The complete genome and proteome of *Mycoplasma mobile*. *Genome Res.* **14**:1447-1461.
24. **Johnston, S. L., and R. J. Martin.** 2005. *Chlamydophila pneumoniae* and *Mycoplasma pneumoniae*: a Role in Asthma Pathogenesis? *Am. J. Respir. Crit. Care Med.* [E-pub ahead of print].
25. **Jordan, J. L., K. M. Berry, M. F. Balish, and D. C. Krause.** 2001. Stability and subcellular localization of cytoadherence-associated protein P65 in *Mycoplasma pneumoniae*. *J. Bacteriol.* **183**:7387-7391.
26. **Kirchhoff, H., and R. Rosengarten.** 1984. Isolation of a motile mycoplasma from fish. *J. Gen. Microbiol.* **130 (Pt 9)**:2439-2445.

27. **Krause, D. C., and M. F. Balish.** 2004. Cellular engineering in a minimal microbe: structure and assembly of the terminal organelle of *Mycoplasma pneumoniae*. *Mol. Microbiol.* **51**:917-924.
28. **Krause, D. C., and J. B. Baseman.** 1983. Inhibition of *Mycoplasma pneumoniae* hemadsorption and adherence to respiratory epithelium by antibodies to a membrane protein. *Infect. Immun.* **39**:1180-1186.
29. **Krause, D. C., D. K. Leith, R. M. Wilson, and J. B. Baseman.** 1982. Identification of *Mycoplasma pneumoniae* proteins associated with hemadsorption and virulence. *Infect. Immun.* **35**:809-817.
30. **Krause, D. C., and D. Taylor-Robinson.** 1992. Mycoplasmas Which Infect Humans, p. 417-444. *In* R. N. M. J. Maniloff, L. R. Finch & J. B. Baseman. (ed.), *In Mycoplasmas- Molecular Biology and Pathogenesis*. American Society for Microbiology, Washington, D.C.
31. **Laemmli, U. K.** 1970. Cleavage of structural proteins during the assembly of the head of bacteriophage T4. *Nature* **227**:680-685.
32. **Layh-Schmitt, G., R. Himmelreich, and U. Leibfried.** 1997. The adhesin related 30-kDa protein of *Mycoplasma pneumoniae* exhibits size and antigen variability. *FEMS Microbiol. Lett.* **152**:101-108.
33. **Lipman, R. P., W. A. Clyde, Jr., and F. W. Denny.** 1969. Characteristics of virulent, attenuated, and avirulent *Mycoplasma pneumoniae* strains. *J. Bacteriol.* **100**:1037-1043.
34. **McBride, M. J.** 2001. Bacterial gliding motility: Multiple mechanisms for cell movement over surfaces. *Annu. Rev. Microbiol.* **55**:49-75.
35. **Meng, K. E., and R. M. Pfister.** 1980. Intracellular structures of *Mycoplasma pneumoniae* revealed after membrane removal. *J. Bacteriol.* **144**:390-399.

36. **Miyata, M., H. Yamamoto, T. Shimizu, A. Uenoyama, C. Citti, and R. Rosengarten.** 2000. Gliding mutants of *Mycoplasma mobile*: relationships between motility and cell morphology, cell adhesion and microcolony formation. *Microbiology* **146**:1311-1320.
37. **Papazisi, L., T. S. Gorton, G. Kutish, P. F. Markham, G. F. Browning, D. K. Nguyen, S. Swartzell, A. Madan, G. Mahairas, and S. J. Geary.** 2003. The complete genome sequence of the avian pathogen *Mycoplasma gallisepticum* strain R(low). *Microbiol.* **149**:2307-2316.
38. **Park, S. J., Y. C. Lee, Y. K. Rhee, and H. B. Lee.** 2005. Seroprevalence of *Mycoplasma pneumoniae* and *Chlamydia pneumoniae* in stable asthma and chronic obstructive pulmonary disease. *J. Korean Med. Sci.* **20**:225-228.
39. **Powell, D. A., P. C. Hu, M. Wilson, A. M. Collier, and J. B. Baseman.** 1976. Attachment of *Mycoplasma pneumoniae* to respiratory epithelium. *Infect. Immun.* **13**:959-966.
40. **Proft, T., and R. Herrmann.** 1994. Identification and characterization of hitherto unknown *Mycoplasma pneumoniae* proteins. *Mol. Microbiol.* **13**:337-348.
41. **Proft, T., H. Hilbert, G. Layh-Schmitt, and R. Herrmann.** 1995. The proline-rich P65 protein of *Mycoplasma pneumoniae* is a component of the Triton X-100-insoluble fraction and exhibits size polymorphism in the strains M129 and FH. *J. Bacteriol.* **177**:3370-3378.
42. **Radestock, U., and W. Bredt.** 1977. Motility of *Mycoplasma pneumoniae*. *J. Bacteriol.* **129**:1495-1501.
43. **Razin, S., D. Yogev, and Y. Naot.** 1998. Molecular biology and pathogenicity of mycoplasmas. *Microbiol. Mol. Biol. Rev.* **62**:1094-1156.

44. **Romero-Arroyo, C. E., J. Jordan, S. J. Peacock, M. J. Willby, M. A. Farmer, and D. C. Krause.** 1999. *Mycoplasma pneumoniae* protein P30 is required for cytodherence and associated with proper cell development. *J. Bacteriol.* **181**:1079-1087.
45. **Sambrook, J., E. F. Fritsch, and T. Maniatis.** 1989. *Molecular Cloning: A Laboratory Manual*, 2nd ed. Cold Spring Harbor Laboratory Press, Cold Spring Harbor, NY.
46. **Seto, S., T. Kenri, T. Tomiyama, and M. Miyata.** 2005. Involvement of P1 adhesin in gliding motility of *Mycoplasma pneumoniae* as revealed by the inhibitory effects of antibody under optimized gliding conditions. *J. Bacteriol.* **187**:1875-1877.
47. **Seto, S., G. Layh-Schmitt, T. Kenri, and M. Miyata.** 2001. Visualization of the attachment organelle and cytodherence proteins of *Mycoplasma pneumoniae* by immunofluorescence microscopy. *J. Bacteriol.* **183**:1621-1630.
48. **Seto, S., and M. Miyata.** 2003. Attachment Organelle Formation Represented by Localization of Cytadherence Proteins and Formation of the Electron-Dense Core in Wild-Type and Mutant Strains of *Mycoplasma pneumoniae*. *J. Bacteriol.* **185**:1082-1091.
49. **Seto, S., A. Uenoyama, and M. Miyata.** 2005. Identification of a 521-kilodalton protein (Gli521) involved in force generation or force transmission for *Mycoplasma mobile* gliding. *J. Bacteriol.* **187**:3502-3510.
50. **Sobeslavsky, O., B. Prescott, and R. Chanock.** 1968. Adsorption of *Mycoplasma pneumoniae* to neuraminic acid receptors of various cells and possible role in virulence. *J. Bacteriol.* **96**:695-705.
51. **Spormann, A. M.** 1999. Gliding motility in bacteria: insights from studies of *Myxococcus xanthus*. *Microbiol. Mol. Biol. Rev.* **63**:621-641.

52. **Stevens, M. K., and D. C. Krause.** 1991. Localization of the *Mycoplasma pneumoniae* cytoadherence-accessory proteins HMW1 and HMW4 in the cytoskeletonlike Triton shell. *J. Bacteriol.* **173**:1041-1050.
53. **Talkington, D.F., K. B. Waites, S. B. Schwartz, and R. E. Besser.** 2001 Emerging from obscurity: understanding pulmonary and extrapulmonary syndromes, pathogenesis, and epidemiology of human *Mycoplasma pneumoniae* infections, p. 57-84. *In* W. M. Scheld, W. A. Graig, and J. M. Hughes (ed.), *Emerging Infections 5*. American Society for Microbiology, Washington, D.C.
54. **Towbin, H., T. Staehelin, and J. Gordon.** 1979. Electrophoretic transfer of proteins from polyacrylamide gels to nitrocellulose sheets: procedure and some applications. *Proc. Natl. Acad. Sci. U.S.A.* **76**:4350-4354.
55. **Tully, J. G., R. F. Whitcomb, H. F. Clark, and D. L. Williamson.** 1977. Pathogenic mycoplasmas: cultivation and vertebrate pathogenicity of a new spiroplasma. *Science* **195**: 892-894.
56. **Uenoyama, A., A. Kusumoto, and M. Miyata.** 2004. Identification of a 349-kilodalton protein (Gli349) responsible for cytoadherence and glass binding during gliding of *Mycoplasma mobile*. *J. Bacteriol.* **186**:1537-1545.
57. **Waldo, R. H., 3rd, P. L. Popham, C. E. Romero-Arroyo, E. A. Mothershed, K. K. Lee, and D. C. Krause.** 1999. Transcriptional analysis of the *hmw* gene cluster of *Mycoplasma pneumoniae*. *J. Bacteriol.* **181**:4978-4

CHAPTER 3

TERMINAL ORGANELLE DEVELOPMENT IN THE CELL WALL-LESS BACTERIUM MYCOPLASMA PNEUMONIAE¹

¹ Hasselbring *et al.* 2006. *Proceedings of the National Academy of Sciences*. 103:16478-83
Reprinted here with permission of publisher.

Abstract

Mycoplasmas are cell wall-less bacteria considered among the smallest and simplest prokaryotes known, and yet several species including *Mycoplasma pneumoniae* have a remarkably complex cellular organization highlighted by the presence of a differentiated terminal organelle, a membrane-bound cell extension distinguished by an electron-dense core. Adhesin proteins localize specifically to the terminal organelle, which is also the leading end in gliding motility. Duplication of the terminal organelle is thought to precede cell division, but neither the mechanism of its duplication nor its role in this process is understood. Here we utilized fluorescent protein fusions and time-lapse digital imaging to study terminal organelle formation in unprecedented detail in growing cultures of *M. pneumoniae*. Individual cells ceased gliding as a new terminal organelle formed adjacent to an existing structure, which then migrated away from the transiently stationary nascent structure. Multiple terminal organelles often formed before cytokinesis was observed. The separation of terminal organelles was impaired in a non-motile mutant, indicating a requirement for gliding in normal cell division. Examination of cells expressing two different fluorescent protein fusions concurrently established their relative order of appearance, while changes in the fluorescence pattern over time suggested that nascent terminal organelles originated de novo rather than from an existing structure. In summary, spatial and temporal analysis of terminal organelle formation has yielded new insights into the nature of *M. pneumoniae* cell division and the role of gliding motility in that process.

Mycoplasma pneumoniae causes chronic infections of the human respiratory tract, including bronchitis and primary atypical or “walking” pneumonia, accounting for up to 30%

of all community-acquired pneumonia, particularly among older children and young adults. *M. pneumoniae* infections can result in chronic or permanent lung damage, and a growing body of evidence supports a correlation with the onset, exacerbation, and recurrence of asthma. Furthermore, extrapulmonary sequelae are not uncommon, reflecting both invasive and immunopathological components to *M. pneumoniae* disease (1).

In addition to its significant impact on public health, *M. pneumoniae* is intriguing from a biological perspective. Mycoplasmas have no cell wall and are among the smallest known cells, with *M. pneumoniae* having a cell volume only about 5% of that of *Escherichia coli*. Likewise, at 816 kb the *M. pneumoniae* genome is among the smallest known for a cell capable of a free-living existence, lacking genes for cell wall production, de novo synthesis of nucleotides and amino acids, and two-component or other common bacterial transcriptional regulators (2, 3). Nevertheless, a remarkable level of structural complexity underlies what are otherwise considered minimal cells (4). Thus, experimental evidence indicated the presence of cytoskeletal structure and function in *M. pneumoniae* well before cytoskeleton-like elements were described in walled bacteria (5, 6). Furthermore, *M. pneumoniae* cells possess a complex, differentiated polar extension of the cell body that mediates both adherence to host cells (cytadherence) and gliding motility (7, 8). Adhesin proteins including P1 and P30, as well as cytadherence-associated proteins of undefined function such as P41 and P65 (9) localize to this structure. The terminal organelle is defined by an electron-dense core that is also a component of the Triton X-100-insoluble, cytoskeletal fraction (5, 6). Loss of certain cytadherence-accessory proteins results in failure to assemble a core or to exhibit the polarity characteristic of wild-type *M. pneumoniae* cells (10, 11). By conventional electron microscopy of thin sections the electron-dense core appears as two parallel flattened rods (12, 13) but recent analysis by electron cryotomography has revealed a complex, multi-subunit composition to this structure (14,

15). Nevertheless, little is known regarding its molecular architecture or functional mechanisms.

By light microscopy *M. pneumoniae* cell division appears to begin with formation of a second terminal organelle adjacent to the first and the migration of one structure towards the opposite cell pole (16). Limits of resolution and the small size of the mycoplasma cell restrict the conclusions that might be drawn by light microscopy, but cell images by electron microscopy (17) as well as data correlating DNA content and the number and location of terminal organelles in fixed cells (18) are consistent with this model. Here we used fluorescent protein fusions with terminal organelle proteins P30, P41, and P65 and time-lapse digital imaging to observe directly the formation and maturation of the terminal organelle in individual cells during *M. pneumoniae* growth. Gliding ceased as a new terminal organelle formed adjacent to an existing structure at a cell pole, and P41 appeared to precede P30 and P65 in terminal organelle development. Migration of an existing terminal organelle was responsible for separation from the nascent structure, a process which was impaired in a non-motile mutant, indicating a requirement for gliding function for normal cell division. Finally, incorporation of P30, P41, and P65 into nascent terminal organelles appeared to result from new protein synthesis rather than from an existing organelle, as has been suggested by electron microscopy images (13).

Results

Visualization of terminal organelle development in growing *M. pneumoniae* cultures.

Protein P30 is a terminal organelle component required for cytodherence and gliding motility (19, 20). A recombinant P30 fusion with yellow fluorescent protein (YFP) introduced by transposon delivery localizes to the terminal organelle and restores cytodherence and gliding to a mutant lacking P30 (20); transformants with the recombinant transposon in an

intergenic site exhibit a phenotype essentially indistinguishable from wild-type *M. pneumoniae* producing P30-YFP. As P30-YFP also yielded the strongest signal of the fluorescent protein fusions examined here (data not shown), we focused initially on this fusion. We monitored mycoplasma cells having a single P30-YFP focus for the formation of nascent terminal organelles, seen as the appearance of additional fluorescent foci over time. Ten phase contrast / fluorescence time-lapse digital movies were generated and analyzed, three with observation periods of 8-12 h and image capture at 0.5-1.5-h intervals, and seven of at least 2 h and image capture at 6-20-min intervals. Each had ≥ 20 cells per field initially, most in clusters or stationary with >1 P30-YFP focus (Fig. 3.1A). 69 of 296 cells examined had 1 P30-YFP focus; nearly 90% of these were gliding, similar to published values (20). A new P30-YFP focus appeared adjacent to the single existing focus and coincident with cessation of gliding in 38% of the motile cells during the observation period (Fig. 3.1B, 3.1C). However, even with image capture at 6-min intervals it was not possible to establish more precisely the sequence of these events, as the impact of photobleaching on detection, enhanced by the small cell size, restricted the number of fluorescence images possible per field. The remaining motile cells glided beyond the field of view, collided with other cells, or failed to form a new terminal organelle during the observation period. In Fig. 3.1B cell gliding ceased and a second P30-YFP focus appeared adjacent to the first between the 6- and 12-min time points. Over the next 18 min the original and new foci appeared to decrease and increase in fluorescence intensity, respectively. The same pattern was seen in Fig. 3.1C, where longer observation made it possible to see the initial focus (yellow arrowhead) move away from the new focus (green arrowhead), which remained relatively fixed. In Fig. 3.1D a single cell (circled in Fig. 3.1A) was monitored over 11 h. Again the appearance of a second P30-YFP focus coincided with gliding cessation, although the

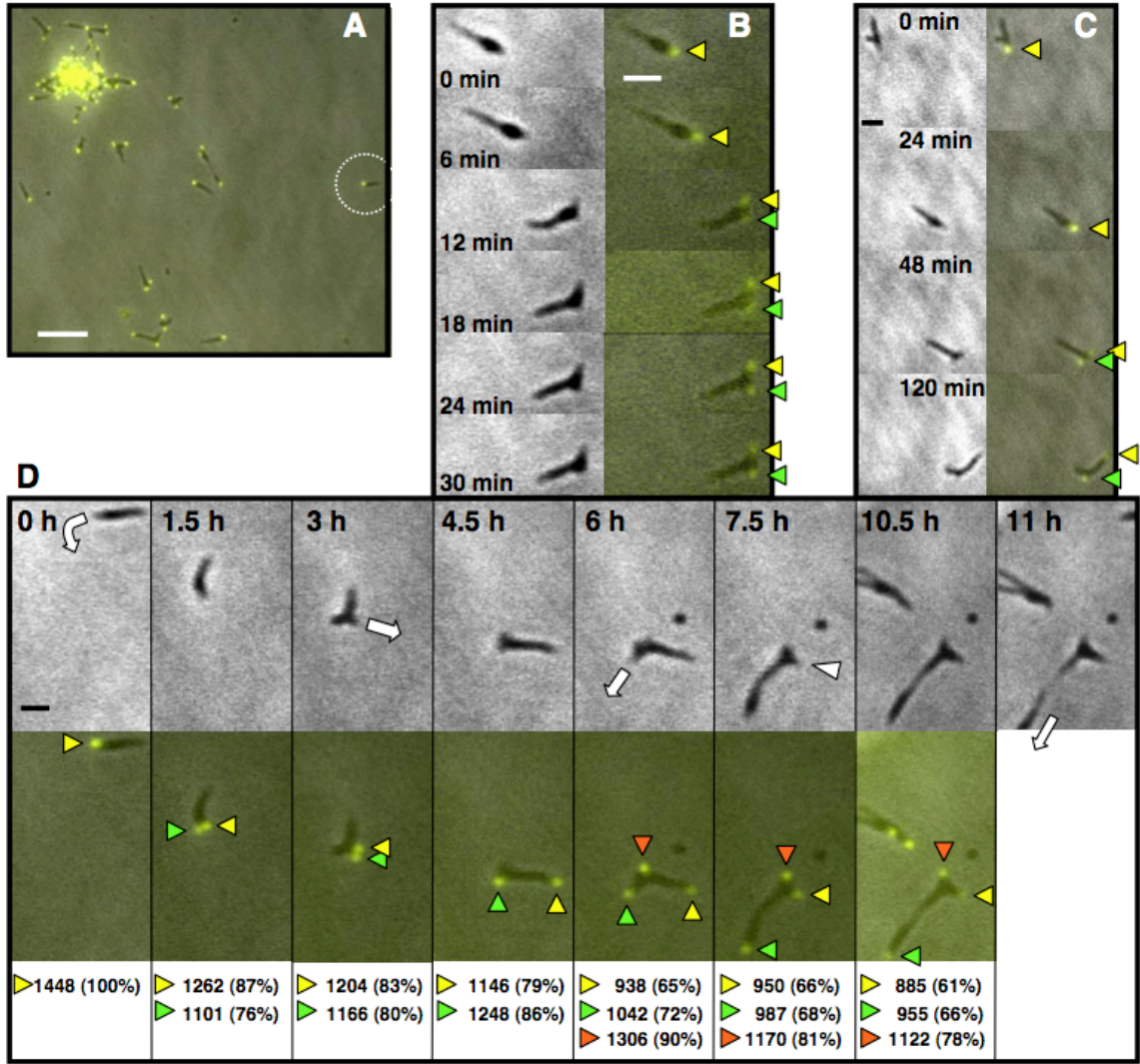


Fig. 3.1. Time-lapse phase contrast / fluorescence microscopy of terminal organelle appearance, development and separation during *M. pneumoniae* growth. Mutant II-3 + recombinant P30-YFP has a wild-type phenotype (20); shown are phase contrast and fluorescence images of II-3 + P30-YFP taken at various intervals over observations of 30 min to 11 h. **(A)** A representative field for analysis of terminal organelle development. Circle, individual cell monitored in panel D over 11 h. Scale, 5 μm . **(B)** Images were captured over a 30-min period at 6-min intervals. Left panels, phase contrast images; right panels, merged P30-YFP fluorescence / phase contrast images; yellow arrowheads, original focus; green arrowheads, nascent focus. Scale, 1 μm . See also supplementary movie 1. **(C)** Selected frames over a 2-h observation; arrowheads and scale same as in (B); see also supplementary movie 2. **(D)** Selected frames over an 11-h observation. Upper panels, phase contrast images; lower panels, merged P30-YFP fluorescence / phase contrast images. White arrows indicate direction of cell gliding; white arrowhead indicates cell retraction. Yellow, green and orange arrowheads indicate the first, second, and third terminal organelles, respectively. Numbers below indicate relative fluorescence units, and in parentheses those values standardized to the single focus at 0 h. Scale, 1 μm . See also supplementary movie 3.

interval between observations does not permit more precise sequencing of these events. Nascent foci were initially less intense than existing foci and required up to 3 h from initial detection to achieve maximum fluorescence (Fig. 3.1D, 0-3 h). During this time cells were not motionless, but gliding of whole cells was not observed. Original and nascent foci separated, in most cases the result of the former moving away from the latter (Fig. 3.1C, 3.1D). Cytokinesis, when observed, generally required an additional 3 h minimum, but usually a third and occasionally a fourth new P30-YFP focus formed before daughter cell separation was observed (Fig. 3.1D, 6-10.5 h and data not shown).

Gliding motility is required for normal cell division. While the appearance of nascent P30-YFP foci coincided with cessation of gliding, subsequent terminal organelle separation and cytokinesis appeared to result from transient resumption of gliding, almost without exception with an older fluorescent focus moving away from a new focus. Only rarely was the converse true or were both foci seen to separate simultaneously. In Fig. 3.1D the original focus (but not the entire cell) glided to the right (3.0 and 4.5 h; yellow arrowheads) while the nascent focus (green arrowheads) remained relatively stationary except for perhaps some rotation. Between 4.5 and 6.0 h a third focus formed (orange arrowheads), and the second focus migrated downward in the field, eventually leading to cytokinesis. This was accompanied by the movement of the initial focus back toward the cell body (7.5 h, white arrowhead), as though detached from the surface to allow cell retraction and partitioning.

The association between *M. pneumoniae* gliding motility and cell division was examined further to determine if separation of P30-YFP foci was impaired in the non-motile mutant III-4, which forms a terminal organelle and localizes P30 to that structure but lacks cytodherence-accessory proteins B & C (10, 11, 21, 22). This mutant formed P30-YFP foci which were not observed to separate over periods of up to 12 h (Fig. 3.2 and data not

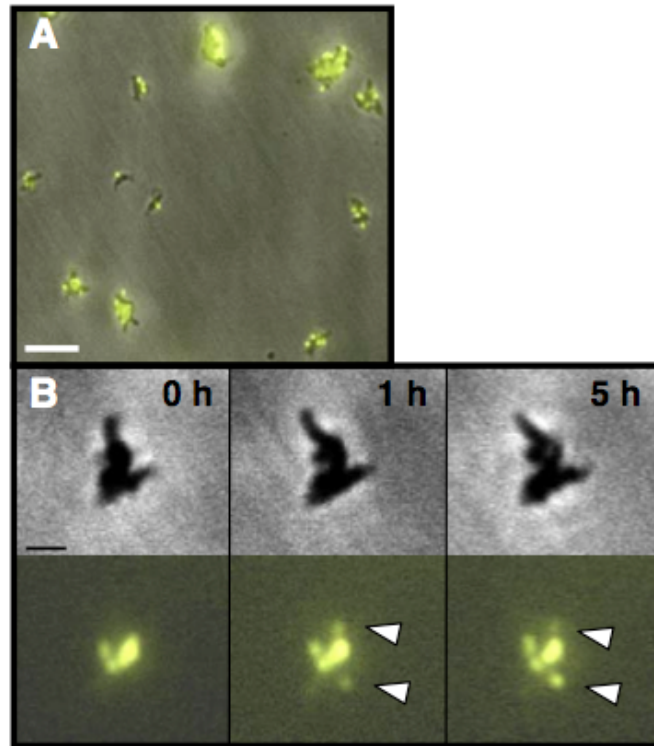


Fig. 3.2. Time-lapse phase contrast / fluorescence microscopy of terminal organelle development without separation during growth of non-motile *M. pneumoniae* mutant III-4. (A) Representative field for examination of non-motile mutant III-4 + P30-YFP. Scale, 5 µm. (B) Non-motile mutant III-4 with selected frames over a 5-h observation during growth in a chamber slide. Top panels, phase contrast images; middle panels, P30-YFP fluorescence images, with white arrowheads indicating new foci evident during the observation period; bottom panels, fluorescence / phase contrast images merged. Scale, 1 µm.

shown), consistent with a requirement for gliding competence for normal cell division. We cannot rule out the possibility that appearance of new foci simply reflects movement of existing foci into the depth of field in these large cell clusters; nevertheless no separation of fluorescent foci was observed in this non-motile mutant.

Examination of assembly sequence using fluorescent protein fusions. The loss of certain *M. pneumoniae* terminal organelle proteins results in accelerated turnover of others and is thought to reflect sequential requirements in the assembly process (9). Cataloging the downstream consequences of loss of essential binding partners has yielded a model for terminal organelle assembly whereby some components are predicted to be incorporated early and others, including P30 and P65, are incorporated later (9, 18, 23). In order to begin to test that model we examined fluorescence patterns in growing mycoplasma cultures producing either P41-YFP or P65-YFP and P30-cyan fluorescent protein (CFP) for their relative timing of appearance. Proteins P65 and P41 are novel cytoskeletal elements of unknown function expressed from the same transcriptional unit in *M. pneumoniae* and localize to the distal end and base, respectively, of the terminal organelle (24, 25). Transformants producing P65-YFP alone exhibited a pattern of new terminal organelle development comparable to that of P30-YFP, and in cells producing both fusions, P30-CFP and P65-YFP were observed in pairs in >95% of the cells examined, suggesting near-concurrent incorporation into the terminal organelle (data not shown).

Results for P41-YFP alone differed from those for P30-YFP and P65-YFP in that 26% of gliding cells had two P41-YFP foci in tandem (Fig. 3.3) compared to <2% for P30-YFP and P65-YFP, suggesting that P41 may precede P30 in the assembly sequence. P30-CFP foci at the tip of terminal organelles were almost exclusively observed paired with P41-YFP at the base of those structures (Fig. 3.4), but in some cells the P30-CFP was faint and diffuse (Fig. 3.4B, circle), and nearly 30% of P41-YFP foci were unpaired with P30-CFP (Fig.

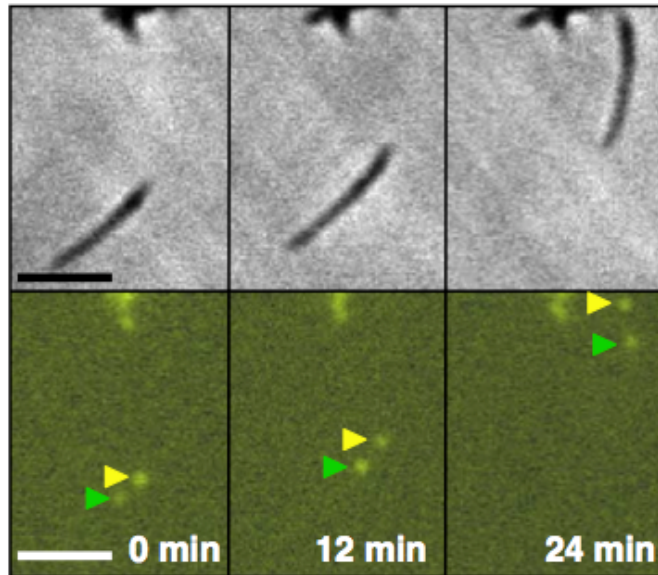


Fig. 3.3. Time-lapse phase contrast / fluorescence microscopy demonstrating the appearance of P41-YFP before cessation of gliding. Selected frames over a 24-min observation during growth in a chamber slide. Yellow arrowheads, leading P41-YFP focus; green arrowheads, trailing P41-YFP focus in a single gliding cell. Scale, 1 μm . See also supplementary movie 4, where the trailing focus can be seen unpaired with P30-CFP.

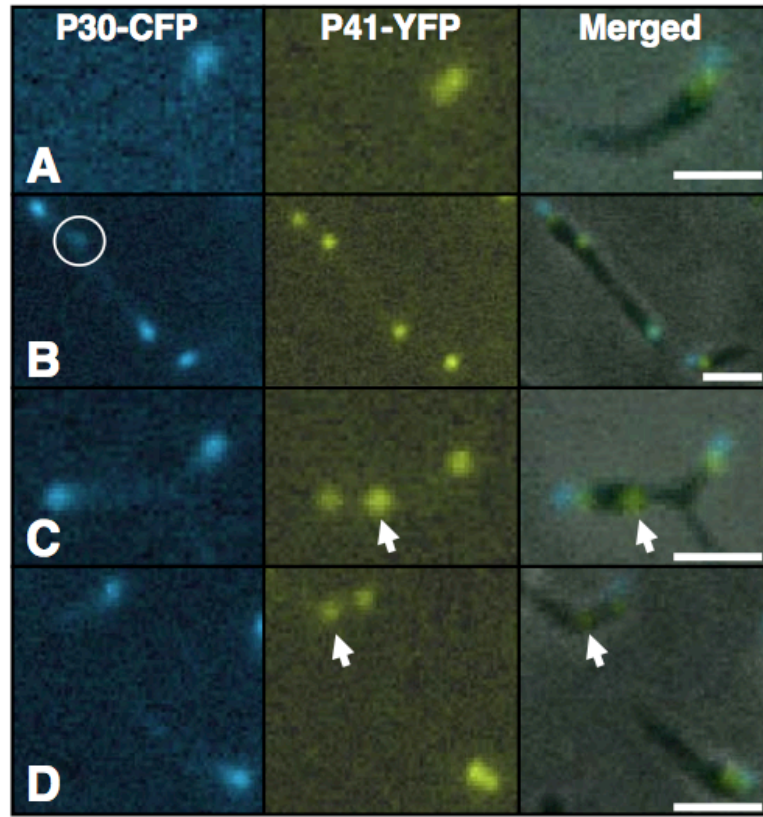


Fig. 3.4. Phase contrast / fluorescence microscopy of *M. pneumoniae* cells producing P30-CFP and P41-YFP. Left column, P30-CFP fluorescence images; middle column, P41-YFP fluorescence images; right column, merged phase contrast and P41-YFP + P30-CFP fluorescence images. Panels **A** and **B** show cells with paired P30-CFP and P41-YFP foci; circle, faint and diffuse P30-CFP focus. Panels **C** and **D** show cells with unpaired P41-YFP foci (arrows).

3.4C, 3.4D, arrows), a frequency similar to that of gliding cells having two P41-YFP foci. Taken together, these observations are consistent with a model where P41 is incorporated into the developing terminal organelle before P30 or P65; time-lapse images were consistent with appearance of P41 before P30, but the toxicity and rapid photobleaching of CFP limited image capture (data not shown). Thus, we were unable, for example, to determine whether new P41 foci invariably matured into terminal organelles on the basis of subsequent acquisition of a P30 focus. However, those new P41 foci were observed in phase contrast images to gain adherence and gliding function (data not shown).

Quantitation of fluorescence suggests that new foci develop de novo. Electron microscopic images of the *M. pneumoniae* terminal organelle splitting at the distal end (13) suggest that its duplication may occur by a semi-conservative process. By this scenario one would predict a rapid decrease in fluorescence intensity of an existing P30-YFP focus when a new focus appeared. Preliminary analysis of relative fluorescence intensities of existing and nascent P30-YFP foci over time suggested that no such decrease occurred (Fig. 3.1D). However, for a more systematic examination we compared P30-YFP fluorescence intensity over time for existing foci in cells that were not dividing, with that in cells forming a second focus during the observation period (Fig. 3.5). Each group exhibited the same gradual decline in fluorescence of the existing P30-YFP focus, suggesting that P30 accumulating at a nascent terminal organelle did not originate from a pre-existing terminal organelle but from new protein synthesis. Interestingly, the maximum intensity of new P30-YFP foci appearing during each observation was typically lower than that of existing foci at 0 h, suggesting that some photobleaching of P30-YFP occurred prior to localization, providing a parameter by which it might be possible to establish the timeframe from synthesis to focus formation. Finally, to test the requirement for new protein synthesis directly in the appearance of new P30-YFP foci during mycoplasma growth, we examined wild-type cells over time in the

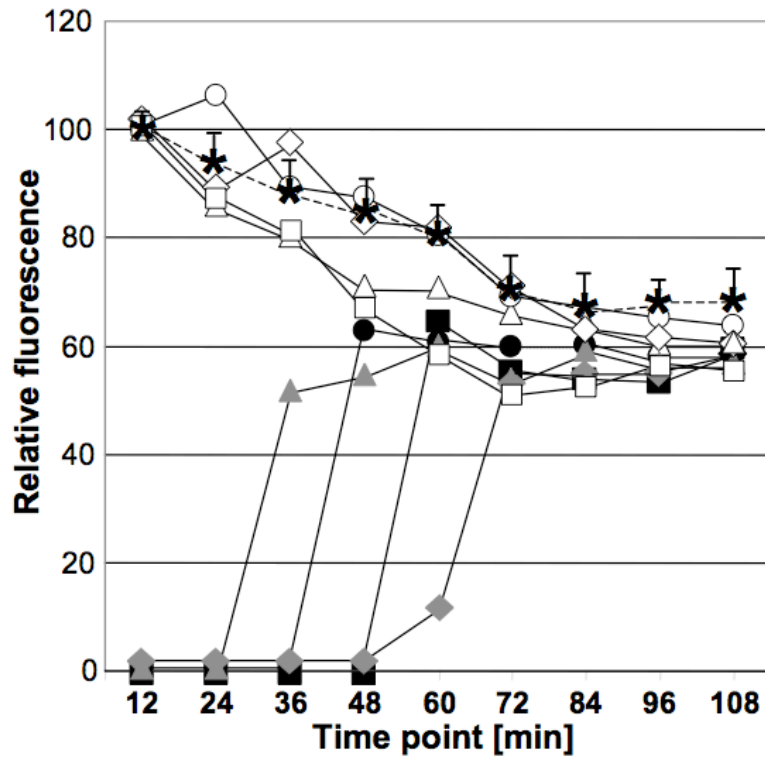


Fig. 3.5. Quantitation of P30-YFP fluorescence intensity over time. Fluorescence was measured at 12-min intervals for ten cells that formed new P30-YFP foci during the observation period and ten cells that did not. The average fluorescence for the latter group (asterisks / dashed line with positive standard deviations indicated) is compared to fluorescence of existing (open shapes) and new (solid shapes) P30-YFP foci in four individual, representative cells which began with a single fluorescent focus that was duplicated at approximately the same time point during the observation period and for which no collisions or other contact with neighboring cells was observed.

presence of chloramphenicol (30 µg/ml). Inhibition of protein synthesis blocked formation of new fluorescent foci, while a normal pattern of terminal organelle appearance returned with removal of the chloramphenicol (data not shown).

Discussion

Early studies by light microscopy and microcinematography suggested that the terminal organelle of *M. pneumoniae* duplicates prior to cell division. However, the exceptionally small size of *M. pneumoniae* cells, the limits of resolution, and therefore the inability to identify terminal organelles definitively, made a conclusive determination impossible. More recently Seto et al. correlated the number and position of terminal organelles with genome content (18), but their technique required cell fixation, hence it was not possible to document the sequence of events that led to those images or to rule out the potential introduction of fixation artifacts. In the current study we used fluorescent protein fusions and digital image analysis to examine assembly and function of the terminal organelle over time in growing cultures, confirming that *M. pneumoniae* terminal organelle duplication and separation precede cell division. Moreover, our findings add considerable detail regarding development and gain of function for nascent terminal organelles and demonstrate that, contrary to previous thinking (18), multiple new terminal organelles often form before cell division is observed.

The coordination of gliding motility and cell division was noted previously (8, 16, 26); our findings support and extend the current understanding of that relationship. Gliding ceased as nascent P30 foci emerged, as expected. However, the frequent presence of nascent P41-YFP foci in gliding cells suggests that assembly of the new terminal organelle begins earlier than previously recognized. Furthermore, subsequent separation of terminal organelles was a function of resumption of gliding as opposed to migration of the nascent

structure along the cell body to the opposite pole by some undefined mechanism, as has been considered (26). Almost without exception (>98% of the cells examined), an existing terminal organelle initiated gliding and separation while the newest structure remained transiently fixed. For example in Fig. 3.1D, between 3 and 4.5 h the 2nd focus (green arrowhead) remained fixed while the first focus (yellow arrowhead) glided to the right, and between 6 and 7.5 h the 2nd focus acquired gliding capacity and moved downward in the field while the 3rd focus (orange arrowhead, now the newest), remained fixed. Thus, P30 is required for both adherence and gliding motility (20, 27), but acquisition of the capacity to adhere occurred rapidly, while the initiation of gliding by a nascent terminal organelle was delayed, hence the localization P30 to a nascent terminal organelle was not sufficient for gliding competence. In addition, at times terminal organelles appeared to release from the glass to allow retraction of the cell body (Fig. 3.1D, white arrowhead). We saw no change in the appearance of a fluorescent focus for P30, P41 or P65 during retraction, and the molecular mechanism responsible for release from the glass is not known. Regardless, both gliding and adherence appear to be dynamic functions during mycoplasma development and cell division. Finally, analysis of the non-motile mutant III-4 demonstrated that loss of gliding function impairs normal separation of developing terminal organelles, expanding upon recent findings that cell extension during gliding is responsible for the characteristic filamentous morphology of *M. pneumoniae* (20). Like mutant II-3 in that study, mutant III-4 here grows both on agar and in liquid culture, hence the inability of daughter cells to separate normally is not lethal. However, the large cell clusters characteristic of both mutants in liquid culture (unpublished observation) likely reflect a failure to separate rather than a propensity to aggregate.

On occasion we observed duplication and separation of terminal organelles in wild-type mycoplasmas followed directly by cytokinesis, consistent with the existing model for *M.*

pneumoniae cell division (18). However, for most dividing cells examined additional terminal organelles developed before new daughter cells emerged, representing a major shift in our understanding of *M. pneumoniae* cell division (Fig. 3.6) and indicating that terminal organelle duplication and cytokinesis are not tightly coordinated under these culture conditions. The extent to which terminal organelle duplication is coordinated with DNA replication remains unclear; we did not examine DNA content here, and the studies by Seto et al. (18) correlating DNA content with number and location of terminal organelles were limited to *M. pneumoniae* cells having only one or two terminal organelles.

Images of wild-type *M. pneumoniae* by electron microscopy occasionally reveal cells with a bifurcated terminal organelle (13), suggesting that formation of a nascent structure may begin with the splitting of the existing terminal organelle. However, in the current study the fluorescence intensity patterns in cells forming a second focus during the observation period did not support this model but suggested de novo incorporation into nascent terminal organelles for both P30 (Fig. 3.5) and P65 (data not shown) at the tip of the terminal organelle and P41 (data not shown) at the base of this structure. While it remains to be determined whether the same applies for proteins known to be specifically associated with the electron-dense core, the inhibition of nascent terminal organelle formation in cells under chloramphenicol arrest is consistent with a requirement for new protein synthesis. This conclusion is likewise consistent with electron cryotomography images (14, 15) in which the dimensions of the two rods of the core are not identical, and therefore fail to support a semi-conservative process. Taken together these observations expand our current understanding of terminal organelle development but also raise new questions regarding regulation of synthesis and assembly of this structure and the coordination of the process with cell division, particularly given the dearth of typical transcriptional regulators in *M. pneumoniae* (2).

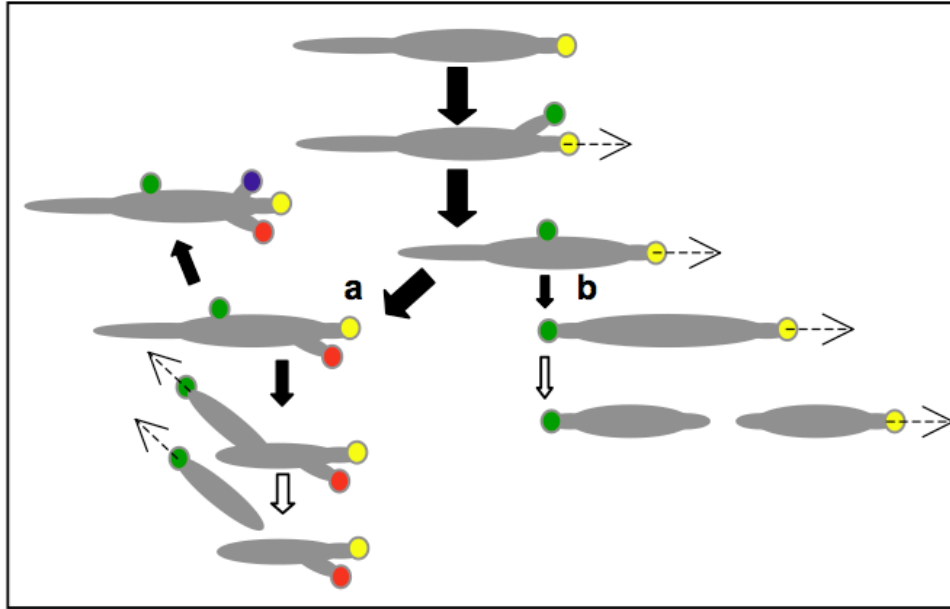


Fig. 3.6. Model for *M. pneumoniae* terminal organelle duplication and growth cycle.

The yellow circle represents the initial terminal organelle, while green, red, and blue circles represent subsequent organelles, appearing in that order. The dashed arrows reflect movement of the indicated terminal organelle, while open arrows indicate cytokinesis. Solid arrows indicate steps in the cell cycle, with arrow size reflecting relative frequency. In most cases multiple duplications of the terminal organelle occur before daughter cells emerge (**a**), although rarely some cells do undergo a single duplication of the terminal organelle followed by cytokinesis (**b**), according to the previous model for cell division in *M. pneumoniae* (18).

Cataloging the downstream consequences of loss of essential binding partners in terminal organelle assembly has yielded a model whereby some components are predicted to be incorporated early and others, including P30 and P65, are incorporated later (9, 18, 23). The ability to follow the relative order of appearance of new fluorescent foci in cells producing two different protein fusions makes it possible to test that model, albeit within the limitations of time-lapse imaging. In pair-wise comparisons P30 and P65 fluorescent foci developed concurrently, consistent with the prediction that both are required relatively late in terminal organelle assembly. In contrast, P41 foci appeared before P30, suggesting that this cytoskeletal protein is required earlier in the assembly sequence. However, it was not possible to follow terminal organelle development for many frames with CFP fusions, which exhibited rapid photobleaching and toxicity.

In conclusion, this study demonstrates the feasibility of spatial and temporal analysis of macromolecular assembly using fluorescent protein fusion technology in mycoplasmas, extraordinarily small cell wall-less bacteria. Furthermore, our findings elucidate further the relationship between the assembly of the terminal organelle, adherence, and gliding motility in mycoplasma cell division. In addition, our results expand the current understanding of the mechanism of terminal organelle duplication and provide evidence for the order of assembly of this complex structure by an otherwise minimal microorganism.

Materials and Methods

Generation of *M. pneumoniae* transformants expressing recombinant protein fusions.

Characterization of recombinant P30-YFP in wild-type *M. pneumoniae* was described previously (20); its introduction into *M. pneumoniae* mutant III-4 in transposon vector pMT85, which delivers recombinant alleles to the mycoplasma chromosome in a random-like manner, was by established protocols (20). YFP fusions to *M. pneumoniae* proteins P65

and P41 were constructed using plasmid pEYFP (Clontech, Mt. View, CA) as described by Kenri et al. (25) with minor primer modifications to facilitate cloning of the PCR amplification products into *Bam*H1 and *Eco*R1 sites in pMT85. *M. pneumoniae* transformants were evaluated for expression of the recombinant fusion proteins by Western immunoblotting and fluorescence microscopy; transformants for which transposition occurred at intergenic loci, as determined by sequencing across the insertion site and comparison with the genome sequence (2, 22), were evaluated further. P30-CFP was constructed as for P30-YFP but using plasmid pECFP (Clontech). For generation of recombinant transposons encoding two fusions in tandem, the gene for P30-CFP was excised using *Xba*I and cloned into the corresponding site within the pMT85 derivatives encoding P41-YFP or P65-YFP described above. Constructs were transformed into wild-type *M. pneumoniae*, and multiple transformants were evaluated for the expression of each recombinant protein by Western immunoblotting and fluorescence microscopy.

Fluorescence microscopy. For analysis of terminal organelle assembly in actively dividing *M. pneumoniae*, frozen stocks (wild-type or the P30 mutant + P30-YFP) were thawed, diluted 1:40 in SP-4 medium containing 3% gelatin, and incubated overnight in chamber slides (20). Digital phase-contrast and fluorescence images were captured with an exposure time of 1.0 sec and frame intervals ranging from 6-60 min on a Leica DM IRM epifluorescence inverted microscope (Wetzlar, Germany) and merged. Fluorescence emission of P30-YFP, P41-YFP, and P65-YFP foci was quantitated for individual cells using the profiling module of Openlab v3.0-4.0 software (Improvision, Lexington, MA). Emission intensities were calculated as the mean level of fluorescence signal emitted relative to the mean background noise of the immediately adjacent cell-free area. Fluorescent intensities were quantified for single pixels (65 nm²) resolving nascent terminal organelles assembling

as near as 130 nm from the parental structure. Co-localization of P30-CFP with P41-YFP or P65-YFP in actively dividing cells was examined using an exposure of 1.0 sec with fluorescence excitation of both signals in rapid succession by alternating between dichroic YFP and CFP filter cubes (Chroma, Rockingham, VT).

Acknowledgements

We thank R. Herrmann for providing pMT85 prior to publication, M. Balish for reading this manuscript and M. Farmer for technical assistance. This work was supported by Public Health Service research grants AI22362 and AI49194 from the National Institute of Allergy and Infectious Diseases to D.C.K.

1. Waites, K. B. & Talkington, D.F. (2004) *Clin. Microbiol. Rev.* **17**, 697-728.
2. Himmelreich, R., Hilbert, H. Plagens, H., Pirkl, E., Li, B.C. & Herrmann, R. (1996) *Nucleic Acids Res.* **24**, 4420-4449.
3. Dandekar, T., Huynen, M., Regula, J.T., Ueberle, B., Zimmermann, C.U., Andrade, M.A., Doerks, T., Sanchez-Pulido, L., Snel, B., Suyama, M., Yuan, Y.P., Herrmann, R. & Bork, P. (2000) *Nucleic Acids Res.* **28**, 3278-3288.
4. Morowitz, H.J. (1984) *Isr. J. Med. Sci.* **20**, 750-753.
5. Gobel, U., Speth, V. & Bredt, B. (1981) *J. Cell. Biol.* **91**, 537-543.
6. Meng, K.E. & Pfister, R.M. (1980) *J. Bacteriol.* **144**, 390-399.
7. Collier, A.M. & Clyde, W.A. Jr. (1974) *Am. Rev. Respir. Dis.* **110**, 765-773.
8. Radestock, U. & Bredt, W. (1977) *J. Bacteriol.* **129**, 1495-1501.
9. Krause, D.C. & Balish, M.F. (2004) *Mol. Microbiol.* **51**, 917-924.
10. Seto, S. & Miyata, M. (2003) *J. Bacteriol.* **185**, 1082-1091.

11. Baseman, J.B., Cole, R.M., Krause, D.C. & Leith, D.K. (1982) *J. Bacteriol.* **151**, 1514-1522.
12. Biberfeld, G. & Biberfeld, P. (1970) *J. Bacteriol.* **102**, 855-861.
13. Hegermann, J., Herrmann, R. & Mayer, F. (2002) *Naturwissenschaften* **89**, 453-458.
14. Henderson, G.P. & Jensen, G.J. (2006) *Mol. Microbiol.* **60**, 376-385.
15. Seybert, A., Herrmann, R. and Franqakis, A.S. (2006) *J. Struct. Biol.* In press.
16. Bredt, W. (1968) *Pathol. Microbiol.* **32**, 321-326.
17. Boatman, E.S. (1979) in *The Mycoplasmas*, eds Barile, M.F. & Razin, S. (Academic Press, New York), Vol. 1, pp. 63-102.
18. Seto, S., Layh-Schmitt, G., Kenri, T. & Miyata, M. (2001) *J. Bacteriol.* **183**, 1621-1630.
19. Baseman, J.B., Morrison-Plummer, J., Drouillard, D., Puleo-Schepke, B., Tryon, V.V. & Holt, S.C. (1987) *Isr. J. Med. Sci.* **23**, 474-479.
20. Hasselbring, B.M., Jordan, J.L. & Krause, D.C. (2005) *J. Bacteriol.* **187**, 6281-6289.
21. Krause, D.C., Leith, D.K., Wilson, R.M., & Baseman, J.B. (1982) *Infect. Immun.* **35**, 809-817.
22. Hasselbring, B.M., Page, C. A., Sheppard, E. S., & Krause, D.C. (2006) *J. Bacteriol.* **188**, 6335-6345.
23. Krause, D.C. & Balish, M.F. (2001) *FEMS Microbiol. Lett.* **198**, 1-7.
24. Krause, D.C., Proft, T., Hedreyda, C.T., Hilbert, H., Plagens, H. & Herrmann, R. (1997) *J. Bacteriol.* **179**, 2668-2677.
25. Kenri, T., Seto, S., Horino, A., Sasaki, Y., Sasaki, T. & Miyata, M. (2004) *J. Bacteriol.* **186**, 6944-6955.
26. Rodwell, A.W. & Mitchell, A. (1979) in *The Mycoplasmas*, eds Barile, M.F. & Razin, S. (Academic Press, New York), Vol. 1, pp. 103-132.

27. Romero-Arroyo, C. E., Jordan, J., Peacock, S.J., Willby, M.J., Farmer, M.A., & Krause, D.C. (1999). *J. Bacteriol.* **181**, 1079-1087.

Materials and Methods, Supplementary

Generation of *M. pneumoniae* transformants expressing recombinant protein fusions.

Generation of recombinant P30-EYFP, its delivery into *M. pneumoniae* and functionality in complementing P30⁻ mutant II-3 have been described in detail previously (20); in the current study P30-EYFP was likewise introduced into wild-type *M. pneumoniae* as well as non-motile mutant III-4 (21). Transformants were filter-cloned and assessed by western immunoblot analysis for the production of P30-EYFP using P30⁻ (19) and GFP⁻ (BD Biosciences) specific antibodies at 1:750 and 1:000, respectively, and by direct fluorescence visualization (20). Transposon insertion sites were determined by sequencing across the insertion site for wild-type transformants (20); only transformants having insertions at intergenic sites were analyzed further.

Sequences required for translation initiation in mycoplasmas are poorly understood hence translational fusions of EYFP to proteins P65 and P41 were constructed as described by Kenri et al. (25) with minor modifications. Wild-type MPN309 and MPN311 alleles, encoding P65 and P41, respectively, were amplified separately by PCR from chromosomal DNA. A *Bsr*G1 restriction site was engineered by mutagenic primer to replace the second and third codons of each gene, and an *Eco*RI restriction site was likewise engineered downstream of the stop codon for each. The resulting PCR products were cloned into the corresponding sites in pEYFP (Clontech), generating plasmids pEYFP-MPN309 and pEYFP-MPN311. The promoter region of the P65 operon, which directs transcription of both MPN309 and MPN311 (24), was amplified by PCR, engineering a *Bam*H1 site upstream of the promoter region and an *Nco*I site replacing the tenth and eleventh codons of MPN309.

The resulting PCR product was cloned into the corresponding sites of pEYFP-MPN309 and pEYFP-MPN311. The P65 promoter-EYFP-MPN309 and P65 promoter-EYFP-MPN311 constructs were then excised by digestion with *Bam*HI and *Eco*RI and cloned separately into the corresponding sites of transposon vector pMT85 (20). Each construct was transformed into wild-type *M. pneumoniae* according to established procedures and the site of pMT85 transposition was determined for multiple filter clones. Transformants for which insertion occurred at intergenic loci were evaluated further. The production and terminal organelle localization (25) of each recombinant fusion was verified by visual screening and by Western immunoblot analysis with P41- and P65-specific sera at 1:1000 and 1:3000, respectively; and GFP-specific antibodies at 1:1000.

To assess the incorporation of P41 and P65 relative to P30 into developing terminal organelles using fluorescent fusions in pairs, a P30-ECFP fusion was constructed as for P30-EYFP, using plasmid pECFP (Clontech) rather than pEYFP. P30-ECFP liberated from pECFP using restriction endonuclease *Xba*I was cloned into the corresponding site in pMT85 containing either the P65 promoter-EYFP-P65 or P65 promoter-EYFP-P41 construct. Each was transformed into wild-type *M. pneumoniae*, and multiple transformants were evaluated for the expression of the recombinant proteins by direct fluorescence visualization and by western analysis as described above.

Fluorescence Microscopy

To analyze terminal organelle development in growing *M. pneumoniae* cultures, frozen log-phase cultures were thawed, diluted 1:40 in fresh SP-4 medium, and incubated overnight in chamber slides (20). For analysis of P30-EYFP, P65-EYFP, or P41-EYFP appearance in nascent terminal organelles, digital phase-contrast and fluorescence images were captured with an exposure time of 1.0 sec and frame intervals ranging from 6-60 min on a Leica DM IRM epifluorescence inverted microscope (Wetzlar, Germany) and merged (20). Co-

localization of P30-ECFP with EYFP-P41 or EYFP-P65 in actively growing cells was likewise determined using exposures of 1.0 sec with fluorescence excitation of both signals recorded in rapid succession by alternating between dichroic EYFP and ECFP filter cubes (Chroma). Images were merged as described (20).

Fluorescence emission of P30-YFP, P41-YFP, and P65-YFP foci was quantitated for individual cells using the profiling module of Openlab v3.0-4.0 software (Improvision, Lexington, MA). Emission intensities were calculated as the mean level of fluorescence signal emitted relative to the mean background noise of the immediately adjacent cell-free area. Fluorescent intensities were quantified for single pixels (65 nm^2) resolving nascent terminal organelles assembling as near as 130 nm from the parental structure.

To assess the effects of translational arrest on terminal organelle development, wild-type cells producing P30-EYFP were incubated overnight as described above. Terminal organelle development was monitored over 2 hr with phase and fluorescence images captured at 12 min intervals, after which chloramphenicol (Cm; $30 \mu\text{g/ml}$) was added to the chamber slides and cultures were monitored an additional 2 hr at 12 min intervals, during which time terminal organelle development was observed to cease. Cm-arrested cultures were monitored an additional 8 hr to verify complete inhibition of terminal organelle formation, after which chamber slides were washed 5x with fresh SP-4 medium, incubated an additional 4-12 hr, and then examined / imaged at 12 min intervals to verify the resumption of terminal organelle development.

Supplementary Movie Legends

Supplementary movie 1. Digital, time-lapse, phase contrast / fluorescence microscopy of terminal organelle appearance and separation during *M. pneumoniae*

growth. Mutant II-3 + recombinant P30-YFP has a wild-type phenotype (20); shown are phase contrast and fluorescence images of II-3 + P30-YFP taken at 6-min intervals over a 30-min observation period. Digital phase contrast and fluorescence images were captured separately and then merged.

Supplementary movie 2. Digital, time-lapse, phase contrast / fluorescence microscopy of terminal organelle appearance, development, and separation during *M. pneumoniae* growth. Shown are phase contrast and fluorescence images of II-3 + P30-YFP as in supplementary movie 1, taken at 24-min intervals over a 2-h observation period.

Supplementary movie 3. Digital, time-lapse, phase contrast / fluorescence microscopy of terminal organelle appearance, development, and separation during *M. pneumoniae* growth. Shown are phase contrast and fluorescence images of II-3 + P30-YFP as in supplementary movie 1, taken at 10-min intervals over an 11-h observation period.

Supplementary movie 4. Digital, time-lapse, phase contrast / fluorescence microscopy demonstrating the appearance of P41-YFP before cessation of gliding. Shown are phase contrast and fluorescence images of wild-type *M. pneumoniae* + P41-YFP (yellow) and P30-CFP (blue) taken over a 24-min observation period. Digital phase contrast and fluorescence images were captured separately and then merged.

CHAPTER 4

TRANSPOSON MUTAGENESIS IDENTIFIES GENES ASSOCIATED WITH *MYCOPLASMA PNEUMONIAE* GLIDING MOTILITY¹

¹ Hasselbring *et al.* 2006. *The Journal of Bacteriology*. 188: 6335-45
Reprinted here with permission of publisher.

ABSTRACT

The wall-less prokaryote *Mycoplasma pneumoniae*, a common cause of chronic respiratory tract infections in humans, is considered among the smallest and simplest known cells capable of self-replication yet has a complex architecture with a novel cytoskeleton and differentiated terminal organelle which function in adherence, cell division, and gliding motility. Recent findings have begun to elucidate the hierarchy of protein interactions required for terminal organelle assembly, but the engineering of its gliding machinery is largely unknown. In the current study we assessed gliding in cytoadherence mutants lacking terminal organelle proteins B, C, P1, and HMW1. Furthermore, we screened over 3500 *M. pneumoniae* transposon mutants individually to identify genes associated with gliding but dispensable for cytoadherence. Forty-seven transformants having motility defects were characterized further, with transposon insertions mapping to 32 different ORFs widely distributed about the *M. pneumoniae* genome; 30 of these were dispensable for cytoadherence. We confirmed clonality of selected transformants by Southern blot hybridization and PCR analysis and characterized satellite growth and gliding by microcinematography. For some mutants satellite growth was absent or developed more slowly than wild-type. Others produced lawn-like growth largely devoid of typical microcolonies, while still others had a dull, asymmetrical leading edge or a filamentous appearance to colony spreading. All mutants exhibited substantially reduced gliding velocities and/or frequencies. These findings expand significantly our understanding of the complexity of *M. pneumoniae* gliding and the identity of possible elements of the gliding machinery, providing a foundation for detailed analysis of the engineering and regulation of motility in this unusual prokaryote.

The cell wall-less prokaryote *Mycoplasma pneumoniae* establishes chronic infections of the human respiratory tract resulting in bronchitis and atypical or "walking" pneumonia and accounting for up to 30% of all community-acquired pneumonia (49). With a minimal genome lacking genes for typical transcriptional regulators, two-component systems, and pathways for de novo synthesis of most macromolecular building blocks including nucleotides and amino acids (8, 21), *M. pneumoniae* is considered to be among the simplest organisms capable of self replication. And yet this unusual species exhibits remarkable architectural complexity, with a dynamic cytoskeleton and a specialized, membrane-bound polar cell extension or terminal organelle having an elaborate macromolecular core (2, 12, 20, 33). The terminal organelle functions in diverse cellular processes that include adherence to host epithelium (cytadherence) and cell division (7, 17, 40) and engages as the leading end as *M. pneumoniae* cells glide over solid surfaces (3). Recent studies have begun to establish the assembly sequence in terminal organelle development and the hierarchy of protein interactions required for core stability and adhesin trafficking (17, 26, 41), but the macromolecular components and engineering of the gliding machinery are unknown. Inspection of the 816-kbp *M. pneumoniae* genome reveals no homology to proteins that function in bacterial motility of any type in walled species, and even within the genus *Mycoplasma* there appear to be distinct gliding mechanisms, as known components of the *Mycoplasma mobile* gliding machinery are not found in *M. pneumoniae* (23, 42, 47, 48).

Analysis by electron cryotomography suggests that the *M. pneumoniae* terminal organelle core is conformationally flexible, prompting speculation that this structure powers gliding by cyclic contraction and extension (20). Although the constituents of the terminal organelle core are largely unknown, proteins HMW1, HMW2, and HMW3 are believed to be involved in core architecture, as they localize to the terminal organelle, are required for core

development and stability, and partition in the Triton X-100-insoluble cytoskeletal fraction, of which the terminal organelle core is a prominent component (12, 26, 33). However, the impact of loss of these proteins on cell gliding has not been assessed. Furthermore, about 100 proteins comprise the *M. pneumoniae* cytoskeletal fraction (36), many of which have no assigned function.

Cytadhesins P1 and P30 are the only *M. pneumoniae* proteins to date for which a role in gliding has been implicated. Gliding velocity and substrate binding are reduced in the presence of P1-specific antibodies (39), and loss of P30 renders *M. pneumoniae* non-cytadherent and non-motile (15). A wild-type phenotype is restored in the P30⁻ mutant with transposon delivery of the wild-type MPN453 allele encoding P30 (15). In contrast, the altered P30 allele P30R, differing from P30 by 17 residues in the middle of the protein, confers cytodherence at about 70% of wild-type but a gliding velocity at only 5% of wild-type (15). Cytodherence and gliding are also separable in the closely related *Mycoplasma genitalium*, where transposon insertion in MG200 or MG386 significantly reduces cell gliding velocity and frequency but only marginally affects cytodherence (34).

In the current study we established that the *M. pneumoniae* terminal organelle proteins HMW1 as well as B and/or C are required for gliding motility. Furthermore, we identified *M. pneumoniae* genes specifically associated with cell gliding but dispensable for cytodherence. Over 3500 transformants were screened individually, approximately 100 of which had a satellite growth-altered (SGA) phenotype, indicating a likely gliding defect (15). This manifested as the complete absence or impaired development of satellite growth, the production of a lawn-like growth largely devoid of typical microcolonies, the presence of a dull, asymmetrical leading edge to colony spreading, or a filamentous appearance to spreading. Gene disruptions were defined for each SGA mutant, identifying 47 distinct transposon insertions in 32 genes, which were grouped according to predicted function.

Hemadsorption (HA) was assessed for each, identifying 30 genes associated with gliding motility but dispensable for cytodherence. Gliding by individual cells was measured by microcinematography, for selected mutants, each exhibiting substantially reduced gliding velocities and/or gliding frequencies. Finally, representative transformants were evaluated for likely polar effects on transcription based on transposon orientation relative to flanking genes and the position of probable promoter sequences.

MATERIALS AND METHODS

Mycoplasma strains and culture conditions. Wild-type *M. pneumoniae* strain M129 (31), mutant II-3 with recombinant Tn4001 carrying a wild-type P30 allele [II-3/P30WT; (15)], and cytodherence mutants III-4, IV-22 (27), and M6 (29) were described previously (Table 4.1). Wild-type M129 was transformed with transposon Tn4001.2065 (25) in four independent electroporations according to established procedures (19). Mixed transformant populations were transferred to tissue culture flasks containing 25 ml Hayflick medium (18) + 18 $\mu\text{g/ml}$ gentamicin and grown to mid-log phase. Gentamicin selection was maintained for subsequent culture of transformants except as indicated. Polystyrene-adherent cells were recovered in order to enrich for transformants likely to retain cytodherence. These were diluted in fresh medium in tissue culture flasks, again enriched for polystyrene adherence, collected in fresh medium, aliquoted, and stored at $-80\text{ }^{\circ}\text{C}$.

Isolation of motility mutants. Mixed transformant populations were thawed, passed twice through $0.22\text{ }\mu\text{m}$ filters to disperse aggregates, diluted, and plated on PPLO agar (6). After 7 d at 37°C plates were over-laid with blood agar, and 2 d later colonies were visible as hemolytic plaques, making it easier to pick individual transformants. These were selected at random, cultured in $400\text{ }\mu\text{l}$ Hayflick medium to mid-log phase (6-8 days), and stored at $-80\text{ }^{\circ}\text{C}$. Individual transformants were later thawed, diluted, and inoculated into

600 μ l Hayflick medium containing 3% gelatin in individual wells of 24-well tissue culture plates. Satellite growth around microcolonies was evaluated by phase-contrast microscopy using a Nikon DIAPHOT microscope (20X objective) at 24-h intervals after 4-8 d, relative to positive controls [wild-type *M. pneumoniae* and strain II-3/P30WT (15)]. Transformants exhibiting reduced or altered satellite growth were screened two additional times in separate experiments to verify the altered phenotype before cataloging and storage.

Insertion mapping and filter cloning. Transposon Tn4001.2065 contains within the IS256L element a HindIII site immediately downstream of a promoterless β -galactosidase gene, an *Escherichia coli* replication origin, and a β -lactamase gene (25). To map transposon insertion sites, genomic DNA isolated from individual *M. pneumoniae* transformants was digested with HindIII, diluted, re-ligated, and transformed into *E. coli*. Plasmid DNA isolated from ampicillin-resistant *E. coli* clones was sequenced across the insertion site using the transposon-specific, outward-directed primer 5'-CACTCCAGCCAGCTTTCCGGCACCGCTTCT-3' for comparison with the published genome sequence (8, 21). Each primary transformant stock was then filtered sequentially through 0.45 and 0.22 μ m pore-size filters, serially diluted, and plated on PPLO agar. Eight progeny colonies were isolated for each and re-evaluated for satellite growth as described. Southern hybridization was performed (38) using multiple probes to ensure presence of Tn4001.2065 in single copy and that IS256 had not duplicated independently and inserted elsewhere in the genome.

Western immunoblotting. Samples were analyzed by sodium dodecylsulfate polyacrylamide gel electrophoresis and Western immunoblotting as described (15), using monoclonal P30-specific antibody (1) or rabbit antisera to P1 (50), P24 (10), P65 (35), P41 (10), B (50), C (50), HMW1 (43), HMW2 (53), or HMW3 (44).

Analysis of glass binding and HA. Binding of mycoplasmas to glass was measured as described (15). HA is a convenient model for *M. pneumoniae* cytoadherence and was measured qualitatively as described (27) except using sheep blood.

Time-lapse analysis of satellite growth. Satellite growth was evaluated for a minimum of three filter-cloned progeny per primary transformant. Cultures were diluted in SP-4 medium (45) + 3% gelatin, inoculated into 4-well borosilicate glass chamber slides (Nunc Nalgene, Naperville, IL), and incubated at 37°C. Satellite growth around colonies was recorded at 12-h intervals (15).

Quantitation of cell gliding. Average and corrected gliding velocities, gliding frequencies, and percent-time resting were quantitated as described (15) for individual cells using the Openlab measurements module v3.51-4.0.4 (Improvision; Lexington, MA), with generally 20-100 cells per field at the start of image capture, and gliding velocities and frequencies measured for a minimum of 30 cells per transformant from at least two independent experiments (15). A resting period was assigned when no net cell movement of greater than 1 pixel (0.0645 μm) occurred between sequential frames (in most cases 1 frame per second; 15). Corrected gliding velocities were calculated as distance traveled by a cell divided by total time of the field interval minus the amount of time spent in resting periods.

RESULTS

Gliding capacity of cytoadherence mutants M6, III-4, and IV-22. *M. pneumoniae* cytoadherence mutant II-3 is non-motile, indicating a requirement for the cytoadherence-associated protein P30 in cell gliding (15). Proteins B and C, also designated P90 and P40, respectively, are thought to function as a complex with P30 and the adhesin P1 in receptor binding (28, 37, 50). To assess their requirement in gliding we examined cytoadherence

mutants III-4 and IV-22 for satellite growth and cell gliding (Table 4.1). Neither mutant produced satellite growth over 96 h (Fig. 4.1) or extended incubations up to 168 h (not shown), and time-lapse digital microcinematography confirmed a non-motile phenotype. Likewise, no motility was observed for cytoadherence mutant M6 (Fig. 4.1), which produces a truncated P30 and lacks HMW1 (29), and as a result fails to assemble an electron-dense core or localize P1 properly (41, 53). For reasons that are not clear the leading edge of mutant M6 colonies had a filamentous appearance compared to the smooth edge seen with mutants III-4 and IV-22, indicating that cell motility alone does not determine colony appearance by this technique. We measured glass binding by each mutant under conditions identical to those used to examine cell gliding. Glass binding ranged from 78-104% of wild-type (Table 4.1), indicating that except perhaps for mutant IV-22, the loss of gliding motility was not a function of poor binding to the inert surface.

Isolation of SGA transformants. We used transposon mutagenesis to identify additional *M. pneumoniae* genes associated with gliding motility. Over 3500 transformants were screened individually for satellite growth; approximately 100 of these exhibited abnormal growth patterns relative to wild-type controls. The nature of the altered satellite growth varied considerably: some transformants had a dull, asymmetrical leading edge to colony spreading (Fig 4.2B-C), while others exhibited a filamentous spreading (Fig. 4.2D). Many produced satellite growth radiating symmetrically but at a much lower density than wild-type (Fig 4.2E-F), while still others exhibited lawn-like growth devoid of typical microcolonies (Fig 4.2G) or barely discernable satellite growth (Fig 4.2H). Each SGA insertion mutant was evaluated in three separate experiments to verify the altered phenotype.

TABLE 4.1. Protein profiles, gliding capacity, and glass binding by wild-type *M. pneumoniae* (WT) and the indicated cytoadherence-negative mutants.

Strain	Levels of Cytadherence-Associated Proteins						Gliding velocity ($\mu\text{m}/\text{sec}$)	Cell gliding frequency	Glass-binding capability
	P1	P40 /P90	P30	HMW1	HMW2	HMW3			
WT	+++ ^a	+++	+++	+++	+++	+++	0.32	28%	100
III-4	+++	-	+++	+++	+++	+++	0	0	104
IV-22	-	-	+++	+++	+++	+++	0	0	78 ^c
M6	+++	+++	++ ^b	-	+	+	0	0	92

^a Relative levels of the indicated proteins: +++, wild-type levels; ++, slightly

reduced levels; +, substantially reduced levels; -, protein absent

^b Protein truncated

^c Significantly lower than ($p < 0.05$)

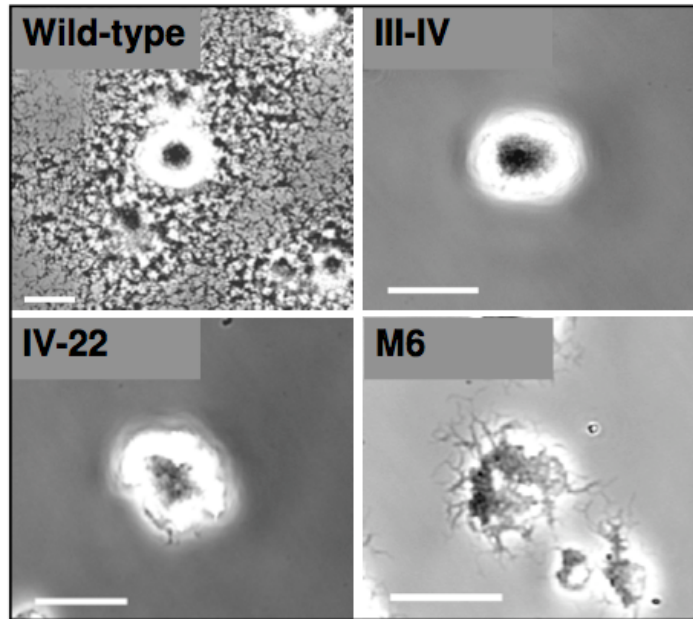


FIG. 4.1. Analysis of *M. pneumoniae* cytoadherence mutant satellite growth. Colony morphology of wild-type, mutant III-4, mutant IV-22, and mutant M6 cultured on glass in SP-4 medium + 3% gelatin. Images were captured at 96 h post-inoculation. Scale bars: 30 μ m.

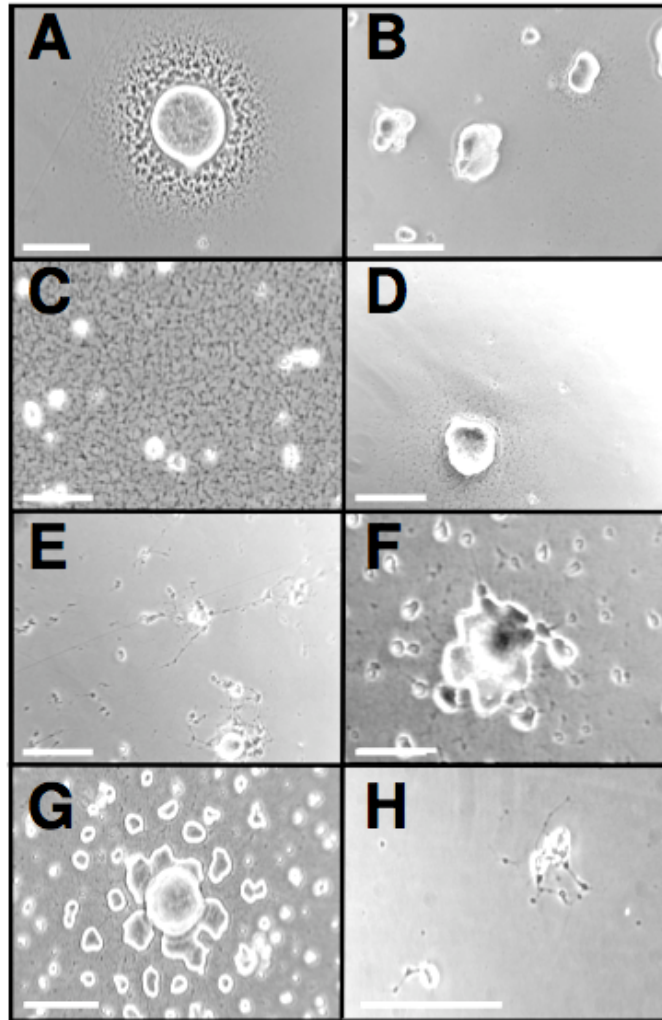


FIG. 4.2. Representative satellite growth patterns of *M. pneumoniae* SGA mutants. Satellite growth for selected SGA mutants cultured on polystyrene in SP-4 medium + 3% gelatin was recorded at 96 h post-inoculation. **A**, mutant II-3/WT P30 (positive control; 14); **B**, mutant 320-30; **C**, mutant 359-130; **D**, mutant 311-22; **E**, mutant 308-274; **F**, mutant 110-112; **G**, mutant 254-70; **H**, mutant 387-2. Scale bars: 40 μ m.

Identification of transposon-disrupted genes. SGA transformants were sequenced across the transposon-insertion site. Several transformants had identical insertion sites and were likely siblings, reinforcing the fidelity of the screening protocol. Sequencing revealed more than one insertion site for about 30% of the SGA transformants, indicating likely mixed populations; these were retained but not examined further here. Likewise, SGA transformants with Tn4001 at intergenic sites were retained but not characterized further here. Among the 47 SGA transformants characterized further (Table 4.2), 32 putative gliding-associated genes were identified scattered around the chromosome rather than clustered. These were grouped according to predicted function of their gene products (8): (i) metabolic enzymes and transport system components; (ii) DNA- or protein-modifying enzymes, and (iii) conserved or genus-specific proteins of unknown function (Table 4.2). The designation for each mutant reflects the disrupted gene (8) and the residue at which its predicted protein product was disrupted, e.g. transformant 311-22 had a transposon insertion in MPN311 disrupting the predicted protein product at residue 22 (Table 4.2). The first group of 12 mutants included genes for two proteins reported in the *M. pneumoniae* proteome (22, 36) and annotated as hypothetical, but which appear to be permease components of ABC-type transport systems (MPN333 and MPN335). Notably each was disrupted independently at two and three distinct sites, respectively. Also disrupted were the only predicted *M. pneumoniae* lipase (MPN407), a putative amino acid transporter (MPN308), and ThyA (MPN320), which converts dUMP to dTMP. Among the genes disrupted in the second group of 9 mutants were the only predicted protein phosphatase (MPN247), as well as methyltransferase and/or DNA specificity subunits of separate gene clusters predicted to encode DNA modification systems. While *M. pneumoniae* genes of unknown function constitute less than 20% of the genome (8), the third class of 26 mutants accounted for over 50% of the SGA mutants characterized. These

Table 4.2. Insertion site identification for *M. pneumoniae* SGA mutants.

Mutant ^a	Site ^b	Description ^c	<i>M. genitalium</i>	<i>M. gallisepticum</i>	<i>M. mobile</i>
Transport and Metabolism					
MPN114-566	150,449	Cat, Carnitine O-acetyltransferase, hypothetical	None ^d	None	None
MPN308-274	363,224	Amino acid transporter	MG225	MGA0287	MMOB2220
MPN320-30	380,633	ThyA, Thymidilate synthase	MG227	MGA0699	MMOB0340
MPN333-32	393,007	Predicted ABC transport system, permease component	None	MGA1302	None
MPN333-614	394,752	Predicted ABC transport system, permease component	None	MGA1302	None
MPN335-38	396,248	Predicted ABC transport system, permease component	None	MGA1302	None
MPN335-377	397,263	Predicted ABC transport system, permease component	None	MGA1302	None
MPN335-595	397,917	Predicted ABC transport system, permease component	None	MGA1302	None
MPN407-137	489,736	Predicted GDSL-like lipase/acylhydrolase	None	None	None
MPN493-20	600,912	UlaD, 3-keto-L-gulonate 6-phosphate decarboxylase	None	None	None
MPN509-145	621,408	Mycoplasma-specific export protein	MG288	None	None
MPN510-42	624,124	Mycoplasma-specific export protein	MG288	None	None
DNA / Protein Modification					
MPN107-68	139,495	Predicted DNA methylase	None	None	None
MPN107-152	139,746	Predicted DNA methylase	None	None	None
MPN110-112	143,608	Predicted restriction endonuclease	None	None	None
MPN153-35	202,490	Superfamily I DNA/RNA helicase	MG140	MGA0793	None
MPN247-100	298,631	PrpC, Serine/threonine protein phosphatase	MG108	MGA0461	MMOB5580
MPN294-96	350,687	Similar to ATP-independent intracellular protease	None	MGA0998	None
MPN342-324	408,833	Restriction-modification system methyltransferase	None	MGA0537	None
MPN342-362	408,949	Restriction-modification system methyltransferase	None	MGA0537	None
MPN607-64	727,792	MsrA, Peptide methionine sulfoxide reductase	MG408	MGA0571	MMOB4950
Unknown Function					
MPN083-62	104,127	Uncharacterized mycoplasma-specific lipoprotein	MG067	MGA1162	None
MPN104-29	134,672	Uncharacterized mycoplasma-specific protein	None	None	None
MPN254-70	305,278	CinA, Uncharacterized protein (competence-induced)	MG115	None	None
MPN281-61	333,465	Uncharacterized mycoplasma-specific lipoprotein	MG185	MGA0674	None
MPN311-22	371,006	P41, Uncharacterized mycoplasma-specific protein	MG218.1	None	None
MPN311-161	371,454	P41, Uncharacterized mycoplasma-specific protein	MG218.1	None	None
MPN358-485	429,136	Uncharacterized mycoplasma-specific protein	MG255	None	None
MPN359-12	429,550	Hypothetical mycoplasma-specific protein	MG256	None	None
MPN359-54	429,675	Hypothetical mycoplasma-specific protein	MG256	None	None
MPN359-93	429,792	Hypothetical mycoplasma-specific protein	MG256	None	None
MPN359-130	429,904	Hypothetical mycoplasma-specific protein	MG256	None	None
MPN359-131	429,906	Hypothetical mycoplasma-specific protein	MG256	None	None
MPN359-132	429,909	Hypothetical mycoplasma-specific protein	MG256	None	None
MPN359-160	429,994	Hypothetical mycoplasma-specific protein	MG256	None	None
MPN359-175	430,040	Hypothetical mycoplasma-specific protein	MG256	None	None
MPN376-744	450,763	Uncharacterized mycoplasma-specific protein	None	None	None
MPN376-626	451,116	Uncharacterized mycoplasma-specific protein	None	None	None
MPN376-335	451,988	Uncharacterized mycoplasma-specific protein	None	None	None
MPN387-2	465,051	Uncharacterized mycoplasma-specific protein	MG269	None	None
MPN403-114	485,469	Hypothetical mycoplasma-specific protein	MG284	MGA1027 ^e	MMOB2170
MPN404-42	485,600	Hypothetical mycoplasma-specific protein	MG285	MGA1029 ^e	None
MPN524-74	645,829	Uncharacterized mycoplasma-specific protein	None	None	None
MPN582-82	704,868	Uncharacterized mycoplasma-specific lipoprotein	MG395	MGA1162	None
MPN614-33	738,065	Hypothetical mycoplasma-specific protein	MG414	None	None
MPN634-134	760,807	Uncharacterized mycoplasma-specific protein	None	None	None
MPN648-107	773,430	Hypothetical mycoplasma-specific protein	MG441	None	None

^a ORF numbering according to reference 7

^b Current study

^c Based on reference 7 and updated by current BLAST analysis

^d homology assigned when greater than 25% sequence identity exists over at least 50% of the *M. pneumoniae* protein, except as indicated

^e 25% identity over greater than 40% of the protein sequence

included MPN254, encoding an ortholog of a highly conserved competence-induced protein of unknown function (CinA), and MPN311 encoding P41, a cytoskeletal protein of unknown function localizing to the base of the terminal organelle (24). Additional genus-specific genes disrupted included MPN376 and MPN387, encoding previously identified cytoskeletal proteins of unknown function (36). Finally, more than one independent insertion was identified for seven genes, with MPN359 and MPN376 having insertions at eight and three distinct sites, respectively (Table 4.2), reinforcing the correlation between gene disruption and phenotype and reflecting a level of mutagenesis likely approaching saturation.

Filter cloning and HA. Primary transformant stocks were filter-cloned, with eight progeny isolated and re-screened for satellite growth for each. In most cases filter clones retained an SGA phenotype, but rarely some progeny reacquired wild-type satellite growth, probably from *Tn4001* transposition to a secondary site; only clones retaining an SGA phenotype were analyzed further. Each mutant was uniformly HA⁺ except 407-137 and 153-35, encoding a predicted lipase and helicase, respectively; these were not characterized further here (Table 4.2).

Filter-cloned progeny from 17 selected HA⁺ SGA mutants representing 13 gliding-associated genes (Table 4.3) were evaluated by Southern hybridization using transposon- and IS256-specific probes to ensure the presence of *Tn4001* in single copy with no independent duplication and insertion of IS256 at secondary loci. Each probe hybridized to a specific band of the predicted size based upon the genome sequence for all filter clones examined, with no duplicate integrated copy of the transposon or IS element evident (data not shown). Clonality was also assessed by PCR using primers flanking each disrupted gene. Rarely, filter clones appearing clonal by Southern analysis yielded a faint PCR product, probably from *Tn4001* excision from the original insertion site in a very low

percentage of the population. Only transformants clonal by all parameters above were characterized further.

Western immunoblotting analysis of SGA mutants. To assess possible spontaneous or secondary loss of known cytodherence-associated proteins in the 17 SGA transformants analyzed further, several filter-cloned isolates of each were assessed by Western immunoblotting using sera specific for cytodherence-associated proteins B, P1, P30, P41, and HMW1 (data not shown). Only MPN311 and MPN387 insertion mutants exhibited profiles distinct from wild-type and were subsequently re-screened with a battery of additional antisera (Fig. 4.3 and data not shown). As expected, disruption of MPN311 resulted in loss of protein P41, encoded by that gene. In addition, the products of the genes immediately upstream (P28) and downstream (P24) were reduced. Disruption of MPN387 was accompanied by drastically reduced levels of HMW3, P28, P30, P41, and P65, and moderately reduced levels of HMW1 and C, while B, HMW2, P1, and P24 were largely unaffected (Fig 4.3 and data not shown). An excision revertant of the MPN387 mutant had a wild-type profile and satellite growth pattern, suggesting that loss of the MPN387 gene product was indeed responsible for reduced steady-state levels of these terminal organelle proteins (data not shown).

Time-lapse analysis of satellite growth and cell gliding. Satellite growth (Fig. 4.4) and cell gliding (Table 4.3) were characterized by time-lapse microcinematography for the 17 selected insertion mutants. MPN311 insertion mutants produced sparse satellite growth that appeared as thickened elongated filaments extending from microcolonies. MPN247 and MPN254 mutants both exhibited lawn-like growth lacking microcolonies, raising the possibility that the defect in each affects related cellular processes. For most SGA insertion mutants such as MPN376, satellite growth simply developed at a slower rate

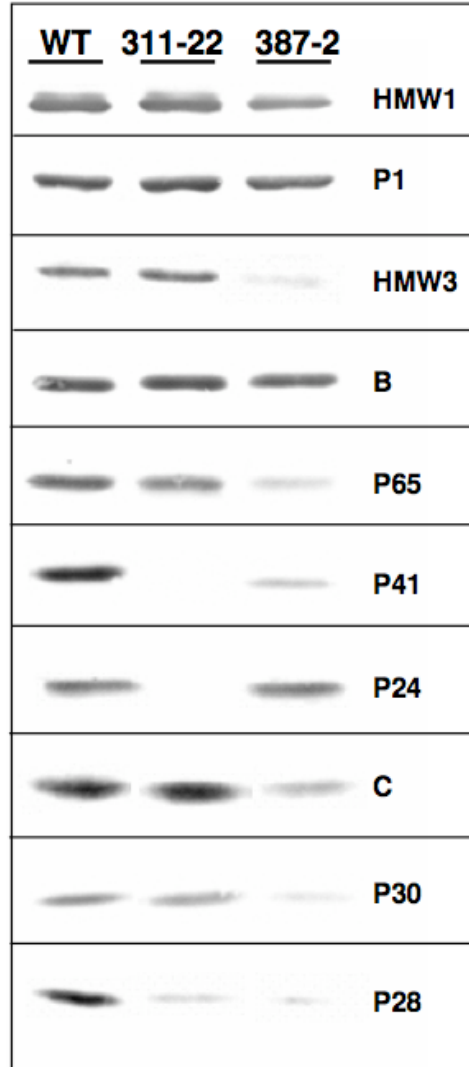


FIG. 4.3. Western immunoblot analysis of selected SGA transformants. **WT**, wild-type *M. pneumoniae* profile; **311-22** and **387-2**, SGA transformants with insertions in MPN311 and MPN387, respectively. 10 μ g protein was loaded per lane and samples were analyzed on a 4-10% polyacrylamide gradient gel. Antisera are indicated to the right.

Table 4.3. Characterization of cell gliding and glass binding for wild-type *M. pneumoniae* and selected SGA mutants.

Satellite growth alteration	Insertion mutant(s)	Mean cell gliding frequency ^b	Average cell velocity ^b	Mean percent-time resting ^b	Mean glass-binding capability ^c
Wild-type	NA	27.8 ± 0.3	100.0 ± 9.4	29.5 ± 0.5	100.0 ± 3.2
Lawn-like growth lacking microcolony formation	MPN247-100	2.8 ± 1.9	42.3 ± 24.9	58.8 ± 14.6	101.3 ± 4.0
	MPN254-70	11.0 ± 3.9	53.4 ± 0.5	48.2 ± 1.8	106.5 ± 12.5
Filamentous spreading	MPN311-22/161 ^a	3.7 ± 1.4	29.7 ± 4.5	54.3 ± 1.2	107.9 ± 1.3
Reduced spreading, confluence by 168 h	MPN083-62	18.8 ± 3.0	56.0 ± 11.6	45.3 ± 0.3	91.5 ± 7.7
	MPN342-324/362 ^a	11.8 ± 5.8	53.6 ± 5.5	47.3 ± 4.8	95.2 ± 2.9
	MPN359-54/130 ^a	8.1 ± 5.1	43.1 ± 1.3	53.0 ± 1.9	90.7 ± 4.9
	MPN376-626/744 ^a	6.8 ± 0.6	54.9 ± 12.7	50.4 ± 7.3	110.1 ± 1.6
Reduced spreading, no confluence by 168 h	MPN104-29	12.4 ± 0.3	87.2 ± 5.0	31.0 ± 5.3	93.7 ± 5.4
	MPN281-61	8.2 ± 3.6	41.8 ± 9.6	55.9 ± 4.7	78.5 ± 1.5
	MPN387-2	0	0	100	100.4 ± 16.8
	MPN403-114	7.6 ± 2.6	57.7 ± 3.3	46.0 ± 4.1	103.6 ± 2.2
	MPN404-42	11.3 ± 1.9	50.8 ± 2.5	48.6 ± 3.4	78.4 ± 7.8
	MPN524-74	12.8 ± 3.2	52.8 ± 7.8	49.1 ± 4.9	68.2 ± 2.0

^a Data were combined for the indicated insertion mutants for these ORFs

^b Data presented as the means ± standard error of the mean from 2 filter clones for each SGA mutant, with measurements for 30-50 individual cells for each, except for MPN247 and MPN311 insertion mutants, where mean gliding frequencies were much lower.

^c In each case glass binding was measured for the 2 filter clones from which gliding values were derived and normalized relative to wild-type.

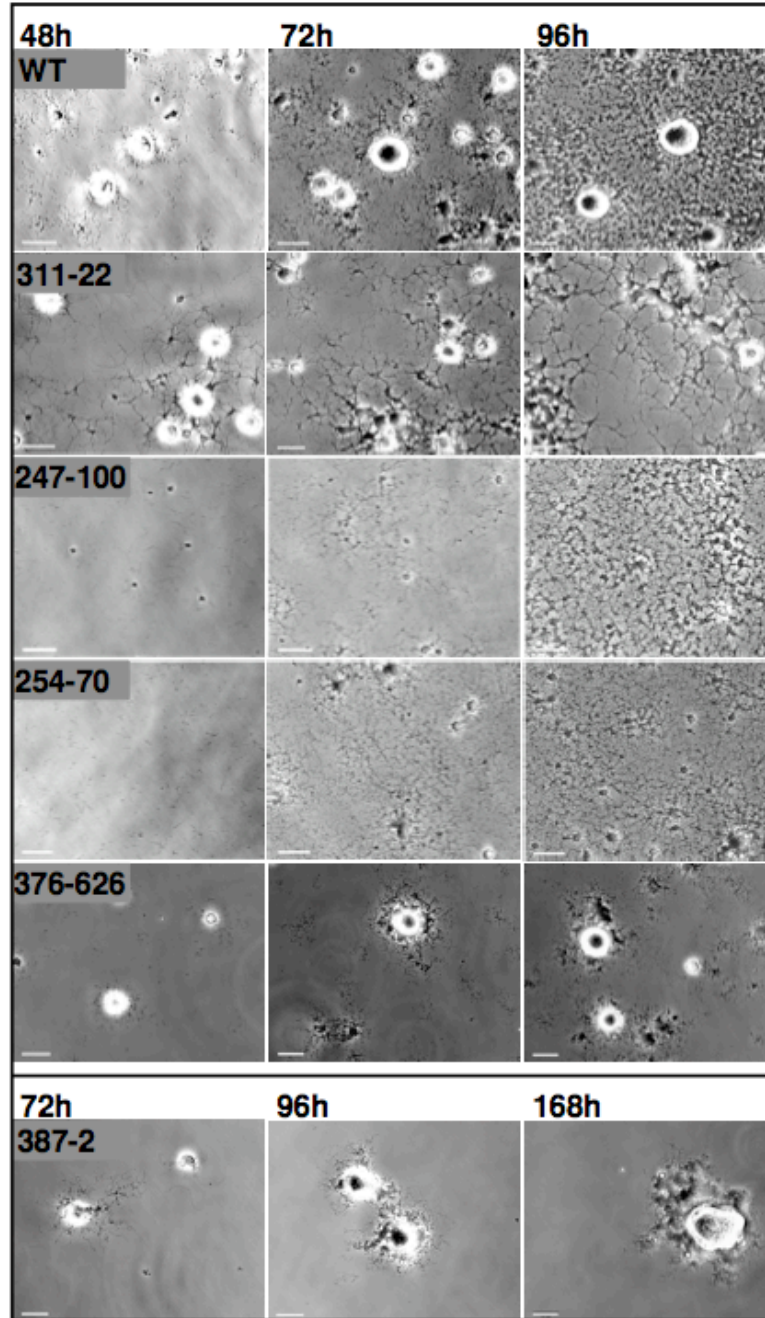


FIG. 4.4. Analysis of satellite growth formation over time for representative SGA mutant phenotypes. Cultures were incubated for 168 h with images captured at 12-h intervals and selected frames shown here for the indicated mutants. Scale bars, 15 μ m.

but otherwise appeared like wild-type. However, other mutants including MPN387 failed to establish the satellite growth typical of wild-type *M. pneumoniae*, even with extended incubation up to 168 h. No individual cell gliding was observed for this mutant over extended frame intervals, although some cell movement was apparent and probably reflected cell growth. Wild-type controls exhibited a gliding frequency of approximately 28%, as expected (15), while gliding frequencies were reduced for all mutants, in most cases ranging from 11-13% (or about 40% of wild-type) but considerably lower for MPN247, MPN311, MPN359, and MPN403 (Table 4.3). Likewise, in most cases average mutant gliding velocities ranged from 36-58% of wild-type, although no cell gliding was seen with MPN387. However, slowest velocities did not necessarily correlate with lowest gliding frequencies. For example, the MPN247 mutant had an extremely low gliding frequency (2.8%, or 10% of wild-type) but an intermediate cell velocity (42.3% of wild-type), while the MPN104 mutant had a high gliding velocity (87.2% of wild-type) but an intermediate gliding frequency (12.4%, or 44% of wild-type). This was also the only mutant to exhibit a normal percent-time resting, suggesting a normal capacity to move once gliding was initiated. Finally, no clear correlation was observed between the specific SGA phenotype and the gliding behavior of individual cells (Table 4.3).

Analysis of glass binding. To rule out the possibility that poor binding to the inert surface was responsible for altered gliding, attachment to glass was measured for each of 13 selected SGA mutants (Table 4.3). Only mutants 281-61, 404-42, and 524-74 exhibited significantly reduced glass binding ($P < 0.05$), at 78.5, 78.4, and 68.2 % of wild-type levels, respectively. All other mutants examined bound to glass at levels ranging from 90-110% of wild-type.

Assessment of potential polar effects. Definitive correlation of gene disruption with altered gliding for each mutant will require isolation and characterization of excision

revertants and genetic complementation, which are not trivial procedures in mycoplasmas (10, 34). However, the likelihood of polar effects of transposon insertion can be assessed on the basis of other parameters. The IS256 at one end of Tn4001.2065 has an outward-directed promoter (P_{out} ; 5, 25) that functions well in *M. pneumoniae* (13), while the corresponding sequence in the IS256 element at the opposite end of the transposon has been disrupted (25). P_{out} can direct the transcription of downstream genes in one orientation but might inhibit translation upstream by RNA interference (RNAi) from anti-sense transcript in the reverse orientation. *M. pneumoniae* has a single σ^{70} -RNA polymerase typical of Gram (+) species (21); while -35 sequences are divergent in *M. pneumoniae*, the -10 sequence is conserved, with a consensus of TAx₃T (51, 52). The insertion mutants in Table 4.3 were evaluated for the likelihood of upstream and downstream polar effects based on the orientation of the transposon with respect to P_{out} and the presence of the -10 consensus within 300 bp of the 5' end of flanking genes (Fig. 4.5). By these criteria no polar effect on flanking genes was predicted for seven of the seventeen mutants analyzed further, with only the MPN311 mutants clearly predicted to have a polar effect downstream, as supported by the data in Fig. 4.3. Upstream polar effects for the remaining mutants would require translational knock-down by RNAi, although this has not been demonstrated in *M. pneumoniae*. Genetic complementation studies will be required to rule out potential polar effects associated with translational coupling (50).

DISCUSSION

Mycoplasmas are considered simple organisms and yet *M. pneumoniae* and related species have a complex cytoskeletal structure and differentiated terminal organelle (2, 12, 20, 33) that function in gliding motility (16), although neither the molecular components nor the mechanics of the gliding machinery have been established. Electron cryotomography

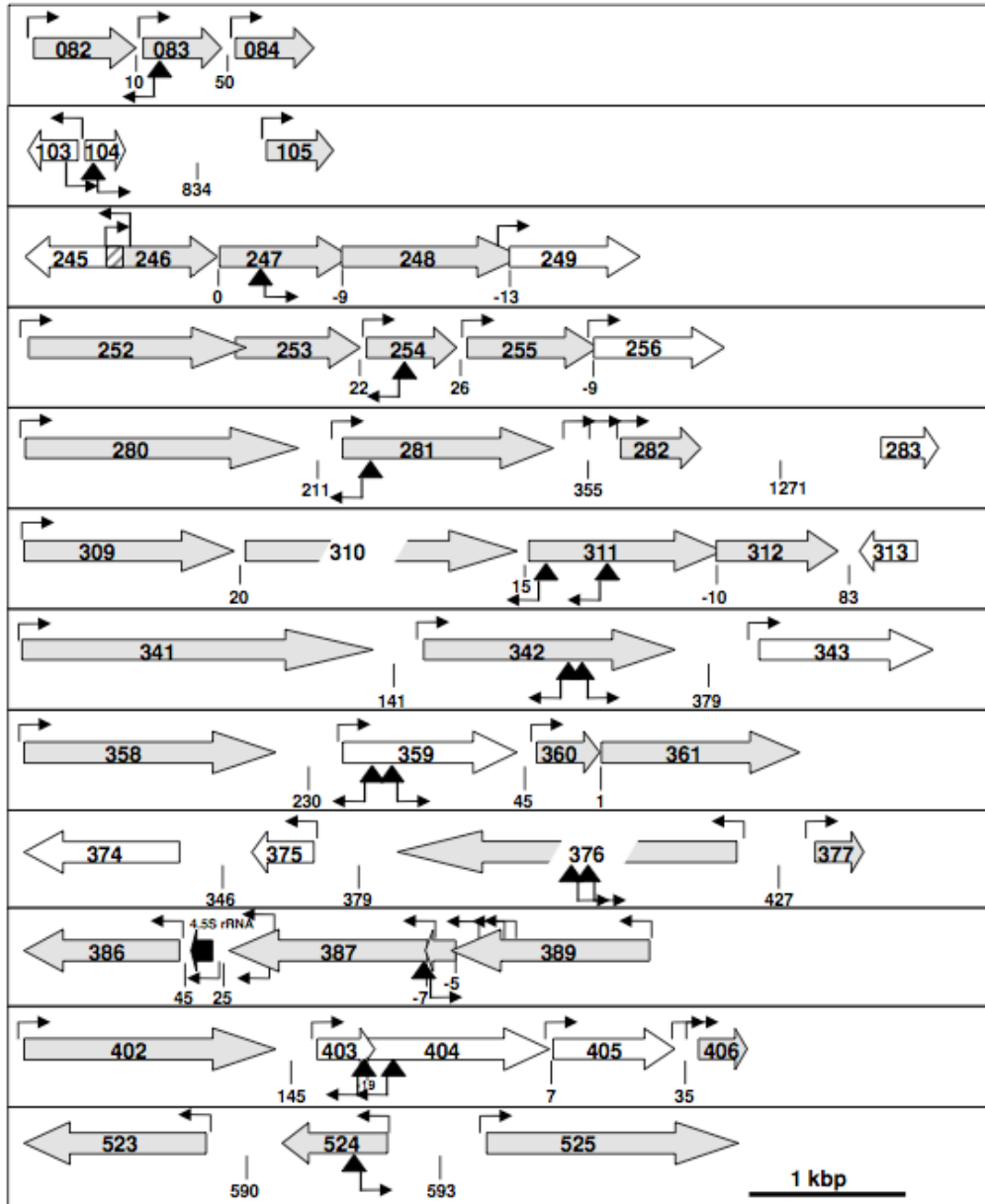


FIG. 4.5. Schematic diagram of disrupted loci for selected SGA mutants to assess likelihood of polar consequences of transposon insertions. ORFs (8) are indicated by large open arrows, gray and white indicating the reported presence or absence, respectively, of the protein product in the *M. pneumoniae* proteome (22, 46). ORF overlap is indicated by overlapping arrows except for MPN245 / MPN246 overlap, which is cross-hatched. The spacing between ORFs is indicated below each locus. Inverted triangles correspond to transposon insertions, with predicted polar effects as detailed in the key. Small arrows originating from the inverted triangles indicate the orientation of a promoter in IS256 that is functional in *M. pneumoniae* (5). Other small arrows indicate the location and orientation of predicted promoters based upon the consensus TAx_{xx}T (51, 52). Scale is approximate, as indicated at the bottom.

imaging reveals a three-dimensional core architecture that suggests conformational flexibility, prompting speculation that alternating contraction and extension of the core propels gliding, utilizing core-tethered surface adhesins for force transmission (20). In the current study we examined gliding by *M. pneumoniae* cytoadherence mutants III-4 and IV-22 to investigate the requirement for the major cytoadhesin P1 and accessory proteins B and C in cell gliding. These proteins are linked at the levels of transcription, translation, protein stability, and subcellular localization and likely function as a multiprotein complex in receptor binding (28, 50). That mutants III-4 and IV-22 are also non-motile indicates that at a minimum proteins B and/or C (Table 4.1) are likewise required in gliding motility. HMW1 is required for P1 localization to the terminal organelle (14), and loss of HMW1 is accompanied by failure to glide (this study). However, P1 localizes to the terminal organelle in mutant II-3 (37), which lacks P30 and is also non-motile (1, 15), hence P1 localization alone is not sufficient for gliding function. Whether P1 and P30 are the core-tethered surface proteins in the model of Henderson and Jensen (20) is unknown and requires more detailed characterization of the protein linkages between core components and the mycoplasma membrane.

Analysis of *M. pneumoniae* mutants defective in both gliding and cytoadherence does not allow for identification of gliding-specific components or for determination of the contribution of gliding to colonization and pathogenesis. Therefore we combined transposon mutagenesis with screening for altered satellite growth and HA to identify *M. pneumoniae* proteins associated with cell gliding but dispensable for cytoadherence. Thirty-two different ORFs were disrupted among 47 transformants, 30 of which were dispensable for HA. Individual cell gliding was quantitated for 13 of these, all of which exhibited reduced gliding velocity and/or frequency. It remains to be determined whether the impact on gliding for each is primary or secondary.

SGA mutants were grouped according to predicted functions of the disrupted genes (Table 4.2). Gliding deficiencies resulting from disruption of genes associated with metabolism and transport were not unexpected for an organism with limited metabolic capabilities but were not characterized further here. However, an association between defects in gliding motility and disruption of genes predicted to encode DNA- and protein-modifying enzymes could provide important new insights into *M. pneumoniae* regulatory mechanisms. For example, promoters inactive when methylated might function in hemimethylated DNA during chromosome replication, perhaps providing a means to coordinate expression of genes encoding components for terminal organelle assembly with cell division. We also disrupted MPN247 encoding the only *M. pneumoniae* protein phosphatase (PrpC) annotated to date. This disruption is not likely to affect transcription of the downstream cognate kinase, but we cannot rule out the possibility of a polar effect associated with translational coupling, as these ORFs overlap by 9 nt. In either case this mutant is likely defective in the ability to modify the phosphorylation state of its protein target(s), perhaps including the terminal organelle phosphoproteins HMW1, HMW2, and P1 (9). The 10-fold reduction in gliding frequency for this mutant was among the largest observed here, suggesting that phosphorylation may control activation of the gliding motor. This mutant also exhibited a lawn-like growth pattern largely devoid of microcolonies. Perhaps significantly, loss of PrpC in *Bacillus subtilis* alters biofilm architecture and increases stationary phase cell densities 5-fold (32), prompting speculation that protein phosphorylation may play a part in regulating quorum sensing. Additional studies are required to determine if the altered growth pattern and reduced gliding frequency for this mutant reflect a similar function in *M. pneumoniae*.

Proteins of unknown function represented over 50% of the loci disrupted in SGA mutants, with only MPN254 (CinA) found outside the genus. Expression of *cinA* is

upregulated in *Streptococcus pneumoniae* as part of the ComX quorum sensing pathway, where it is thought to function in the uptake of extracellular DNA in response to increasing culture densities (30). A role in DNA uptake may be nutritionally significant to *M. pneumoniae*, given its inability to synthesize purines and pyrimidines de novo, although it is not clear how this might contribute to the lawn-like growth observed here.

While most gliding-associated genes were identified from single insertion mutants, two or more independent disruptions were observed for several genes; these yielded the same SGA phenotype, reinforcing a cause-and-effect relationship between transposon insertion and phenotype. Eight distinct insertion mutants were isolated for MPN359, none of which were predicted to have polar effects on flanking genes. MPN359 has been found to date only in *M. pneumoniae* and the closely related *M. genitalium*. Its gene product, predicted to have three membrane-spanning domains, was not detected in the proteome (22, 46), perhaps due to its deduced alkaline pI and transmembrane nature. The products of MPN403 and 404 were likewise not detected by proteomic analyses, but like MPN359, orthologs of MPN403 and 404 are present in *M. genitalium*, and given the retention of these genes in both species despite considerable genome reduction, we speculate that their products are synthesized.

The disrupted genus-specific genes associated with gliding included MPN083 and MPN281, encoding putative lipoproteins. *M. pneumoniae* genome annotation indicates a complement of approximately 42 lipoproteins, based largely on homology to putative *M. genitalium* lipoproteins (8), and none with assessed function. Palmitoylation data suggest that 25-30 lipoproteins are synthesized in *M. pneumoniae*, while 30 of the 42 predicted lipoproteins, including the MPN083 and MPN281 products, were detected in the *M. pneumoniae* proteome (21, 22). Polar effects downstream are not predicted, but we cannot rule out the possibility of upstream effects due to RNAi. Nevertheless, our findings represent

the first genetic evidence of function for these *M. pneumoniae* lipoproteins. MPN524 and MPN104 contain a central domain of unknown function (DUF) that is unique to *M. pneumoniae* and designated DUF16 (21). Approximately 20 additional *M. pneumoniae* proteins share this motif, which is predicted to adopt a coil-coil conformation through the DUF motif, but none have been identified in the *M. pneumoniae* cytoskeletal fraction (36). MPN524 has a 40-amino acid C-terminal domain strongly predicted to form a dimeric coiled-coil structure. This domain is absent in MPN104 and other DUF proteins. Glass binding was reduced with disruption of MPN524 but not MPN104, raising the possibility that this C-terminal domain has functional significance.

The gliding defects associated with disruption of MPN376, MPN311, and MPN387 were among the most severe observed here. Three independent insertions were identified in MPN376, underscoring the likely correlation between gene disruption and mutant phenotype, and polar effects were not predicted. MPN376 transcripts are among the most abundant in *M. pneumoniae* (52), and the product is a cytoskeletal element of unknown function (36) but predicted to have an N-terminal signal peptide and C-terminal membrane-spanning domain. Both gliding velocity and gliding frequency were reduced with disruption of MPN376, suggesting a requirement for initiation as well as operation of the gliding motor. MPN311 mutants were unique among the SGA variants characterized here in producing filamentous satellite growth. Furthermore, individual cells of this mutant had an unusual elongated morphology, often reaching lengths of 4-8 μm compared to 1 – 2 μm for wild-type cells (data not shown). MPN311 encodes P41, a cytoskeletal protein of unknown function localizing to the base of the terminal organelle (24). MPN311 disruption is not predicted to have downstream effects on MPN312 transcription, but preliminary data indicate that loss of protein P24, encoded by MPN312, accompanies disruption of MPN311 and may be due to translational coupling, as MPN311 overlaps the 5' end of MPN312 by 10 bp.

Complementation studies will be required to determine whether the motility and morphology defects associated with MPN311 disruption are due to loss of P41, P24, or both. Disruption of MPN387 resulted in a complete loss of gliding; some cell movement was observed with extended observation intervals but probably reflects cell growth. The transposon insertion site at the 5' end of MPN387 corresponded to the 3' end of MPN388, hence complementation analyses will be required to assess whether truncation of MPN388 contributes to the phenotype of this mutant. The MPN387 product is a cytoskeletal protein (36) that appears to lack membrane-spanning domains and is predicted to assume an elongated coiled-coil conformation. Loss of MPN387 did not affect appreciably the steady-state levels of B, HMW2, P1, or P24, but the levels of other known terminal organelle proteins were moderately or drastically reduced, thus it was somewhat surprising that this mutant retained an HA+ phenotype, although erythrocyte binding was not assessed quantitatively. It has been proposed that P1, B & C are incorporated into the terminal organelle by a separate pathway than HMW1, HMW3, P65, and P30 (26). The destabilization of protein C in addition to HMW1, P28, P30, P41, and P65 with disruption of MPN387 suggests that the MPN387 gene product participates in both putative assembly pathways. Significantly, an MPN387 excision revertant had a wild-type satellite growth pattern and protein profile (data not shown), indicating that the destabilization of cytodherence-associated proteins was indeed a consequence of the transposon insertion and not a secondary defect.

Eighteen of the 32 ORFS associated here with *M. pneumoniae* gliding are also found in the closely related *M. genitalium*. Global transposon mutagenesis has established what may approach a minimal genomic complement for laboratory growth in *M. genitalium* (11); among the 18 gliding-associated ORFs shared with *M. genitalium* (Table 4.2) only the MPN247 ortholog was not identified as dispensable (11). As each of the 482 *M. genitalium*

ORFs are represented in *M. pneumoniae*, the gliding machinery of both species is likely similar. Nevertheless, transposon mutagenesis and screening for altered satellite growth in *M. genitalium* yielded only MG200 and MG386 (34), corresponding to MPN119 and MPN567 respectively in *M. pneumoniae*, and thus a common subset of gliding-associated genes was not identified for both species. However, in separate studies we have identified insertion mutants in MPN119 and MPN567, and preliminary analysis indicates an altered gliding phenotype (unpublished data).

Over 200 mycoplasmas have been described to date, but gliding motility has been reported in only five species, including *M. gallisepticum*, *M. pulmonis*, and *M. mobile*, in addition to *M. pneumoniae* and *M. genitalium* (4). As genes required for gliding in *M. mobile* (23) are found in *M. pulmonis* but not in *M. pneumoniae*, *M. genitalium*, or *M. gallisepticum*, we assessed whether the gliding-associated genes identified here for *M. pneumoniae* are found in *M. gallisepticum* and *M. mobile*, in addition to *M. genitalium* (Table 4.2). Even using a relatively low stringency for this determination, only one genus-specific gene of unknown function associated with gliding in *M. pneumoniae* was conserved in *M. mobile* compared with twelve in *M. genitalium* and five in *M. gallisepticum*, consistent with a distinct gliding mechanism in *M. mobile* from the other mycoplasmas compared here.

In conclusion the current study represents the first widespread genetic analysis of gliding motility in *M. pneumoniae*. The generation and initial characterization of gliding mutants provides strong evidence associating a number of mycoplasma genes with this novel cellular locomotion in *M. pneumoniae* and sets the stage for future studies into the engineering and regulation of the gliding machinery. Analysis of existing cytoadherence mutants has established a clear requirement for protein P30 (15) and now proteins HMW1, as well as B and/or C, in *M. pneumoniae* gliding. Moreover, global transposon mutagenesis identified 30 additional genes, insertions in which resulted in altered satellite growth with no

effect on HA as evaluated qualitatively. A quantitative assessment of binding by these mutants to erythrocytes as well as other cell types is still required. Each of the 17 representative SGA mutants analyzed further exhibited substantially reduced gliding frequencies, gliding velocities, or both, identifying on a genetic basis a number of mycoplasma proteins with no previously assigned function having an association with gliding. Furthermore, our findings raise the possibility of regulatory roles in *M. pneumoniae* for DNA methylation and protein phosphorylation in terminal organelle function in gliding. Finally, the isolation of cytoadherence-positive gliding mutants should allow for elucidation of the contribution of gliding to colonization of bronchial epithelium and pathogenesis.

ACKNOWLEDGEMENTS

We thank C. Minion for providing Tn4001.2065, R. Herrmann for antisera, M. Farmer, R. Krause, M. Hamrick and L. Sellers for technical assistance, and J. Piñol for providing data prior to publication. This work was supported by Public Health Service grant AI49194 from the National Institute of Allergy and Infectious Diseases to D.C.K.

REFERENCES

1. **Baseman, J. B., J. Morrison-Plummer, D. Drouillard, B. Puleo-Schepke, V. V. Tryon, and S. C. Holt.** 1987. Identification of a 32-kilodalton protein of *Mycoplasma pneumoniae* associated with hemadsorption. *Isr. J. Med. Sci.* **23**:474-479.
2. **Biberfeld, G., and P. Biberfeld.** 1970. Ultrastructural Features of *Mycoplasma pneumoniae*. *J. Bacteriol.* **102**:855-861.
3. **Bredt, W.** 1968. Motility and multiplication of *Mycoplasma pneumoniae*. A phase contrast study. *Pathol. Microbiol.* **32**:321-326.

4. **Bredt, W.** 1979. Motility, p. 141-155. *In* M.F. Barile and S. Razin (ed.), *The Mycoplasmas*, Vol. I, Cell Biology. Academic Press, New York, N.Y.
5. **Byrne, M. E., D. A. Rouch, and R. A. Skurray.** 1989. Nucleotide sequence analysis of IS256 from the *Staphylococcus aureus* gentamicin-tobramycin-kanamycin-resistance transposon Tn4001. *Gene* **81**:361-367.
6. **Chanock, R. M., L. Hayflick, and M. F. Barile.** 1962. Growth on artificial medium of an agent associated with atypical pneumonia and its identification as a PPLO. *Proc. Natl. Acad. Sci. U.S.A.* **48**:41-49.
7. **Collier, A. M., W. A. Clyde, Jr., and F. W. Denny.** 1971. *Mycoplasma pneumoniae* in hamster tracheal organ culture: immunofluorescent and electron microscopic studies. *Proc. Soc. Exp. Biol. Med.* **136**:569-573.
8. **Dandekar, T., M. Huynen, J. T. Regula, B. Ueberle, C. U. Zimmermann, M. A. Andrade, T. Doerks, L. Sanchez-Pulido, B. Snel, M. Suyama, Y. P. Yuan, R. Herrmann, and P. Bork.** 2000. Re-annotating the *Mycoplasma pneumoniae* genome sequence: adding value, function and reading frames. *Nucleic Acids Res.* **28**:3278-3288.
9. **Dirksen, L. B., K. A., and D. C. Krause.** 1994. Phosphorylation of cytoadherence-accessory proteins in *Mycoplasma pneumoniae*. *J. Bacteriol.* **176**:7499-7505.
10. **Fisseha, M., H. W. Gohlmann, R. Herrmann, and D. C. Krause.** 1999. Identification and complementation of frameshift mutations associated with loss of cytoadherence in *Mycoplasma pneumoniae*. *J. Bacteriol.* **181**:4404-4410.
11. **Glass, J. I., N. Assad-Garcia, N. Alperovich, S. Yooseph, M. R. Lewis, M. Maruf, C. A. Hutchison III, H. O. Smith, and J. C. Venter.** 2006. Essential genes of a minimal bacterium. *Proc. Natl. Acad. Sci. U.S.A.* **103**: 425-430.

12. **Gobel, U., V. Speth, and W. Bredt.** 1981. Filamentous structures in adherent *Mycoplasma pneumoniae* cells treated with nonionic detergents. *J. Cell Biol.* **91**:537-543.
13. **Hahn, T. W., K. A. Krebs, and D. C. Krause.** 1996. Expression in *Mycoplasma pneumoniae* of the recombinant gene encoding the cytoadherence-associated protein HMW1 and identification of HMW4 as a product. *Mol. Microbiol.* **19**:1085-1093.
14. **Hahn, T. W., M. J. Willby, and D. C. Krause.** 1998. HMW1 is required for cytoadhesin P1 trafficking to the attachment organelle in *Mycoplasma pneumoniae*. *J. Bacteriol.* **180**:1270-1276.
15. **Hasselbring, B. M., J. L. Jordan, and D. C. Krause.** 2005. Mutant analysis reveals a specific requirement for protein P30 in *Mycoplasma pneumoniae* gliding motility. *J. Bacteriol.* **187**:6281-6289.
16. **Hasselbring, B. M. and D. C. Krause.** 2006. Gliding motor of the wall-less prokaryote *Mycoplasma pneumoniae*. Submitted.
17. **Hasselbring, B. M., J. L. Jordan, R. W. Krause, and D. C. Krause.** 2006. Terminal organelle development in the cell wall-less prokaryote *Mycoplasma pneumoniae*. Submitted.
18. **Hayflick, L.** 1965. Tissue cultures and mycoplasmas. *Tex. Rep. Biol. Med.* **23**:Suppl 1:285+.
19. **Hedreyda, C. T., K. K. Lee, and D. C. Krause.** 1993. Transformation of *Mycoplasma pneumoniae* with Tn4001 by electroporation. *Plasmid* **30**:170-175.
20. **Henderson, G. P., and G. J. Jensen.** 2006. Three-dimensional structure of *Mycoplasma pneumoniae*'s attachment organelle and a model for its role in gliding motility. *Mol. Microbiol.* **60**:376-385.

21. **Himmelreich, R., H. Hilbert, H. Plagens, E. Pirkl, B. C. Li, and R. Herrmann.** 1996. Complete sequence analysis of the genome of the bacterium *Mycoplasma pneumoniae*. *Nucleic Acids Res.* **24**:4420-4449.
22. **Jaffe, J. D., H. C. Berg, and G. M. Church.** 2004. Proteogenomic mapping as a complementary method to perform genome annotation. *Proteomics* **4**:59-77.
23. **Jaffe J.D., N. Stange-Thomann, C. Smith, D. DeCaprio, S. Fisher, J. Butler, S. Calvo, T. Elkins, M. G. FitzGerald, N. Hafez, C. D. Kodira, J. Major, S. Wang, J. Wilkinson, R. Nicol, C. Nusbaum, B. Birren, H. C. Berg, and G. M. Church.** 2004. The complete genome and proteome of *Mycoplasma mobile*. *Genome Res.* **14**:1447-1461.
24. **Kenri, T., S. Seto, A. Horino, Y. Sasaki, T. Sasaki, and M. Miyata.** 2004. Use of fluorescent-protein tagging to determine the subcellular localization of *Mycoplasma pneumoniae* proteins encoded by the cytoadherence regulatory locus. *J. Bacteriol.* **186**:6944-6955.
25. **Knudtson, K. L., and F. C. Minion.** 1993. Construction of Tn4001lac derivatives to be used as promoter probe vectors in mycoplasmas. *Gene* **137**:217-222.
26. **Krause, D. C., and M. F. Balish.** 2004. Cellular engineering in a minimal microbe: structure and assembly of the terminal organelle of *Mycoplasma pneumoniae*. *Mol. Microbiol.* **51**:917-924.
27. **Krause, D. C., D. K. Leith, R. M. Wilson, and J. B. Baseman.** 1982. Identification of *Mycoplasma pneumoniae* proteins associated with hemadsorption and virulence. *Infect. Immun.* **35**:809-817.
28. **Layh-Schmitt, G. and R. Herrmann.** 1994. Spatial arrangement of gene products of the P1 operon in the membrane of *Mycoplasma pneumoniae*. *Infect. Immun.* **62**:974-979.

29. **Layh-Schmitt, G., H. Hilbert, and E. Pirkl.** 1995. A spontaneous hemadsorption-negative mutant of *Mycoplasma pneumoniae* exhibits a truncated adhesin-related 30-kilodalton protein and lacks the cytoadherence-accessory protein HMW1. *J. Bacteriol.* **177**:843-846.
30. **Lee, M.S. and D.A. Morrison.** 1999. Identification of a new regulator in *Streptococcus pneumoniae* linking quorum sensing to competence for genetic transformation. *J. Bacteriol.* **181**:5004-5016.
31. **Lipman, R. P., and W. A. Clyde, Jr.** 1969. The interrelationship of virulence, cytoadsorption, and peroxide formation in *Mycoplasma pneumoniae*. *Proc. Soc. Exp. Biol. Med.* **131**:1163-1167.
32. **Madek, E., A. Laszkiewicz, A. Iwanicki, M. Obuchowski, and S. Seror.** 2002. Characterization of a membrane-linked Ser/Thr protein kinase in *Bacillus subtilis*, implicated in developmental processes. *Mol. Microbiol.* **46**:571-586.
33. **Meng, K. E., and R. M. Pfister.** 1980. Intracellular structures of *Mycoplasma pneumoniae* revealed after membrane removal. *J. Bacteriol.* **144**:390-399.
34. **Pich, O. Q., R. Burgos, M. Ferrer-Navarro, E. Querol, and J. Piñol.** 2006. *Mycoplasma genitalium* *mg200* and *mg386* genes are involved in gliding motility but not in cytoadherence. *Mol. Microbiol.* In press.
35. **Proft, T., and R. Herrmann.** 1994. Identification and characterization of hitherto unknown *Mycoplasma pneumoniae* proteins. *Mol. Microbiol.* **13**:337-348.
36. **Regula, J.T., G. Boguth, A. Gorg, J. Hegermann, F. Mayer, R. Frank, and R. Herrmann.** 2001. Defining the mycoplasma 'cytoskeleton': the protein composition of the Triton X-100 insoluble fraction of the bacterium *Mycoplasma pneumoniae* determined by 2-D gel electrophoresis and mass spectrometry. *Microbiol.* **147**:1045-1057.

37. **Romero-Arroyo, C. E., J. Jordan, S. J. Peacock, M. J. Willby, M. A. Farmer, and D. C. Krause.** 1999. *Mycoplasma pneumoniae* protein P30 is required for cytodherence and associated with proper cell development. *J. Bacteriol.* **181**:1079-1087.
38. **Sambrook, J., E. F. Fritsch, and T. Maniatis.** 1989. *Molecular Cloning: A Laboratory Manual*, 2nd ed. Cold Spring Harbor Laboratory Press, Cold Spring Harbor, NY.
39. **Seto, S., T. Kenri, T. Tomiyama, and M. Miyata.** 2005. Involvement of P1 adhesin in gliding motility of *Mycoplasma pneumoniae* as revealed by the inhibitory effects of antibody under optimized gliding conditions. *J. Bacteriol.* **187**:1875-1877.
40. **Seto, S., G. Layh-Schmitt, T. Kenri, and M. Miyata.** 2001. Visualization of the attachment organelle and cytodherence proteins of *Mycoplasma pneumoniae* by immunofluorescence microscopy. *J. Bacteriol.* **183**:1621-1630.
41. **Seto, S., and M. Miyata.** 2003. Attachment organelle formation represented by localization of cytodherence proteins and formation of the electron-dense core in wild-type and mutant strains of *Mycoplasma pneumoniae*. *J. Bacteriol.* **185**:1082-1091.
42. **Seto, S., A. Uenoyama, and M. Miyata.** 2005. Identification of a 521-kilodalton protein (Gli521) involved in force generation or force transmission for *Mycoplasma mobile* gliding. *J. Bacteriol.* **187**:3502-3510.
43. **Stevens, M. K., and D. C. Krause.** 1991. Localization of the *Mycoplasma pneumoniae* cytodherence-accessory proteins HMW1 and HMW4 in the cytoskeletonlike Triton shell. *J. Bacteriol.* **173**:1041-1050.

44. **Stevens, M. K. and D. C. Krause.** 1992. *Mycoplasma pneumoniae* cytoadherence phase-variable protein HMW3 is a component of the attachment organelle. J. Bacteriol. **174**:4265-4274.
45. **Tully, J. G., R. F. Whitcomb, H. F. Clark, and D. L. Williamson.** 1977. Pathogenic mycoplasmas: cultivation and vertebrate pathogenicity of a new spiroplasma. Science **195**:892-894.
46. **Ueberle, B., R. Frank, and R. Herrmann.** 2002. The proteome of the bacterium *Mycoplasma pneumoniae*: comparing predicted open reading frames to identified gene products. Proteomics. 2: 754-764.
47. **Uenoyama, A., A. Kusumoto, and M. Miyata.** 2004. Identification of a 349-kilodalton protein (Gli349) responsible for cytoadherence and glass binding during gliding of *Mycoplasma mobile*. J. Bacteriol. **186**:1537-1545.
48. **Uenoyama, A., and M. Miyata.** 2005. Identification of a 123-kilodalton protein (Gli123) involved in machinery for gliding motility of *Mycoplasma mobile*. J. Bacteriol. **187**:5578-5584.
49. **Waites, K. B., and D. F. Talkington.** 2004. *Mycoplasma pneumoniae* and its role as a human pathogen. Clin. Microbiol. Rev. **17**:697-728.
50. **Waldo, R. H., 3rd, and D. C. Krause.** 2006. Synthesis, stability, and function of cytoadhesin P1 and accessory protein B/C complex of *Mycoplasma pneumoniae*. J. Bacteriol. **188**:569-575.
51. **Waldo, R. H., 3rd, P. L. Popham, C. E. Romero-Arroyo, E. A. Mothershed, K. K. Lee, and D. C. Krause.** 1999. Transcriptional analysis of the *hmw* gene cluster of *Mycoplasma pneumoniae*. J. Bacteriol. **181**:4978-4985.
52. **Weiner, J., 3rd, R. Herrmann, and G. F. Browning.** 2000. Transcription in *Mycoplasma pneumoniae*. Nucleic Acids Res. **28**:4488-4496.

53. **Willby, M. J., M. F. Balish, S. M. Ross, K. K. Lee, J. L. Jordan, and D. C. Krause.**
2004. HMW1 is required for stability and localization of HMW2 to the attachment
organelle of *Mycoplasma pneumoniae*. *J. Bacteriol.* **186**:8221-8228.

CHAPTER 5

CYTOSKELETAL PROTEIN P41 IS REQUIRED TO ANCHOR THE TERMINAL ORGANELLE OF THE WALL-LESS PROKARYOTE *MYCOPLASMA PNEUMONIAE*¹

¹ B. M. Hasselbring and D. C. Krause. 2007. *Molecular Microbiology*. In press.
Reprinted here with permission of publisher.

Summary

The cell wall-less prokaryote *Mycoplasma pneumoniae* approaches the minimal requirements for a cell yet produces a complex terminal organelle that mediates cytodherence and gliding motility. Here we explored the molecular nature of the *M. pneumoniae* gliding machinery, utilizing fluorescent protein fusions and digital microcinematography to characterize gliding-altered mutants having transposon insertions in MPN311, encoding the cytoskeletal protein P41. Disruption of MPN311 resulted in loss of P41 and P24, the downstream gene product. Gliding ceases in wild-type *M. pneumoniae* during terminal organelle development, which occurs at the cell poles adjacent to an existing structure. In contrast, terminal organelle development in MPN311 mutants did not necessarily coincide with gliding cessation, and new terminal organelles frequently formed at lateral sites. Furthermore, new terminal organelles exhibited gliding capacity quickly, unlike wild-type *M. pneumoniae*. P41 and P24 localize at the base of the terminal organelle; in their absence this structure detached from the cell body of motile and dividing cells but retained gliding capacity and thus constitutes the gliding apparatus. Recombinant wild-type P41 restored cell integrity, establishing a role for this protein in anchoring the terminal organelle to the cell body.

Introduction

Mycoplasmas are cell wall-less, obligate parasitic bacteria colonizing a variety of plant, invertebrate, and vertebrate hosts, with some species severely impacting agriculture and public health (Razin *et al.*, 1998). *Mycoplasma pneumoniae* is a major pathogen in humans, establishing chronic infections of the respiratory tract resulting in bronchitis and atypical or “walking” pneumonia. *M. pneumoniae* accounts for up to 20% of all cases of community-

acquired pneumonia and is the leading cause of pneumonia in older children and young adults (Waites and Talkington, 2004). Extra-pulmonary sequelae are not uncommon and often have an immunopathological basis, although isolation of *M. pneumoniae* from non-respiratory tissues reflects a capacity to spread systemically (Waites and Talkington, 2004).

Apart from its importance to human health, *M. pneumoniae* is also intriguing from a biological perspective. With a minimal genome of only 816 kbp and lacking genes for cell wall production, de novo synthesis of nucleotides and amino acids, and common transcriptional regulatory circuits and two-component signaling pathways (Himmelreich *et al.*, 1996; Dandekar *et al.*, 2000), this species approaches the minimal requirements for a free-living existence. *M. pneumoniae* cells are likewise extremely small, with a volume only 5-10% of that of model prokaryotes. Nevertheless, a remarkable degree of cellular complexity underlies this novel bacterium. Despite having no cell wall, *M. pneumoniae* cells exhibit a distinctive morphology imparted by a cytoskeleton-like structure and highlighted by a polar, differentiated terminal organelle that functions in complex and seemingly disparate cellular processes that include adherence to host cells (cytadherence) and cell division (Göbel *et al.*, 1981; Krause and Balish, 2004; Meng and Pfister, 1980). This membrane-bound extension of the cell body has an electron-dense core which appears as two parallel rods oriented longitudinally, having a jointed, multi-subunit architecture, and enlarging to form a terminal button at the distal end (Biberfeld and Biberfeld, 1970; Hegermann *et al.*, 2002; Henderson and Jensen, 2006). Several cytadherence-associated proteins including the adhesins P1 and P30 localize predominantly or exclusively to the terminal organelle, but the composition of the core remains undefined (Krause and Balish, 2004). Development of a new terminal organelle adjacent to an existing structure precedes cell division (Hasselbring *et al.*, 2006a; Rodwell and Mitchell, 1979; Seto *et al.*, 2001), and recent studies have begun to establish the sequence for macromolecular assembly, including protein

interactions required for core stability and the proper trafficking of adhesin proteins (Krause and Balish, 2004; Hasselbring *et al.*, 2006a).

The terminal organelle is also the leading end as *M. pneumoniae* cells glide across surfaces. Gliding is intermittent at a velocity of approximately 0.3 $\mu\text{m}/\text{sec}$ (Hasselbring *et al.*, 2005; Radestock and Bredt, 1977), but neither the biological significance nor the molecular mechanism of gliding is known, although it has been proposed that conformational changes in the core may drive gliding by an inchworm-like process (Henderson and Jensen, 2006). Genome analysis reveals no homology to proteins known to be involved in motility of any type in walled bacteria. Furthermore, distinct gliding mechanisms are likely employed even within the genus *Mycoplasma*, as no homologs of proteins required for motility in *Mycoplasma mobile* have been identified in *M. pneumoniae* (Seto *et al.*, 2005b; Uenoyama *et al.*, 2004; Uenoyama and Miyata, 2005), and very few genes associated with gliding in *M. pneumoniae* are found in *M. mobile* (Hasselbring *et al.*, 2006b).

We recently utilized global transposon mutagenesis to dissect further the *M. pneumoniae* gliding apparatus, screening transformants individually for atypical satellite growth phenotypes. Two transformants exhibited sparse, highly filamentous satellite growth; transposon insertions for each mapped to MPN311 (Hasselbring *et al.*, 2006b), the third of four ORFs of the P65 operon (Fisseha *et al.*, 1999; Fig. 5.1). MPN311 encodes protein P41, a component of the mycoplasma terminal organelle and the Triton X-100-insoluble, cytoskeletal fraction (Kenri *et al.*, 2004). In the current study insertional inactivation of MPN311 resulted in loss of both P41 and P24, the product of the ORF immediately downstream. Gliding by wild-type *M. pneumoniae* ceases during terminal organelle development, and nascent terminal organelles form at a cell pole adjacent to an existing structure and generally do not initiate gliding for up to 3 h (Hasselbring *et al.*, 2006a). However, terminal organelle development appeared to be poorly coordinated spatially and

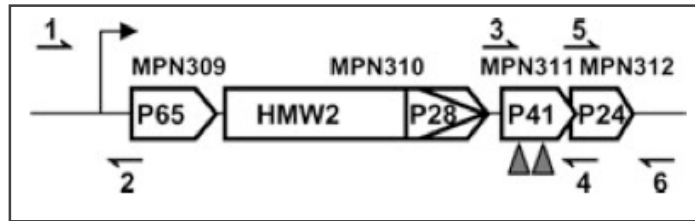


Fig. 5.1. Organization of the P65 operon in *M. pneumoniae*. The ORF designations (Dandekar *et al.*, 2000) are given above each gene product. The arrow indicates the promoter for the operon. Transposon insertions were mapped to distinct sites in MPN311 corresponding to residues 22 and 161 of P41 (arrowheads). The numbered half-arrows correspond to the following PCR primers, with underlined sequences corresponding to the indicated restriction sites.

1. 5'-TAGTTTTGTAAGGATCCCAAGCTTTGCCGTCAT-3' *Bam*HI
2. 5'-AATTATATCCATTTTGTACAGGTAAAAGGTGCC-3' *Bsr*GI
3. 5'-TAAATAAGGAAGATGTACAAGATGACTAATGAT-3' *Bsr*GI
4. 5'-CAGTTGGCAATTAGGCCICTAAAGCAGTCG-3' *Stu*I
5. 5'-TACAGGAATTAGATGTACATAATGAAGGATAGT-3' *Bsr*GI
6. 5'-TACTTGTTTAGAAGGCCTGAAACAAACAGCCAG-3' *Stu*I

temporally with gliding in MPN311 mutants. Furthermore, loss of P41 and P24 was accompanied by separation of the terminal organelle from the *M. pneumoniae* cell body. Detached terminal organelles retained gliding capacity, demonstrating definitively that this structure constitutes the *M. pneumoniae* gliding motor. Recombinant wild-type P41 in MPN311 mutants restored a wild-type cell morphology, normal satellite growth, and stable linkage of the terminal organelle to the cell body.

Results

Characterization of MPN311 Mutants

Transposon insertions in two independent transformants exhibiting filamentous satellite growth were mapped to sites in the MPN311 gene corresponding to amino acid residues 22 and 161 of protein P41 (311-22 and 311-161; Hasselbring *et al.*, 2006b). Western immunoblot analysis confirmed the loss of P41 with disruption of MPN311 but also revealed a polar effect downstream resulting in the loss of P24, which co-localizes with P41 at the base of the terminal organelle (Fig. 5.2; Kenri *et al.*, 2004). This downstream polar effect was not unexpected, as the promoter for the P65 operon precedes MPN309 (Krause *et al.*, 1999), and the transposon orientation relative to MPN311 provides no downward-reading promoter from within the transposon (Hasselbring *et al.*, 2006b). Moreover, given the 10-bp overlap between MPN311 and MPN312 it is likely that translation of P24 is coupled to P41 (Krause *et al.*, 1997). HMW2 and P28 are products of the gene immediately upstream of MPN311 (Fig. 5.1); while HMW2 levels were wild-type in the MPN311 insertion mutants, P28 levels were reduced about 4-fold, as shown previously (Hasselbring *et al.*, 2006b). The terminal organelle protein P1 (Hu *et al.*, 1982) and the uniformly distributed membrane protein FtsH (Jordan *et al.*, 2001) were both present at wild-type levels in MPN311 mutants (Fig. 5.2).

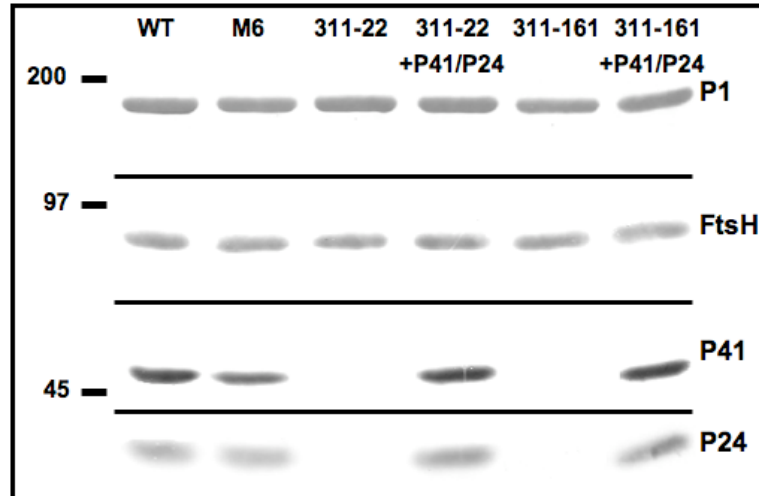


Fig. 5.2. Western immunoblotting of MPN311 mutants. Analysis by Western immunoblotting revealed the complete loss of both P41 and P24. Proteins P1 and FtsH were probed as controls for proteins that localize to the terminal organelle and cell body, respectively. Terminal organelle mutant M6 (Layh-Schmitt *et al.*, 1995) produces reduced levels of P41 (unpublished data) and was included for comparison.

Phase contrast microscopy revealed a distinctive cell morphology for MPN311 transposon-insertion mutants, which appeared as chains of coccoid cells rather than the individual filamentous cells characteristic of wild type *M. pneumoniae* (Fig. 5.3). Furthermore, very small forms approximately 200-300 nm in size were abundant in MPN311 mutant cultures (Fig. 5.3A, arrowheads) but extremely rare in wild-type cultures. These small forms failed to stain with DAPI, indicating the absence of genetic material (Fig. 5.3B). The MPN311 mutant was also examined by immunofluorescence microscopy using antibodies to the cytoadherence-associated protein P30, which localizes to the terminal organelle in wild-type *M. pneumoniae* (Baseman *et al.*, 1987; Fig. 5.3C). A single polar fluorescent focus was observed in wild-type controls as expected (Hasselbring *et al.*, 2005) and occasionally in the MPN311 mutant cells. However, other cells of the MPN311 mutant exhibited only a lateral focus (see below), and some were completely devoid of a P30 signal (Fig. 5.3C). Additionally, the smaller detached forms seen by phase contrast microscopy (Fig. 5.3A) labeled intensely with P30-specific antibodies (Fig 5.3C, arrowheads). Proteins P1 and P65 are cytoadherence-associated terminal organelle components like P30, and immunofluorescence analysis with P1- and P65-specific antibodies yielded labeling patterns similar to those seen for P30 (data not shown). Thus, the small forms very likely constitute detached *M. pneumoniae* terminal organelles, and a terminal organelle detachment (TOD) phenotype was associated with loss of P41, P24, or both.

Terminal Organelle Development in TOD Mutants

To investigate further terminal organelle development and function in TOD mutants we examined growing cultures by digital time-lapse microcinematography, with phase contrast images recorded over intervals of up to 30 min. Individual cells were motile but at velocities and gliding frequencies approximately three-fold and eight-fold, respectively, below that of

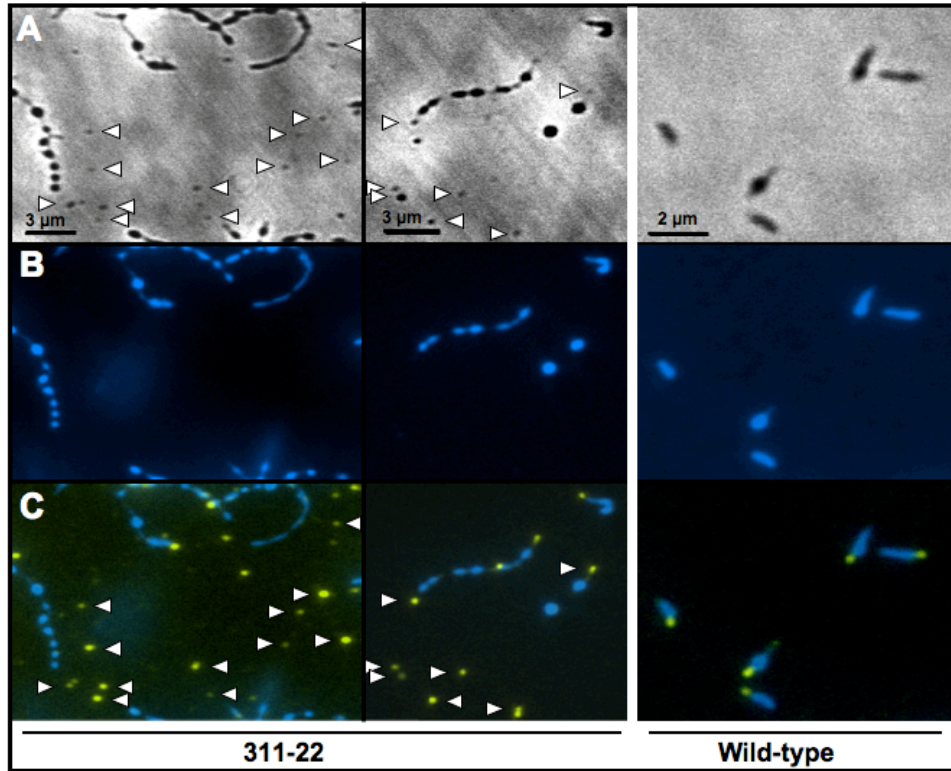


Fig. 5.3. Terminal organelle localization in wild-type and MPN311 mutant cells. (A) Phase contrast image. Mutant MPN311 cells commonly appeared as long chains of coccoid cells rather than as individual, filamentous cells typical of wild-type *M. pneumoniae*. However, a smaller form approximately 300 nm in diameter (arrowheads) was also abundant in mutant cultures. (B) DAPI Fluorescence images of the same fields in panel A. No fluorescence was observed in the smaller forms, indicating the absence of genetic material. (C) Merged images from DAPI and immunofluorescence analysis. Antibodies to the adhesin protein P30 demonstrated that the smaller forms possessed this terminal organelle component. Similar results were observed with antibodies to other terminal organelle proteins (data not shown). Scale as indicated.

wild-type *M. pneumoniae* (Hasselbring *et al.*, 2006b). As with wild-type cells (Fig. 5.4A; supplementary movie 1), gliding was unidirectional with the terminal organelle the leading end. The smaller forms seen in fixed cultures were common in growing cultures and clearly motile, often at approximately wild-type velocities (Fig 5.4B; supplementary movie 2). Their origin first became evident from the observation of gliding mutant cells encountering neighboring cells. When wild-type *M. pneumoniae* traversed cells encountered during gliding, the resulting cell-cell contact reduced the forward velocity but usually resolved with the motile cell continuing its forward progress without morphological alterations (Fig. 5.4A). TOD mutants initially followed a similar pattern, but during progression of the intersection, the cell body became impeded while the leading end, corresponding to the terminal organelle continued its forward progress (Fig. 5.4C, white arrowheads; supplementary movie 3). As a result, cell length but not cell volume increased dramatically until only a thin cellular thread often up to 8 μm in length bound the terminal organelle to the impeded cell body (Fig. 5.4C-E, black arrows). Typically this thread reached a critical point where the terminal organelle detached and the cell body recoiled (Fig. 5.4C-E, black arrowheads; supplementary movies 3-5). Detached terminal organelles typically remained motile for the duration of the observation period while the cell bodies from which they originated remained motionless over that time, but with longer observations formed new terminal organelles and regained motility (see below).

We utilized a P30-yellow fluorescent protein (P30-YFP) fusion to confirm that detaching structures were indeed terminal organelles. P30-YFP forms a fluorescent focus at the terminal organelle and restores gliding and cytoadherence to P30⁻ mutant II-3 (Hasselbring *et al.*, 2005). Gliding motility ceases in wild-type *M. pneumoniae* concurrently with the appearance of a new P30-YFP focus adjacent to a pre-existing structure at a cell pole, and nascent terminal organelles typically do not initiate gliding for up to 3 h

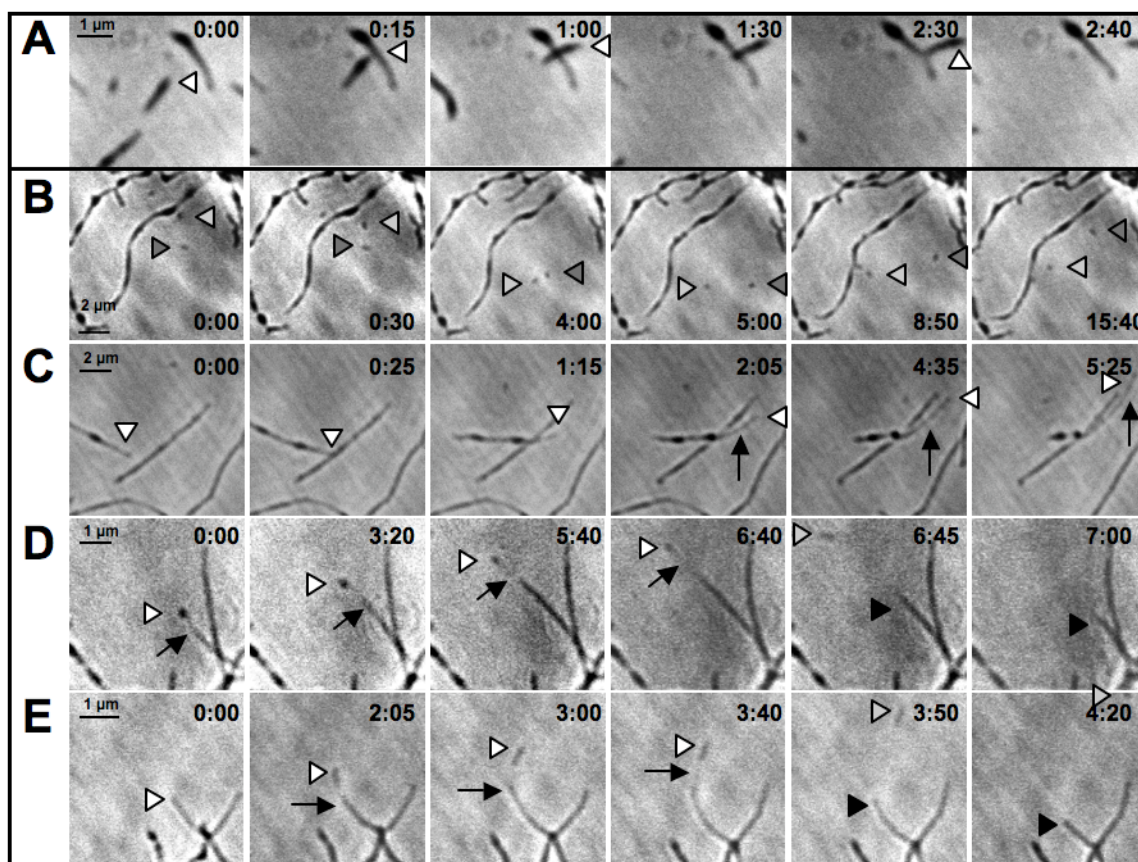


Fig. 5.4. Visualization of wild-type and MPN311 mutant cell gliding. Cultures of wild-type and MPN311 mutant *M. pneumoniae* (panels **A** and **B-E**, respectively) were monitored by microcinematography, capturing phase-contrast images at automated frame-rates of 1 frame per second (wild-type) and 1 frame per 4 seconds (mutants) for intervals of up to 30 min. The small, isolated spherical bodies abundant in MPN311 mutant cultures exhibited gliding capability at approximately wild-type velocities (panel **B**; grey arrowheads). Drag conferred upon motile mutant cells resulted in elongation of the cell body (panels **C-E**, black arrows) until the leading pole (terminal organelle; white arrowheads) detached (panels **D** and **E**; grey arrowheads) and the cell body recoiled (panels **D** and **E**; black arrowheads). Time, min:sec; Scale, as indicated. For panels **A**, **B**, **C**, **D**, and **E**, see supplementary movies 1-5, respectively.

(Hasselbring *et al.*, 2006b). However, in TOD mutants gliding cessation did not generally coincide with the appearance of new P30-YFP foci (Fig. 5.5A-B), which frequently emerged at lateral sites well separated from an existing terminal organelle and initiated gliding within 30 min (Fig. 5.5A-C; supplementary movies 6-8). Nascent structures emerging laterally pulled the cell body to a breaking point (Fig. 5.5C-E, yellow arrowheads) and ultimately detached (Fig. 5.5C, green arrowhead), even in the absence of contact with neighboring cells; detached terminal organelles often remained motile for > 30 min (data not shown). Alternatively, the forward motility of a pre-existing terminal organelle occasionally resulted in detachment of a motionless nascent structure, which remained non-motile if gliding had not initiated before separation (Fig. 5.5D, green arrowhead), consistent with the conclusion that nascent terminal organelles exhibit the capacity to adhere before the capacity to glide (Hasselbring *et al.*, 2006a). Significantly, new P30-YFP foci formed in cells that had lost a pre-existing structure (Fig. 5.5E; supplementary movie 9), in agreement with recent evidence that new terminal organelles develop *de novo* (Hasselbring *et al.*, 2006a; Henderson and Jensen, 2006) rather than by a semi-conservative process involving a pre-existing terminal organelle, as has been suggested (Rodwell and Mitchell, 1979). Finally, occasionally terminal organelles were observed to detach from motile cells but not maintain their motility (supplementary movies 8 and 9).

Complementation of TOD mutants

Methods for allelic exchange have not been developed for *M. pneumoniae*, but it is possible to complement mutants by means of transposon delivery of recombinant wild-type alleles (Fisseha *et al.*, 1999; Romero *et al.*, 1999). We engineered and transformed into each TOD mutant a Tn4001 derivative containing wild-type MPN311 and MPN312 alleles in tandem under the control of the promoter for the P65 operon, which normally directs their expression

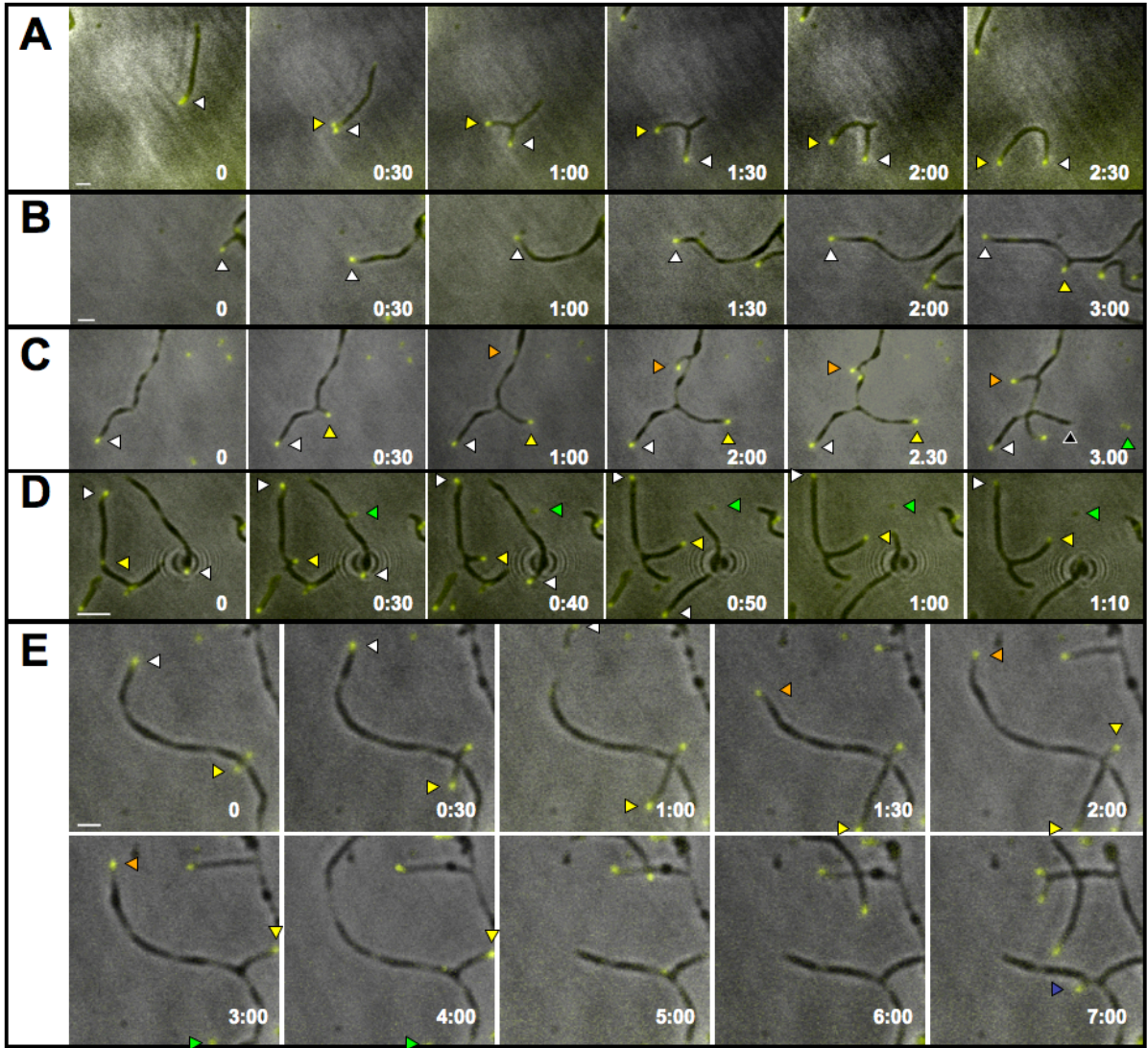


Fig. 5.5. Time-lapse analysis of terminal organelle development in MPN311 mutants.

MPN311 mutants producing P30-YFP were monitored by time-lapse phase-contrast and fluorescence microscopy. Merged images are shown for the indicated time points. Wild-type *M. pneumoniae* typically forms nascent terminal organelles adjacent to pre-existing structures at a cell pole and which require up to 3 h to exhibit gliding competence (Hasselbring *et al.*, 2006b). In contrast, nascent terminal organelles (yellow arrowheads) in MPN311 mutant cells achieved a state of gliding competence very rapidly after P30 incorporation (panel **A**, yellow arrowheads) and often developed at sites lacking a preexisting structure (panels **B–D**, yellow and orange arrowheads). Furthermore, in the absence of P41 and P24, motile nascent terminal organelles stretched the cell body to a breaking point (panels **C** and **E**, orange arrow heads) and detached (panels **C** and **E**, green arrowheads) with the cell body subsequently recoiling (panel **C**, black arrowhead). At other times (panel **D**), nascent terminal organelles detached from the cell body and remained motionless (green arrow heads) with the mycoplasma cell continuing to glide in the direction of a pre-existing terminal organelle (white arrowhead). Over time lost structures were replaced by new terminal organelles (panel **E**, blue arrow head). Time, h:min; scale bar, 1 μm . See supplementary movies 6 - 9 for panels **A – C** and **E**, respectively).

(Fig. 5.1; Krause *et al.*, 1997). Individual transformants were isolated, expanded, and characterized further. The recombinant alleles restored P41 and P24 (Fig. 5.2), conferring wild-type satellite growth, cell morphology, and terminal organelle development, with detached terminal organelles no longer apparent (data not shown). In order to determine whether loss of P41, P24, or both was responsible for the TOD phenotype we cloned each allele individually into the transposon vector, again under the control of the promoter for the P65 operon. We cloned each in-frame at the ATG of MPN309 to circumvent potential problems with translation initiation (Kenri *et al.*, 2004). Western immunoblot analysis established that each recombinant protein was made at wild-type levels (Fig. 5.6A), but P28 was only partially restored (data not shown). Recombinant P41 was sufficient to restore wild-type cell morphology and satellite growth and stable terminal organelle linkage to the cell body (Fig. 5.6B and data not shown). Furthermore, preliminary data indicated normal gliding behavior during terminal organelle formation (data not shown). MPN311 mutants producing recombinant P24 alone retained filamentous satellite growth, altered cell morphology, and the TOD phenotype, suggesting a separate and still undefined role for P24 (Fig. 5.6C and data not shown).

Discussion

The current data establish a clear requirement for P41 to anchor the terminal organelle to the cell body of *M. pneumoniae*; thus in the absence of P41 the terminal organelle detached yet retained gliding function. The capacity for cell-independent gliding by detached terminal organelles provides definitive evidence that this structure constitutes the *M. pneumoniae* gliding motor. Remarkably, mycoplasma cells from which terminal organelles detached remained viable based on the subsequent development of new terminal organelles. The conclusion that the terminal organelle constitutes the molecular motor and drive train for *M.*

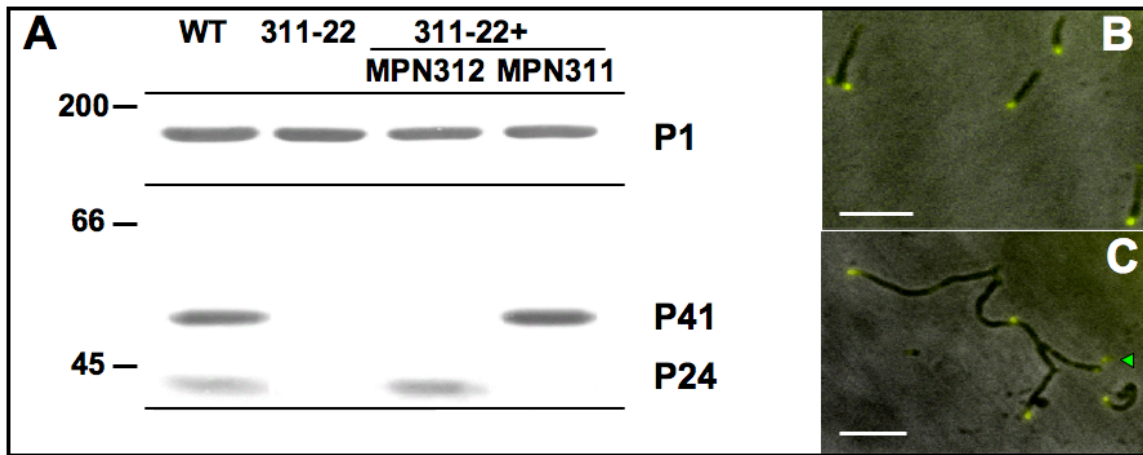


Fig. 5.6. Complementation of MPN311 Mutants with recombinant P41 and P24 individually. (A) Constructs containing MPN311 or MPN312 under control of the P65 promoter were cloned into transposon *Tn4001.2062cat* (Hahn *et al.*, 1999) containing P30-YFP (Hasselbring *et al.*, 2005). Delivery of each construct into MPN311 mutants resulted in reacquisition of P41 or P24 at wild-type levels. (B) MPN311 mutants producing recombinant P41 alone exhibited wild-type cell morphology with terminal organelle detachment no longer apparent. (C) Cells producing recombinant P24 alone retained an elongated morphology and detached terminal organelles remained abundant (green arrowhead). Scale bars, 2 μ m.

pneumoniae gliding is consistent with findings by electron cryotomography that the core itself is conformationally flexible (Henderson and Jensen, 2006). ATP powers cell gliding in the related species *M. mobile* (Jaffe *et al.*, 2004), but *M. mobile* and *M. pneumoniae* are thought to employ distinct gliding mechanisms (Uenoyama *et al.*, 2004; Hasselbring *et al.*, 2005, 2006b; Jaffe *et al.*, 2004b), and additional experiments are required to elucidate the mechanochemical basis for propulsion in *M. pneumoniae*. However, it may now be possible to isolate functional *M. pneumoniae* gliding motors intact, making such studies in this novel bacterium feasible.

Complementation studies demonstrated that loss of P41 was responsible for the TOD phenotype. P41 localizes to the base of the terminal organelle and is thought to have a structural function as a component of the Triton X-100-insoluble, cytoskeletal fraction (Kenri *et al.*, 2004). Analyses by electron microscopy (Hegermann *et al.*, 2002) and electron cryotomography (Henderson and Jensen, 2006) reveal ultrastructural details of the terminal organelle in remarkable clarity, including a differentiated structure at its base and described as wheel-like with spokes radiating from the center (Hegermann *et al.* 2002), or as a convex, bowl-like complex with a component that connects the bowl to the larger of the two rods of the core (Henderson and Jensen, 2006). They suggest that the bowl complex may provide a stable base against which alternating contraction and extension of the electron-dense core is leveraged to propel the mycoplasma cell. As MPN311 insertion mutants retained gliding function, albeit at reduced velocities, and many detached terminal organelles glided at approximately wild-type velocities, we predict based on the Henderson and Jensen model that the bowl complex is intact in motile detached terminal organelles. An attractive hypothesis based on our observations has P41 as a structural element at the base of the bowl, connecting that structure to cytoskeletal filaments that extend into the mycoplasma cell body, as described by others (Meng and Pfister, 1980; Göbel *et al.*, 1981; Hegermann *et al.*,

2002). This hypothesis should be testable by analysis of these mutants by electron cryotomography.

Gliding by wild-type *M. pneumoniae* ceases during formation of a new terminal organelle at a cell pole adjacent to an existing structure, with new P41-YFP foci emerging prior to gliding cessation, and new P30-YFP and P65-YFP foci with gliding cessation or shortly thereafter (Hasselbring *et al.*, 2006a). Nascent terminal organelles generally do not initiate gliding for 2-3 h, and therefore their subsequent separation from existing terminal organelles is a consequence of re-initiation of gliding by the latter (Hasselbring *et al.*, 2006a). The parameters that direct assembly of new terminal organelles to the cell pole, and the mechanism by which this process is coordinated with chromosome replication and cell gliding remain undefined. However, the current analysis of mutants lacking P41 and P24 suggests that both proteins play significant roles in this process.

Loss of P41 and P24 altered gliding function in both existing and nascent terminal organelles relative to wild-type (Hasselbring *et al.*, 2006a), as gliding cessation by the former did not coincide with the appearance of nascent terminal organelles (Fig. 5.5), and the latter initiated gliding rapidly following their appearance. P41 and P24 both localize to the base of the *M. pneumoniae* terminal organelle (Kenri *et al.*, 2004), and while the timing of P24 incorporation into developing terminal organelles has not been investigated, P41 appears to localize to developing terminal organelles before gliding ceases (Hasselbring *et al.*, 2006a). The failure of gliding to cease during terminal organelle development in MPN311 mutants raises the possibility that P41 also coordinates gliding cessation and initiation, for example to allow coordination with chromosome duplication or cell division.

Wild-type *M. pneumoniae* assembles new terminal organelles at a polar site adjacent to an existing terminal organelle (Hasselbring *et al.*, 2006a), but in the absence of P41 and P24 new terminal organelles formed at seemingly random sites along the cell body,

independent of an existing structure (Fig. 5.5). Thus, new terminal organelles do not require a close association with an existing structure for their assembly and function, raising the question why such an association consistently occurs with wild-type *M. pneumoniae* cells. The answer may emerge from recent findings regarding spatial organization of bacterial chromosomes in other bacteria (Gitai, *et al.*, 2005), where the origin and terminus of packaged chromosomes are always oriented in the same position in the bacterial cell from one generation to the next. Thus, an attractive hypothesis would link the site of nascent terminal organelle formation to a chromosomal locus always organized at the cell pole, the duplication of which during chromosome replication would coincide with new terminal organelle formation, and subsequent initiation of gliding by a terminal organelle could then effect chromosome segregation. By this model, cessation and initiation of gliding with terminal organelle development might reflect a need to coordinate gliding function with chromosome replication and segregation. The aberrant terminal organelle development with MPN311 mutants holds significant promise for further exploration of this possibility. The current findings also suggest a function for P24, as preliminary analysis of MPN311 mutants producing recombinant P41 revealed gliding frequencies substantially below wild-type (data not shown). Thus, P24 may partner with P41 in coordinating initiation of gliding. Additional studies are required to pursue this possibility further.

In conclusion, the studies described here provide significant insight into the roles of the terminal organelle components P41 and P24 in the development and function of this structure. Moreover, our observations establish definitively the identity of the gliding motor in *M. pneumoniae*. And finally, our findings establish an excellent foundation for elucidation of *M. pneumoniae* terminal organelle architecture, the regulation of terminal organelle development, the mechanical / chemical basis for mycoplasma propulsion, and the coordination of this process with cell division in this minimal microbe.

Experimental procedures

Mycoplasma strains and genetic engineering

Wild-type *M. pneumoniae* strain M129 and mutants II-3 and M6 were described previously (Krause *et al.*, 1982; Layh-Schmitt *et al.*, 1995). Wild-type *M. pneumoniae* was transformed with transposon Tn4001.2065 (Knudtson and Minion, 1993) by electroporation; mutants 311-22 and 311-161 were isolated by screening colonies of individually isolated transformants for atypical satellite growth, and transposon insertion sites were mapped as described (Hasselbring *et al.*, 2006b). Each transformant was filter-cloned (Tully, 1983), and the clonality of progeny was confirmed by PCR with *M. pneumoniae*- and transposon-specific primers. Confirmation of a single copy of Tn4001.2065 and no additional IS256 copies within clonal MPN311 mutant genomes was confirmed by Southern hybridization analyses. A P30-YFP translational fusion described previously (Hasselbring, *et al.*, 2005) was cloned into the *Sma*I site in transposon Tn4001.2062.cat and electroporated into wild-type *M. pneumoniae*, mutant II-3, 311-22, and 311-161 as described (Hahn *et al.*, 1999). Multiple transformants were isolated from each and expanded (Hasselbring *et al.*, 2005).

In order to complement the TOD mutants, the wild-type MPN311 and MPN312 alleles were amplified by PCR from genomic DNA, with a *Bsr*G1 restriction site engineered by primer modification immediately upstream of the MPN311 start codon, and a *Stu*I restriction site likewise engineered downstream of MPN312 (see Fig. 5.1). The resulting PCR product was cloned into the corresponding sites in pEYFP (Clontech, Mt. View, CA), generating plasmid pEYFP-311/312. The promoter region of the P65 operon was amplified by PCR, engineering an upstream *Bam*HI site and a downstream *Bsr*G1 site immediately before the MPN309 start codon. The resulting PCR product was cloned into the corresponding sites in pEYFP-311/312, replacing *eyfp* with the P65 promoter region. The P65 promoter-MPN311/312 construct was excised by digestion with *Bam*HI and *Stu*I and

cloned into *Tn4001.2062.cat* (Hahn *et al.*, 1999). For complementation of MPN311 mutants with either MPN311 or MPN312 alone, the wild-type alleles for each were amplified separately by PCR to incorporate *Bsr*GI and *Stu*I sites as above. Each PCR product was cloned into the corresponding sites of the P65 promoter-MPN311/312 construct, replacing MPN311/312 with either MPN311 or MPN312. The P65 promoter-MPN311 and P65 promoter-MPN312 constructs were excised by digestion with *Bam*HI and *Stu*I and cloned separately into *Tn4001.2062.cat* for delivery into *M. pneumoniae*. The fidelity of all constructs was confirmed by sequence analysis before transformation into mutants 311-22 and 311-161.

Western immunoblotting analysis

Mycoplasmas were analyzed by sodium dodecylsulfate polyacrylamide gel electrophoresis and Western immunoblotting as described previously (Hasselbring *et al.*, 2005). Rabbit anti-P1, anti-FtsH, anti-P41, anti-P24, and anti-P28 serum (Fisseha *et al.*, 1999; Jordan *et al.*, 2001) were used at 1:2000, 1:500, 1:1000, 1:500, and 1:1000, respectively.

Microscopy

Frozen *M. pneumoniae* stocks in SP-4 medium (Tully *et al.*, 1977) were thawed, inoculated into 4-well chamber-slides (Nalge/Nunc, Naperville, IL) containing SP-4 medium + 3% w/v gelatin (Hasselbring *et al.*, 2005), and incubated overnight at 37°C. Images were captured on a DM IRB inverted microscope (Leica Microsystems, Wetzlar, Germany) and digitally recorded with a Orca ER CCD camera (Hamamatsu Photonics, Hamamatsu City, Japan) with the Openlab program v4.0 (Improvision, Lexington, MA). To monitor cell gliding behavior, fields of approximately 50-100 cells were recorded with phase contrast optics (100X oil-immersion objective, 1.4 numerical aperture) at automated rates as indicated over

intervals of up to 30 min. Alternatively, cultures were fixed in the chamber slides and prepared for immunofluorescence microscopy and nucleoid staining as described (Balish *et al.*, 2001). Monoclonal P30 (Baseman *et al.*, 1987) and P1 (Maine Biotechnology Services) antibodies were used at 1:40; polyclonal P65 antiserum was used at 1:300. Secondary Cy2- or Cy3- conjugated antisera were used at 1:100. Cy2, Cy3, and DAPI exposures for image capture by fluorescence microscopy were 1.0, 0.5, and 0.03 sec, respectively. For analysis of terminal organelle development in *M. pneumoniae* cultures producing P30-YFP, mycoplasmas were inoculated and grown in chamber slides as described above, with phase and fluorescence images captured at 6 and 12 or 30 min intervals, respectively, at an exposure of 1.0 sec, and processed using Openlab v4.0.

Acknowledgements

This work was supported by Public Health Service research grants AI22362 and AI49194 from the National Institute of Allergy and Infectious Diseases to D.C.K.

References

- Balish, M. F., Hahn, T.W., Popham, P.L., and Krause, D.C. (2001) Stability of *Mycoplasma pneumoniae* cytoadherence-accessory protein HMW1 correlates with its association with the triton shell. *J Bacteriol* **183**: 3680-3688.
- Baseman, J. B., Morrison-Plummer, J., Drouillard, D., Puleo-Schepke, B., Tryon, V. V., and Holt, S. C. (1987) Identification of a 32-kilodalton protein of *Mycoplasma pneumoniae* associated with hemadsorption. *Isr J Med Sci* **23**:474-479.
- Biberfeld, G and Biberfeld, P. (1970) Ultrastructural features of *Mycoplasma pneumoniae*. *J Bacteriol* **102**: 855-61.

- Dandekar, T., Huynen, M., Regula, J. T., Ueberle, B., Zimmermann, C. U., Andrade, M. A., Doerks, T., Sanchez-Pulido, L., Snel, B., Suyama, M., Yuan, Y. P., Herrmann, R., and Bork, P. (2000) Re-annotating the *Mycoplasma pneumoniae* genome sequence: adding value, function and reading frames. *Nucleic Acids Res* **28**: 3278-3288.
- Fisseha, M., Gohlmann, H. W., Herrmann, R., and Krause, D. C. (1999) Identification and complementation of frameshift mutations associated with loss of cytoadherence in *Mycoplasma pneumoniae*. *J Bacteriol* **181**:4404-4410.
- Gitai, Z., Thanbichler, M., and Shapiro, L. 2005. The choreographed dynamics of bacterial chromosomes. *Trends Microbiol* **13**:221-228.
- Göbel, U., Speth, V., and Bredt, W. (1981) Filamentous structures in adherent *Mycoplasma pneumoniae* cells treated with nonionic detergents. *J Cell Biol* **91**:537-543.
- Hahn, T.-W., Mothershed, E. A., Waldo, III, R. H., and Krause, D. C. (1999) Construction and analysis of a modified Tn4001 conferring chloramphenicol resistance in *Mycoplasma pneumoniae*. *Plasmid* **41**: 120-124.
- Hasselbring, B. M., Jordan, J. L. and Krause, D.C. (2005) Mutant analysis reveals a specific requirement for protein P30 in *Mycoplasma pneumoniae* gliding motility. *J Bacteriol* **187**:6281-6289.
- Hasselbring, B. M., Jordan, J. L., Krause, R. W., and Krause, D. C. (2006a) Terminal organelle development in the cell wall-less prokaryote *Mycoplasma pneumoniae*. *Proc. Natl. Acad. Sci. USA*. In press.
- Hasselbring, B.M., Page, C. A., Sheppard, E. S., and Krause, D. C. (2006b) Transposon mutagenesis identifies genes associated with *Mycoplasma pneumoniae* gliding motility. *J Bacteriol* **188**: 6335-6345.
- Hegermann, J., Herrmann, R., and Mayer, F. (2002) Cytoskeletal elements in the bacterium *Mycoplasma pneumoniae*. *Naturwissenschaften* **89**: 453-458.

- Henderson, G. P., and Jensen, G. J. (2006) Three-dimensional structure of *Mycoplasma pneumoniae*'s attachment organelle and a model for its role in gliding motility. *Mol Microbiol* **60**:376-385.
- Himmelreich, R., Hilbert, H., Plagens, H., Pirkl, E., Li, B.-C., and Herrmann, R. (1996) Complete sequence analysis of the genome of the bacterium *Mycoplasma pneumoniae*. *Nucleic Acids Res* **24**: 4420-4449.
- Hu, P.-C., Cole, R.M., Huang, Y.S., Graham, J.A., Gardner, D.E., Collier, A.M., and Clyde, W.A., Jr. (1982) *Mycoplasma pneumoniae* infection: role of a surface protein in the attachment organelle. *Science* **216**: 313-315.
- Jaffe, J. D., Miyata, M., and Berg, H. C. (2004) Energetics of gliding motility in *Mycoplasma mobile*. *J Bacteriol* **186**:4254-4261.
- Jordan, J. L., Berry, K. M., Balish, M. F., and Krause, D. C. (2001) Stability and subcellular localization of cytoadherence-associated protein P65 in *Mycoplasma pneumoniae*. *J Bacteriol* **183**: 7387-7391.
- Kenri, T., Seto, S., Horino, A., Sasaki, Y., Sasaki, T., and Miyata, M. (2004) Use of fluorescent-protein tagging to determine the subcellular localization of *Mycoplasma pneumoniae* proteins encoded by the cytoadherence regulatory locus. *J Bacteriol* **186**: 6944-6955.
- Krause, D. C., and Balish, M. F. (2004) Cellular engineering in a minimal microbe: structure and assembly of the terminal organelle of *Mycoplasma pneumoniae*. *Mol Microbiol* **51**:917-924.
- Krause, D. C., Leith, D. K., Wilson, R. M., and Baseman, J. B. (1982) Identification of *Mycoplasma pneumoniae* proteins associated with hemadsorption and virulence. *Infect Immun* **35**:809-817.

- Krause, D. C., Proft, T., Hedreyda, C.T., Hilbert, H., Plagens, H., and Herrmann, R. (1997) Transposon mutagenesis reinforces the correlation between *Mycoplasma pneumoniae* cytoskeletal protein HMW2 and cytodherence. *J Bacteriol* **179**: 2668-2677.
- Knudtson, K. L. and Minion, F. C. (1993) Construction of Tn4001lac derivatives to be used as promoter probe vectors in mycoplasmas. *Gene* **137**: 217-222.
- Layh-Schmitt, G., Hilbert, H., and Pirkl, E. (1995) A spontaneous hemadsorption-negative mutant of *Mycoplasma pneumoniae* exhibits a truncated adhesin-related 30-kilodalton protein and lacks the cytodherence-accessory protein HMW1. *J Bacteriol* **177**: 843-846.
- Meng, K. E., and Pfister, R. M. (1980) Intracellular structures of *Mycoplasma pneumoniae* revealed after membrane removal. *J Bacteriol* **144**:390-399.
- Radestock, U., and Bredt, W. (1977) Motility of *Mycoplasma pneumoniae*. *J Bacteriol* **129**:1495-1501.
- Razin, S., Yogev, D., Naot, Y. (1998) Molecular biology and pathogenicity of mycoplasmas. *Microbiol Mol Biol Rev* **62**:1094-1156.
- Rodwell, A. W. and Mitchell, A. (1979) Nutrition, growth, and reproduction. In *The Mycoplasmas*. Barile, M. F. and Razin, S. (eds). New York: Academic Press, Vol I, pp. 103-139.
- Romero-Arroyo, C.E., Jordan, J., Peacock, S.J., Willby, M.J., Farmer, M.A., and Krause, D.C. (1999) Mycoplasma pneumoniae protein P30 is required for cytodherence and associated with proper cell development. *J Bacteriol* **181**: 1079-1087.
- Seto, S., Kenri, T., Tomiyama, T., and Miyata, M. (2005) Involvement of P1 adhesin in gliding motility of *Mycoplasma pneumoniae* as revealed by the inhibitory effects of antibody under optimized gliding conditions. *J Bacteriol* **187**:1875-1877.

- Seto, S., Layh-Schmitt, G., Kenri, T., and Miyata, M. (2001) Visualization of the attachment organelle and cytoadherence proteins of *Mycoplasma pneumoniae* by immunofluorescence microscopy. *J Bacteriol* **183**: 1621-1630.
- Seto, S., Uenoyama, A., and Miyata, M. (2005b) Identification of a 521-kilodalton protein (Gli521) involved in force generation or force transmission for *Mycoplasma mobile* gliding. *J Bacteriol* **187**:3502-3510.
- Tully, J. G. (1983) New laboratory techniques for isolation of *Mycoplasma pneumoniae*. *Yale J Biol Med* **56**: 511-515.
- Tully, J. G., Whitcomb, R. F., Clark, H. F., and Williamson, D. L. (1977) Pathogenic mycoplasmas: cultivation and vertebrate pathogenicity of a new spiroplasma. *Science* **195**: 892-894.
- Uenoyama, A., Kusumoto, A., and Miyata, M. (2004) Identification of a 349-kilodalton protein (Gli349) responsible for cytoadherence and glass binding during gliding of *Mycoplasma mobile*. *J Bacteriol* **186**:1537-1545.
- Uenoyama, A., and Miyata, M. (2005) Identification of a 123-kilodalton protein (Gli123) involved in machinery for gliding motility of *Mycoplasma mobile*. *J Bacteriol* **187**:5578-5584.
- Waites, K. B. and Talkington, D. F. (2004) *Mycoplasma pneumoniae* and its role as a human pathogen. *Clin Microbiol Rev* **17**:697-728.

Supplementary Movie Legends

Movie S1. **Digital microcinematography of wild-type *M. pneumoniae* cell intersection during gliding.** Shown are phase contrast images of a typical wild-type *M. pneumoniae* cell

intersection during gliding. Captured at 1 frame-per-sec over approximately 3 min, the images are shown here at 6 frames-per-sec.

Movie S2. **Digital microcinematography of cell-independent gliding of detached mutant MPN311 terminal organelles.** Phase contrast images of MPN311 mutant terminal organelles gliding independently after detachment. Captured at 15 frames-per-min over approximately 19 min, the images are shown here at 10 frames-per-sec.

Movie S3. **Digital microcinematography of mutant MPN311 cell intersection during gliding.** Shown are phase contrast images of the intersection of two MPN311 mutant cells. The terminal organelle of the motile cell continues forward after the intersection while the cell body is inhibited in crossing. Captured at 15 frames-per-min over 7 min, the images are shown here at 5 frames-per-sec.

Movie S4. **Digital microcinematography of mutant MPN311 terminal organelle detachment after cell intersection.** Phase contrast images showing detachment of the terminal organelle from an MPN311 mutant cell during intersection. Captured at 15 frames-per-min over approximately 8 min, the images are shown here at 5 frames-per-sec.

Movie S5. **Digital microcinematography of mutant MPN311 terminal organelle detachment after cell intersection.** Phase contrast images showing detachment of the terminal organelle from an MPN311 mutant cell during intersection. Captured at 30 frames-per-min over 14 min, the images are shown here at 6 frames-per-sec.

Movie S6. **Digital phase contrast / fluorescence microscopy of the appearance and gliding of a mutant MPN311 nascent terminal organelle.** Shown are phase contrast and fluorescence images of an MPN311 mutant cell + P30-YFP (yellow) taken over a 2.5-hr observation. Phase contrast and fluorescence images were captured in rapid succession at 30-min intervals. Unlike wild-type cells (Hasselbring *et al.* 2006a), the nascent terminal organelle of the MPN311 mutant initiated gliding rapidly upon P30 incorporation.

Movie S7. **Digital phase contrast / fluorescence microscopy of the lateral development of a mutant MPN311 nascent terminal organelle in a motile cell.** Shown are phase contrast and fluorescence images of an MPN311 mutant cell + P30-YFP (yellow) taken over a 3-hr observation. Phase contrast images were captured at 5-min intervals and fluorescence images were captured at 30-min intervals. Unlike wild-type cells (Hasselbring *et al.* 2006a), the nascent terminal organelle formed in a motile mutant MPN311 cell at a lateral site lacking an existing terminal organelle.

Movie S8. **Digital phase contrast / fluorescence microscopy of lateral development, gliding, and separation of mutant MPN311 nascent terminal organelles.** Shown are phase contrast and fluorescence images of an MPN311 mutant cell + P30-YFP (yellow) taken over a 3-hr observation. Phase contrast images were captured at 5-min intervals and fluorescence images were captured at 30-min intervals. Unlike wild-type cells (Hasselbring *et al.* 2006a), nascent terminal organelles formed at lateral sites lacking existing structures, exhibited gliding rapidly upon the incorporation of P30, and detached from the cell body in the MPN311 mutants.

Movie S9. Digital phase contrast / fluorescence microscopy of development, separation, and re-development of nascent terminal organelles in an MPN311 mutant.

Shown are phase contrast and fluorescence images of an MPN311 mutant cell + P30-YFP (yellow) taken over a 7.5-hr observation. Phase contrast images were captured at 6-min intervals and fluorescence images were captured at 30-min intervals. New terminal organelles formed at sites from which previous terminal organelles had detached.

CHAPTER 6

ANALYSIS OF P41 AND P24 FUNCTION IN *MYCOPLASMA PNEUMONIAE* TERMINAL ORGANELLE DEVELOPMENT AND GLIDING MOTILITY¹

¹ B. M. Hasselbring and D. C. Krause. To be submitted to *The Journal of Bacteriology*

Abstract

Gliding motility and cell division were analyzed in *Mycoplasma pneumoniae* mutants lacking terminal organelle proteins P24 or P41. The P24 mutant exhibited normal cell morphology and gliding velocity, but cell gliding frequency and rate of nascent terminal organelle development were 60% below wild-type values. P24 function required the presence of cytoskeletal element P41, exhibiting dynamic localization patterns and weak or transient association with the *M. pneumoniae* terminal organelle in the absence of P41.

With minimal genomes as small as ~ 580 kbp and cell volumes less than 10% of those of model prokaryotes, mycoplasmas are among the smallest and simplest organisms capable of self-replication. Several are human pathogens, with *Mycoplasma pneumoniae* typically producing infections of the respiratory tract including tracheobronchitis and atypical pneumonia, although extrapulmonary manifestations may also occur and reflect in part a capacity for the organism to spread systemically (Waites and Talkington, 2004).

In addition to its medical significance, *M. pneumoniae* is genuinely intriguing from a biological perspective largely due to its remarkable structural organization, highlighted by a polar, membrane-bound terminal organelle which functions in cellular processes that include cytoadherence (Krause and Balish, 2004) and gliding motility (Bredt, 1968; Hasselbring *et al.*, 2005; Hasselbring and Krause, 2007). Although the molecular mechanism powering gliding and the means by which the terminal organelle gliding motor is regulated are unknown, modulations in motor activation are coordinated with and required for proper cell division (Hasselbring *et al.*, 2006a). Thus, during replication, motile cells cease gliding coincident with the formation of a nascent terminal organelle adjacent to the existing polar structure. Newly-assembled terminal organelles generally require up to 3 hr to become gliding

competent; during this time resumption of gliding by the preexisting organelle displaces the nascent structure to the opposite cell pole prior to cytokinesis (Hasselbring *et al.*, 2006a).

In order to identify *M. pneumoniae* proteins specifically associated with gliding motility, we recently isolated over 30 gliding-deficient transposon-insertion mutants retaining cytodherence (Hasselbring *et al.*, 2006b). Subsequent characterization of two such mutants revealed distinct insertions in gene MPN311 resulting in the loss of its product, cytoskeletal protein P41, as well as the downstream gene product, P24 (Fig. 6.1a) (Hasselbring *et al.*, 2006b; Hasselbring and Krause, 2007; Krause *et al.*, 1997). Both P41 and P24 localize to the base of wild-type terminal organelles (Kenri *et al.*, 2004), and while the relative timing of P24 incorporation into developing structures has not been assessed, newly-synthesized P41 localizes to sites of future terminal organelle development prior to gliding cessation (Hasselbring *et al.*, 2006a) and likely functions early in the hierarchy of events required for terminal organelle assembly coincident with chromosome replication (Seto *et al.*, 2001).

Originally identified on the basis of their highly filamentous satellite growth characteristics (Hasselbring *et al.*, 2006b), MPN311 mutant cells exhibit elongated morphologies, often appearing as chains of coccoid cells (Hasselbring and Krause, 2007). These cells are motile, albeit at velocities and gliding frequencies typically only 10-30% percent of wild-type (Hasselbring *et al.*, 2006b). Strikingly, MPN311 mutants fail to regulate properly the motor activities of existing and nascent terminal organelles during cell division, with the latter often forming at sites devoid of preexisting structures and becoming gliding competent rapidly after the incorporation of protein P30 (Hasselbring and Krause, 2007). Moreover, terminal organelles of MPN311 mutants commonly detach from the cell body during gliding and cell division but remain motile in a cell-independent state for up to 1 hr (Hasselbring and Krause, 2007). Delivery of recombinant P41 but not P24 restores cell morphology to wild-type and suppresses terminal organelle detachment, suggesting a

structural role for P41 in anchoring the terminal organelle to the *M. pneumoniae* cell body but leaving the function of P24 undefined by morphological examination alone (Hasselbring and Krause, 2007). While P41 and P24 are not reciprocally dependent for stability (Hasselbring and Krause, 2007), possible interdependencies governing their localization at the terminal organelle have not been assessed, nor have specific functions of each in terminal organelle development and gliding motility been identified, other than the requirement for P41 to anchor the terminal organelle to the cell body.

Here, we effectively generated recombinant strains solely lacking P24 or P41 while expressing P41 or P24 fluorescent protein fusions, respectively. Yellow fluorescent protein (YFP) fusions were constructed separately at the N-terminus of P41 and P24 and placed under the transcriptional control of the P65 operon promoter, which normally directs their expression (Krause *et al.*, 1997) (Fig. 6.1a and b). Each was cloned into transposon vector Tn4001cat (Hahn *et al.*, 1999) and delivered into MPN311 mutants 311-22 and 311-161. Multiple transformants of each mutant were analyzed for the production of the recombinant alleles. MPN311 mutants receiving YFP-P24 (Y24cat) (Fig. 6.1b) produced the recombinant fusion protein at wild-type levels, while the native copies of P41 and P24 remained absent (Fig. 6.1c), as expected due to the existing transposon disruption in gene MPN311 (Hasselbring and Krause, 2007) (Fig. 6.1a). Delivery of YFP-P41 (Y41cat) (Fig. 6.1b) into the MPN311 mutants likewise resulted solely in the expression of the recombinant fusion at wild-type levels (Fig. 6.1c). Delivery of Y41/24cat and Y41cat, but not Y24cat alone, restored wild-type cell morphology and satellite growth patterns to the MPN311 mutants (Fig. 6.2a, data not shown), indicating that the YFP moiety on the N-terminus of P41 does not affect its ability to stabilize cell morphology (Hasselbring and Krause, 2007). Levels of protein P28, a product of gene MPN310 immediately upstream of MPN311 (Fig. 6.1a) requiring P41 for stability (Hasselbring and Krause, 2007), likewise rebounded with the

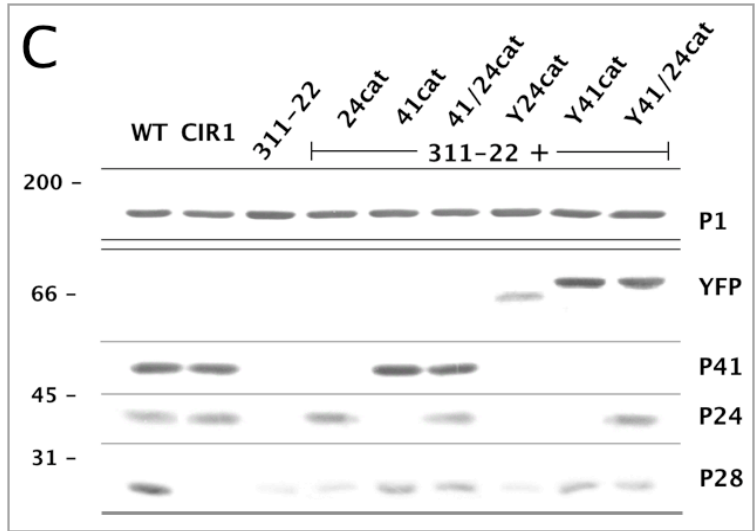
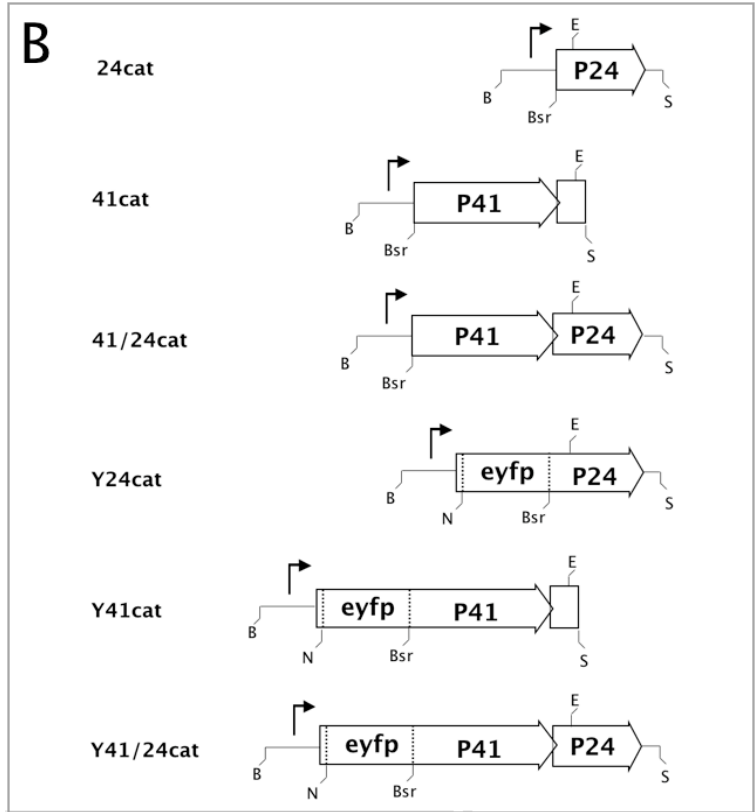
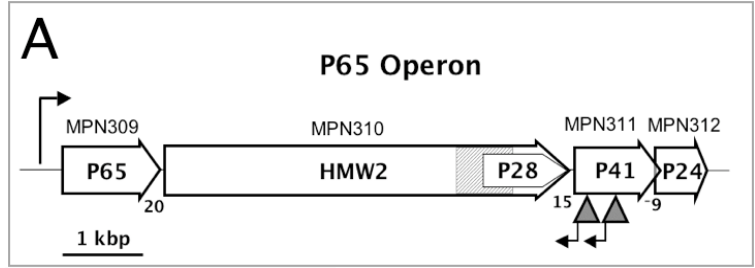


FIG. 6.1. Recombinant alleles generating P41 and P24 mutants. (A) Schematic illustration of the P65 operon (Krause *et al.*, 1997). Gray arrowheads indicate relative locations of Tn4001 insertion in MPN311, generating MPN311 mutants 311-22 and 311-161 lacking P41, as well as the downstream gene product P24 (Hasselbring *et al.*, 2006b; Hasselbring and Krause, 2007). P28, a product of MPN311 immediately upstream of MPN311, requires P41 for stability (Hasselbring and Krause, 2007). The shaded area in gene MPN310 represents a region deleted in P28⁻ mutant C1R1 (Balish *et al.*, 2003), included as a control in all current analyses. (B) Constructs were engineered to generate recombinant strains lacking only P41 or P24. The construction of recombinant MPN311 and MPN312 alleles together (41/24cat) or separately (41cat and 24cat) in transposon vector Tn4001cat (Hahn *et al.*, 1999) was described previously (Hasselbring and Krause, 2007). Vectors pEYFP-MPN311, pEYFP-MPN312, and pEYFP-MPN311/312 (Hasselbring *et al.*, 2006a; Hasselbring and Krause, 2007) were digested with *Nco*I (N) and *Bam*H1 (B), cleaving each at the 5' end of *eyfp*. Transposon vector pMT85 containing a P65-promoter-EYFP-MPN311 construct (Hasselbring *et al.*, 2006a) was digested with *Bam*H1 and *Nco*I to liberate the P65 promoter, which was then cloned into the respective sites of pEYFP-MPN311, pEYFP-MPN312, and pEYFP-MPN311/312. Each was then digested with *Bam*H1 and *Stu*I (S), and the constructs were isolated and cloned into the *Bam*H1 and *Sma*I sites of transposon vector Tn4001cat, generating Y41cat, Y24cat, and Y41/24cat, respectively. (C) Western immunoblot. Delivery of each construct into the MPN311 mutants resulted in the reacquisition of P24, P41, or both, at wild-type levels. YFP fusions to each were stable at levels comparable to those of the native protein. YFP fusion to P41 did not affect its ability to partially stabilize protein P28. Protein profiles are representative for multiple filter clones of each recombinant MPN311 mutant.

delivery of Y41/24cat or Y41cat (Fig. 6.1c).

Cultures of MPN311 mutants expressing the recombinant alleles (Fig. 6.1b) were examined by microcinematography (Hasselbring *et al.*, 2005) to assess the specific contributions of P41 and P24 to *M. pneumoniae* gliding motility. As expected (Hasselbring and Krause, 2007), delivery of both P41 and P24 in vector 41/24cat restored gliding velocities and gliding frequencies of each MPN311 mutant to wild-type parameters; here, YFP-P41 likewise fully complemented each MPN311 mutant when delivered with P24 in vector Y41/24cat (Fig. 6.2b). Recombinant P41 alone, with or without fusion to YFP, was also capable of restoring gliding velocities to wild-type parameters, but gliding frequencies remained a significant 60% below wild-type in the absence of P24 (Fig. 6.2b). This observation suggested a function of P24 in gliding motor activation, hence we expected MPN311 mutants expressing P24 or YFP-P24 alone (effectively P41 mutants), to exhibit wild-type gliding frequencies. This was not the case, however, as the cell gliding frequencies of P41 mutants remained similar to those of the parental MPN311 mutants (Fig. 6.2b). Sustained reductions in gliding frequencies and velocities were not due to the failure to stabilize P28 in the absence of P41 (Fig. 6.1c), as P28 mutant C1R1 exhibited gliding velocities and gliding frequencies at levels approximately 110% and 90% of wild-type, respectively (Fig. 6.2b). Furthermore, these gliding deficiencies appeared to stem solely from the absence of P41 rather than from possible detrimental effects caused by the recombinant YFP-P24, protein as wild-type *M. pneumoniae* harboring Y24cat exhibited no reductions in gliding capability (data not shown).

To assess contributions of P24 and P41 during terminal organelle development and cell division, growing cultures of recombinant P24 and P41 mutants expressing a functional YFP fusion to terminal organelle protein P30 (P30-YFP) (Hasselbring *et al.*, 2005; Hasselbring *et al.*, 2006a) were monitored by time-lapse microcinematography, capturing

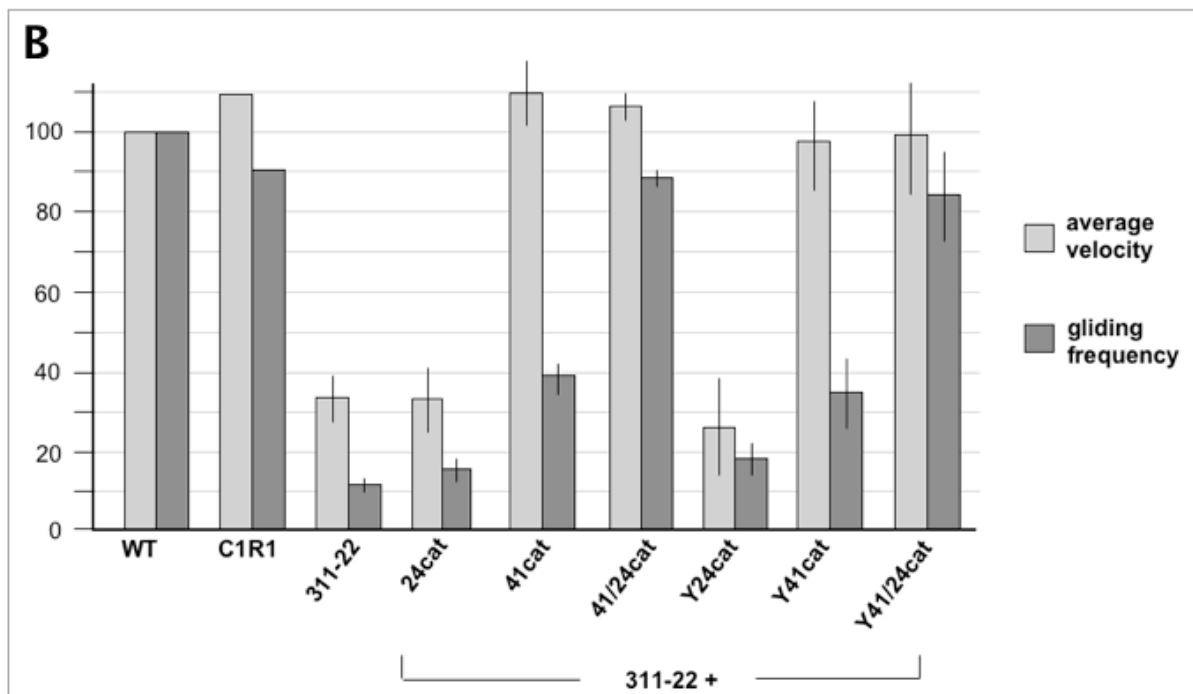
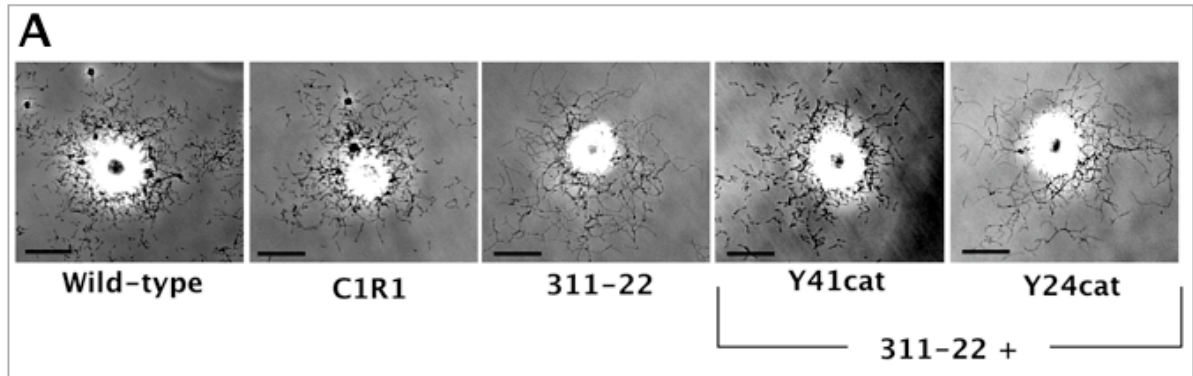


FIG. 6.2. Function of P41 and P24 in *M. pneumoniae* gliding motility. (A). Satellite growth pattern of wild-type *M. pneumoniae*, recombinant MPN311 mutants, and P28⁻ mutant C1R1, analyzed as described (Hasselbring *et al.*, 2005). Fusion of YFP to P41 did not affect its ability to restore wild-type satellite growth to the MPN311 mutants. The inability of YFP-P24 or P24 to rescue satellite growth is not attributable to reduced P28 levels, as evident by the normal satellite growth pattern of mutant C1R1. Scale: 15 μ m. (B) Cell gliding capabilities were assessed quantitatively as described (Hasselbring *et al.*, 2005). Delivery of P41 or YFP-P41 was sufficient to restore wild-type cell gliding velocities to the MPN311 mutants, but the additional presence of P24 was required to bring cell gliding frequencies to wild-type levels. In the absence of P41, expression of P24 or YFP-P24 failed to restore the mutants to wild-type. This was not due to the failure of these proteins to stabilize P28. For the recombinant MPN311 mutants, error bars represent the standard error of the mean between recombinant clones of mutant 311-22 versus mutant 311-161.

phase contrast and fluorescence images in rapid succession at 12 min intervals over 2 hr. Phase contrast and fluorescence images from each time point were merged, revealing terminal organelle location(s) within each cell (Fig. 6.3a) and allowing the sites of nascent terminal organelle development over the ensuing time-course to be assessed relative to the position of each original structure. For P41 mutants, initial P30-YFP focal patterns were similar to the parental MPN311 mutants, being equally distributed among polar and lateral sites (Fig. 6.3a). Cell gliding behaviors of the P41 mutants during nascent terminal organelle development were likewise indistinguishable from the original MPN311 mutants; thus, gliding cessation did not correlate with nascent terminal organelle assembly, and newly-formed terminal organelles achieved gliding competence rapidly and detached from the cell body (Fig. 6.3a, and data not shown). Initial terminal organelle locations for the P24 mutants mirrored those of wild-type, P28⁻ mutant C1R1, and recombinant MPN311 mutants receiving both P41 and P24: approximately 75% of P30 foci occupied polar positions, and the remaining 25% were observed at lateral sites (Fig. 6.3a). Time-lapse observation revealed that the absence of P24 likewise had little effect on the location of terminal organelle assembly, with over 90% of the nascent structures forming adjacent to the preexisting structure at the cell pole (Fig. 6.3b). For the low percentage of P24⁻ cells that were motile gliding ceased coincident with this process but was reinitiated by the existing polar terminal organelle to displace the nascent structure to the opposite cell pole, thus accounting for the observation of some lateral terminal organelles at the initial time-point. However, in the absence of P24, the percentage of individual cells either initiating or completing terminal organelle development during the 2 hr observations was approximately 60% below the values observed for wild-type *M. pneumoniae*, mutant C1R1, the original MPN311 mutants, and MPN311 mutants complemented with 24 alone or with both P41 and P24 (Fig. 6.3c, and data not shown).

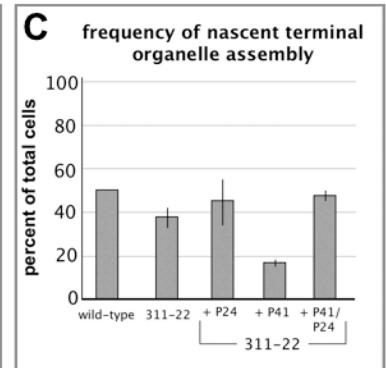
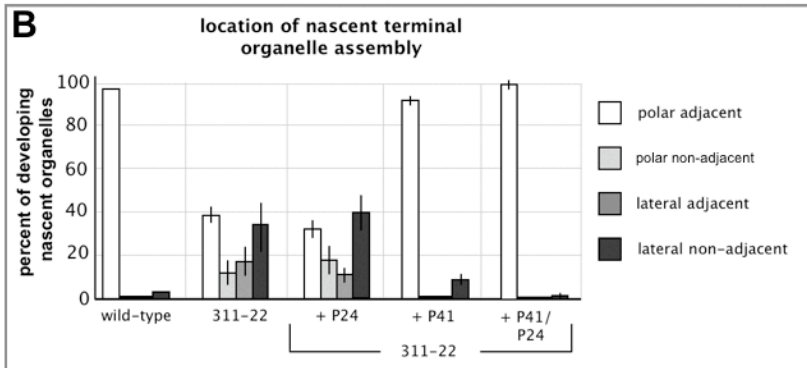
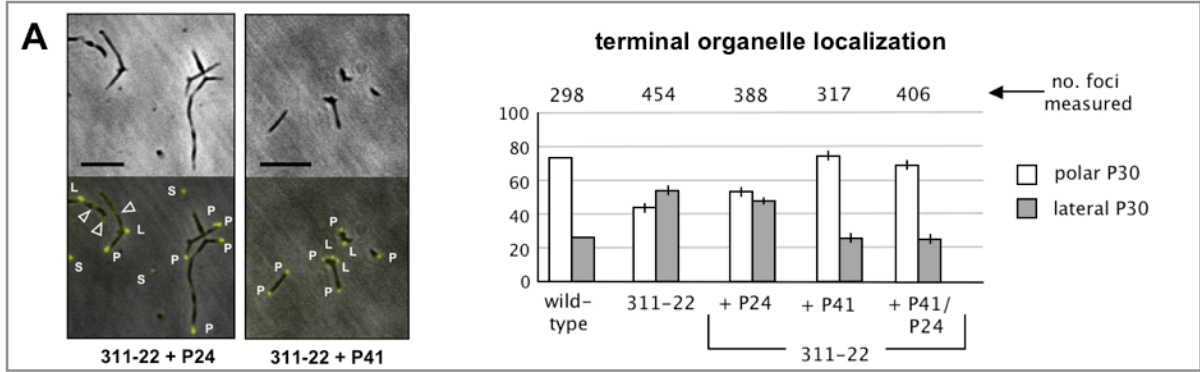


FIG. 6.3. Function of P41 and P24 in *M. pneumoniae* terminal organelle development.

A functional P30-YFP fusion (Hasselbring *et al.*, 2005), cloned in tandem with P24, P41, or P41/P24 in Tn4001cat and delivered into MPN311 mutants as described (Hasselbring and Krause, 2007) was utilized here to assess terminal organelle development patterns of P41 and P24 mutants. (A) As seen with the parental MPN311 mutants, in the absence of P41 terminal organelles were observed at approximately equal frequencies at polar (P) and lateral (L) positions along the cell body, and also in separated forms (S) after terminal organelle detachment. Delivery of recombinant P41 alone suppressed terminal organelle detachment and resulted in patterns of terminal organelle placement comparable to wild-type or MPN311 mutants complemented with both P41 and P24. Scale bar, 4 μm . Arrowheads represent sites of developing terminal organelles not yet exhibiting full P30-YFP incorporation. (B) Time lapse analysis of terminal organelle development revealed that in MPN311 mutants + P41 alone, terminal organelles assembled predominantly at the cell pole, adjacent to the existing structure. However, providing MPN311 mutants with P24 alone failed to restore normal localization of nascent terminal organelle development, which commonly occurred at sites lacking existing structures (non-adjacent) either laterally along the cell body or at a cell pole. (C) *M. pneumoniae* cells solely lacking protein P24 initiated terminal organelle development at frequencies approximately 60% below wild-type values. For (A), (B), and (C), error bars represent standard error of the mean between clones of mutants 311-22 and 311-161.

For the recombinant P24 mutants, the reductions in frequency of nascent terminal organelle development frequency their percent-reductions in cell gliding frequency, suggesting a direct and possibly related role for P24 in both processes. However, these possible regulatory functions for P24 were only evident provided P41 was present (Figs. 6.2 and 6.3). Thus, we were interested in determining whether P24 and P41 are reciprocally-dependent for localization to the terminal organelle. To localize P24 or P41 in P41⁻ or P24⁻ backgrounds, respectively, relative to the terminal organelle, P30-CFP (Hasselbring *et al.*, 2006a) was cloned separately into transposon vectors Y41cat, Y41/24cat, and Y24cat, and each was delivered into wild-type *M. pneumoniae*, C1R1, and the MPN311 mutants. As expected in wild-type *M. pneumoniae* P30-CFP and YFP-P41 localized to the base and the distal end of the terminal organelle, respectively (Fig. 6.4a). The same pattern was observed here for C1R1 and for MPN311 mutants expressing P30-CFP/YFP-P41 (Fig. 6.4a, and data not shown), demonstrating that neither P28 nor P24 is required for P41 to localize to the terminal organelle. For each recombinant strain, patterns of P30-CFP localization were similar to those observed earlier for P30-YFP, and each lateral P30 focus was paired with P41, likely indicating nascent foci in the process of displacement to the opposite cell pole (Fig. 6.4a, and data not shown). Furthermore, as P41 localizes to sites of future terminal organelle assembly prior to gliding cessation and the incorporation of P30 (Hasselbring *et al.*, 2006a), as expected, cells possessing a single P30-P41 pair at the terminal organelle commonly exhibited a second, unpaired P41 focus directly proximal to the terminal organelle (data not shown). For wild-type and C1R1, these adjacent, unpaired P41 foci represented approximately 18% of the total P41 foci (Fig. 6.4a), values consistent with previous studies (Hasselbring *et al.*, 2006a) and which indicated here that loss of P28 does not affect the frequency of nascent terminal organelle development. However, in the absence of P24, unpaired P41 foci accounted for only 8% of the total, approximately 55%

less than that in wild-type or C1R1 (Fig. 6.4a) and consistent with the reduced rate of initiation of terminal organelle development described above. MPN311 mutants expressing P30-CFP and YFP-P41 together with P24 (construct P30-CFP/YFP-P41/P24 in *Tn4001cat*) had frequencies of unpaired P41 foci at approximately 20% (data not shown), these data further supported a role for P24 in facilitating nascent terminal organelle development.

Whereas P41 was able to localize to the terminal organelle in the absence of P24, in the absence of P41, P24 exhibit highly-dynamic patterns of localization and appeared to be only weakly or transiently associated with the terminal organelle. In wild-type, as expected (Kenri *et al.*, 2004), and here in C1R1, P24 localized to the base of the terminal organelle relative to P30, which localized to the distal end (Fig. 6.4b, data not shown). Polar P30 foci were always paired with a P24 focus, as were P30 foci at lateral positions, likely representing terminal organelles in the process of displacement to the opposite cell pole (Fig. 6.4b, data not shown). Furthermore, in wild-type and C1R1 cells, unpaired P24 foci were occasionally evident directly proximal to the P30/P24 pair at the terminal organelle, although this accounted for only about 7% of the total P24 foci in these cells compared to ~18% for P41 (Fig. 6.4a, data not shown), suggesting that P24 incorporates into developing structures subsequent to P41 but prior to P30. Remarkably, in P41 mutant cells, unpaired P24 foci accounted for approximately 50% of the total P24 foci and were evident at both lateral (~40%) and polar (~10%) positions (Fig. 6.4b). As expected (Hasselbring and Krause, 2007) (Fig. 6.3a), detached terminal organelles were common in these cultures (Fig. 4b). However, only approximately 40% of the separated terminal organelles exhibited YFP-P24 signal, close to the percentage of cell-associated P30 foci with an accompanying P24 focus (Fig. 6.4b). Interestingly, in separated terminal organelles, YFP-P24 signal was typically weaker than cell-associated YFP-P24 (Fig. 6.4b). This was not the case for P30-CFP (Fig. 6.4b), suggesting the possibility that unpaired, cell-associated P24 foci could

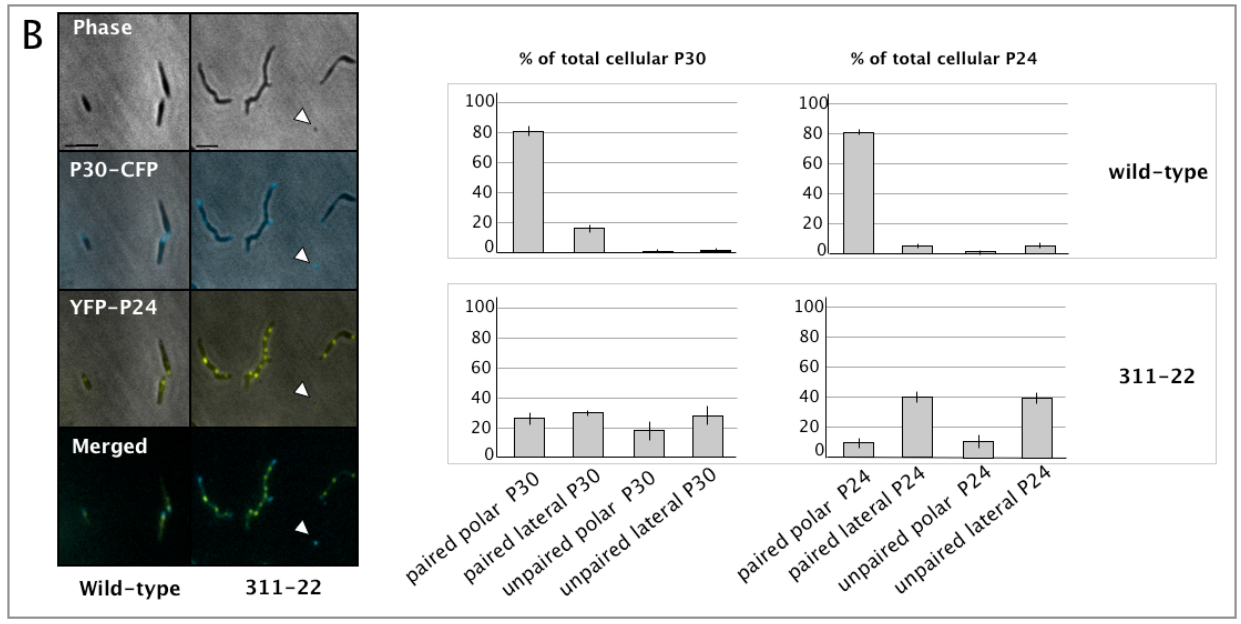
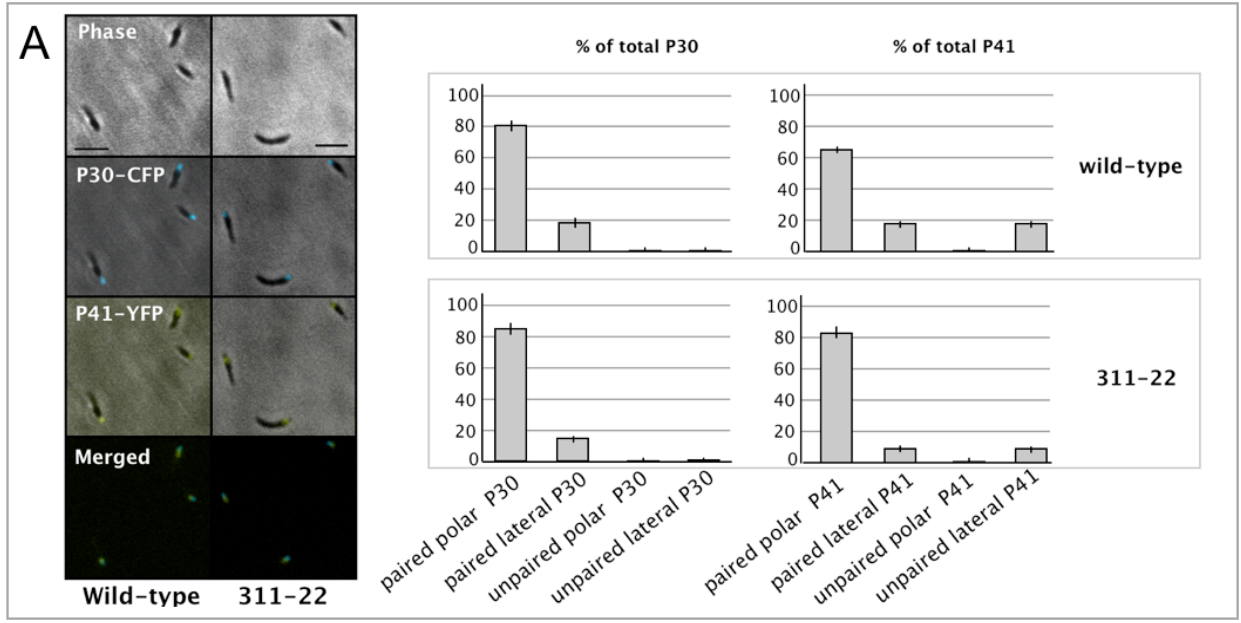


FIG. 6.4. Investigation of reciprocal dependency between P41 and P24 for terminal organelle localization. Locations of YFP-P24 and YFP-P41 in P41⁻ and P24⁻ backgrounds, respectively, were analyzed relative to terminal organelle reporter P30-CFP (Hasselbring and Krause, 2007). (A) In the absence of P24, cell morphology was indistinguishable from wild-type, as were P41 localization patterns with YFP-P41 pairing with P30-CFP at the terminal organelle. P41 foci lacking an accompanying P30 signal were evident directly proximal to the terminal organelle in ~18% of wild-type cells but only ~8% of P24⁻ cells, reflecting the incorporation of P41 into developing terminal organelles prior to P30. (B) In the absence of P41, YFP-P24 foci were distributed randomly along the cell body, with over 50% unpaired with P30, while P30-CFP focal patterns were indistinguishable from the original MPN311 mutants, although over 50% of these were unpaired with P24 foci. Detached terminal organelles containing P30 were common (arrowhead), although less than half of the detached terminal organelles contained P24. When present in the separated structures, the fluorescence intensity of YFP-P24 was typically weaker than the cell-associated YFP-P24 foci. Scale bars, panel (A), 1 μm ; panel (B) 2 μm . Wild-type error bars represent standard error of the mean between wild-type and C1R1 values. Error bars for recombinant MPN311 mutant 311-22 represent standard error of the mean against the same recombinant forms of MPN311 mutant 311-161.

originate during terminal organelle detachment; thus in the absence of P41, P24 may only weakly associate with the terminal organelle and remain in the cell body upon terminal organelle detachment. Due to the rapid photobleaching of P30-CFP (Hasselbring *et al.*, 2006a), we were unable to co-localize P24 and P30 over multiple time-lapse images to investigate this possibility further. However, even if terminal organelle detachment were accountable for the high occurrence of unpaired, cell-associated P24 foci, this would still not account for the equal occurrence of cell-associated P30 foci lacking an accompanying P24 signal (Fig. 6.4b). As transient interactions rather than weak, static interactions between P24 and the terminal organelle could account for the occurrence of unpaired P24 and P30 foci, P41 mutants expressing P24-YFP were examined by time-lapse microcinematography to monitor YFP-P24 dynamics. In capturing phase-contrast and fluorescence images in rapid succession over ten minute intervals, we observed that in both motile and non-motile P41 mutant cells, P24 foci appeared to migrate laterally within the cell body (Fig. 6.5). When encountering another P24 focus, the two appeared to merge, yielding a more intense fluorescence signal, which often dissipated by the next time-lapse image, although new foci had appeared elsewhere (Fig. 6.5). We could not discern whether this apparent migration through the cell body truly represented lateral displacement of distinct foci or the rapid aggregation, dissolution, and re-aggregation of P24 into discrete foci elsewhere in the cell body. Even when imaged at intervals as frequently as 2 min, the same patterns were evident, and there were no apparent differences in the distances between the new and former locations of P24 between time-frames (data not shown). Attempts to monitor these behaviors in real-time were unsuccessful, as YFP-P24 exhibited only about 10 sec of photostability under constant-excitation. Significantly, these dynamic patterns were not evident for YFP-P24 foci in wild-type or C1R1 cells, nor did P30 foci exhibit these patterns in

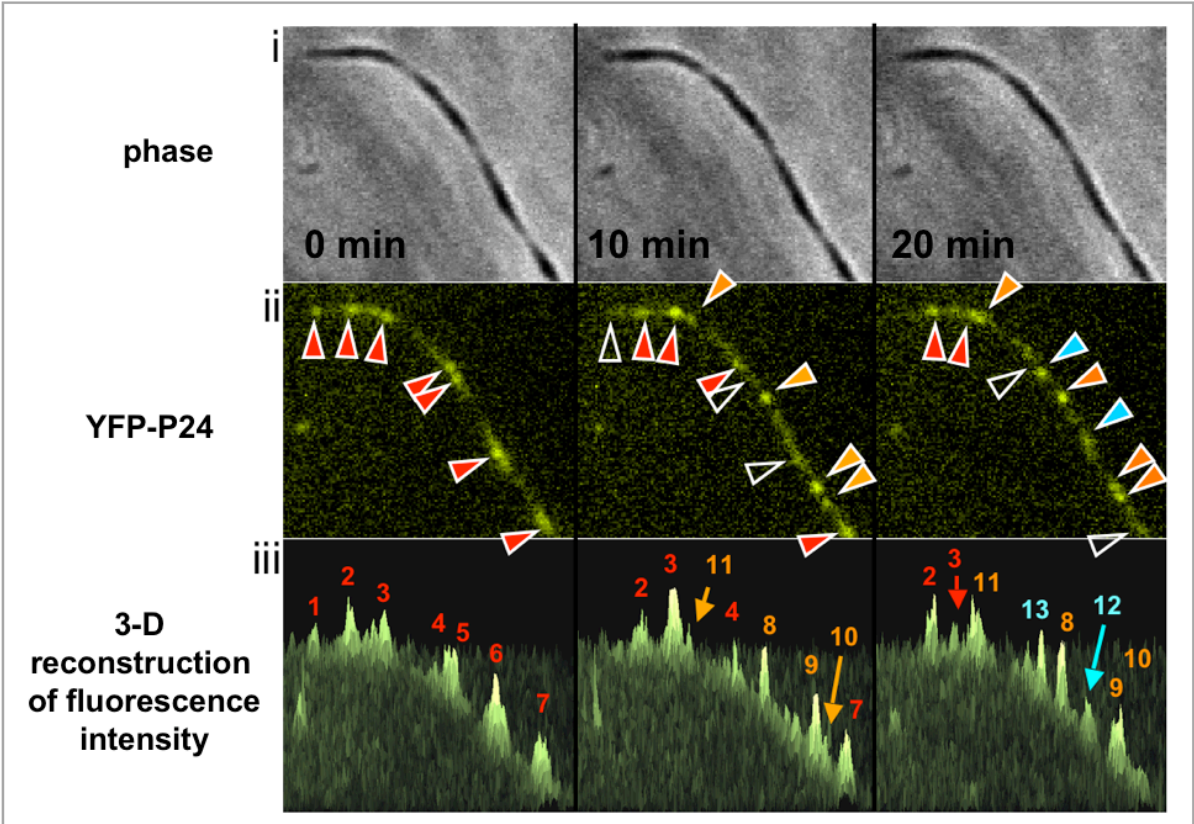


FIG. 6.5. Dynamic P24 focal organizations in the absence of P41. Examination of YFP-P24 localization in growing cultures of P41⁻ mutants revealed P24 focal dynamics not seen in wild-type *M. pneumoniae* or mutant CIRI. In progressive time-lapse images, P24 foci appeared to either migrate and/or rapidly disperse and reform elsewhere in the cell body, along the cell axis, suggesting that the elongated morphology of the P41 mutant truly represented a single, continuous cell rather than a chain of individual cells, the difference in which we were previously unable to discern (Hasselbring and Krause, 2007). In the representative cell shown, at each time point 7 major focal peaks were evident, although over the observation interval, these 7 major foci occupied 13 separate locations along the length of the cell body. In panel ii, red arrowheads represent the original locations of the 7 major foci, numbered in panel iii. After 10 minutes YFP-P24 fluorescence intensity at locations originally occupied by foci 1, 5, and 6 were below detection (empty arrowheads panel ii, 10 min) while new foci were evident at peaks 8, 9, and 10, shown at the 10 min time-point in panel iii (orange arrowheads). At the 20 minute timepoint only 1 original focus was retained, focus 2 (foci lost from 10 to 20 min are shown with empty arrowheads at 20 min, panel ii). Foci 8, 9, and 10 remained present although 9 and 10 appeared to merge somewhat (panels ii and iii, 10 vs. 20 min), and 3 new foci had emerged elsewhere as shown in panel ii with blue arrowheads (foci 11-13). Panel i: phase-contrast images; panel ii: YFP-P24 fluorescence, 1.0 sec exposure; panel iii: 3-dimensional reconstruction of fluorescence intensity (rendered by the Profiling module of the computer program Openlab v.4.5, which was used to digitize images in panel ii).

the absence, suggesting a requirement for P41 not only in anchoring the terminal organelle to the *M. pneumoniae* body, but also in sequestering P24 at the structure.

While P24 is not required for activation of the *M. pneumoniae* terminal organelle gliding motor or for terminal organelle development, the current studies suggest that P24 functions in the regulation of both processes provided P41 is present, although the current data do not resolve whether P41 and P24 interact directly or if P24 requires hitherto unknown P41-dependent proteins for its association with the terminal organelle. The similar percent-reductions in cell gliding and nascent terminal organelle development frequencies suggest a related role for P24 in both processes. Examination of the P30-CFP and YFP-P24 patterns in wild-type demonstrated that P24, like P41, incorporates into developing terminal organelles prior to P30. However, the lower percentage of unpaired P24 foci versus unpaired P41 foci suggests that P24 incorporation follows P41. While additional studies will be required to assess the relative sequence of events, it is tempting to speculate that P24 may function as a “gate-keeper” or check-point during terminal organelle assembly, facilitating or allowing the incorporation of components subsequent to the arrival of P41. In this capacity, the loss of P24 could account for the reductions in the frequency of nascent terminal organelle assembly (observed here by monitoring P30-YFP, which is thought to arrive late in the terminal organelle developmental pathway) as well as the reduced cell gliding frequencies if the high percentage of non-motile cells represent cells that have ceased gliding upon the start of nascent terminal organelle assembly but are inhibited in the resolution of the process. In conclusion, the current analyses have identified the first protein appearing to be involved in the regulation of *M. pneumoniae* terminal organelle assembly and function. From here, future examinations of P24 function and its apparent interactions with P41 hold promise for elucidating the specific mechanisms by which gliding motor regulation is achieved, as well as other regulated aspects *M. pneumoniae* cell biology such

as the temporal association between terminal organelle development and chromosome replication.

References

- Balish, M.F., Ross, S.M., Fisseha, M., and Krause, D.C. (2003) Deletion analysis identifies key functional domains of the cytoadherence-associated protein HMW2 of *Mycoplasma pneumoniae*. *Mol Microbiol* **50**: 1507-1516.
- Bredt, W. (1968) Motility and multiplication of *Mycoplasma pneumoniae*. A phase contrast study. *Pathol Microbiol (Basel)* **32**: 321-326.
- Hahn, T.W., Mothershed, E.A., Waldo, R.H., 3rd, and Krause, D.C. (1999) Construction and analysis of a modified Tn4001 conferring chloramphenicol resistance in *Mycoplasma pneumoniae*. *Plasmid* **41**: 120-124.
- Hasselbring, B.M., Jordan, J.L., and Krause, D.C. (2005) Mutant analysis reveals a specific requirement for protein P30 in *Mycoplasma pneumoniae* gliding motility. *J Bacteriol* **187**: 6281-6289.
- Hasselbring, B.M., Jordan, J., Krause, R.W., and Krause, D.C. (2006a) Terminal organelle development in the cell wall-less bacterium *Mycoplasma pneumoniae*. *Proc Natl Acad Sci U S A* **103**: 16478-16483.
- Hasselbring, B.M., Page, C.A., Sheppard, E.S., and Krause, D.C. (2006b) Transposon mutagenesis identifies genes associated with *Mycoplasma pneumoniae* gliding motility. *J Bacteriol* **188**: 6335-6345.
- Hasselbring, B.M., and Krause, D.C. (2007) Cytoskeletal protein P41 is required to anchor the terminal organelle of the wall-less prokaryote *Mycoplasma pneumoniae*. *Mol Microbiol*: in press.

- Kenri, T., Seto, S., Horino, A., Sasaki, Y., Sasaki, T., and Miyata, M. (2004) Use of fluorescent-protein tagging to determine the subcellular localization of *Mycoplasma pneumoniae* proteins encoded by the cytoadherence regulatory locus. *J Bacteriol* **186**: 6944-6955.
- Krause, D.C., Proft, T., Hedreyda, C.T., Hilbert, H., Plagens, H., and Herrmann, R. (1997) Transposon mutagenesis reinforces the correlation between *Mycoplasma pneumoniae* cytoskeletal protein HMW2 and cytoadherence. *J Bacteriol* **179**: 2668-2677.
- Krause, D.C., and Balish, M.F. (2004) Cellular engineering in a minimal microbe: structure and assembly of the terminal organelle of *Mycoplasma pneumoniae*. *Mol Microbiol* **51**: 917-924.
- Seto, S., Layh-Schmitt, G., Kenri, T., and Miyata, M. (2001) Visualization of the attachment organelle and cytoadherence proteins of *Mycoplasma pneumoniae* by immunofluorescence microscopy. *J Bacteriol* **183**: 1621-1630.
- Waites, K.B., and Talkington, D.F. (2004) *Mycoplasma pneumoniae* and its role as a human pathogen. *Clin Microbiol Rev* **17**: 697-728.

CHAPTER 7

Dissertation Summary

Less than two decades after the culture on *M. pneumoniae* on artificial medium and its acceptance as eubacterial status (Chanock *et al.*, 1962), examinations by electron and phase contrast microscopy had identified the presence and basic ultrastructural details of its unique terminal organelle and implicated the structure to function in the seemingly distinct processes of cytoadherence, gliding motility, and cell division. By the early 1980's, Baseman *et al.* had identified the majority of the currently-known cytoadherence-associated proteins (Krause and Baseman, 1982; Krause *et al.*, 1982), and, over the last 15 years, Krause *et al.* have elucidated a delicate array of protein-interdependencies required for their stability and localization to the terminal organelle (Krause and Balish, 2004). And yet, the basic mechanism and kinetics of terminal organelle development, specifically regarding how the process is directed spatially and regulated temporally to coincide with chromosome replication, have remained only speculative (Seto *et al.*, 2001). Furthermore, since its preliminary characterizations almost 40 years ago, *M. pneumoniae* gliding motility has largely been ignored. Thus the molecular content, location, and mechanism of the *M. pneumoniae* gliding machinery, and the relationships between gliding motility, cytoadherence, and cell division, were all undescribed as recently as four years ago.

While the studies in this dissertation have failed to define the energetics and mechanism of the *M. pneumoniae* gliding motor, I have presented the first genetic and molecular investigations into *M. pneumoniae* gliding motility and have provided novel insights into terminal organelle development, function, and architecture. Here I summarize the content and significance of the previous chapters, concentrating on the relatedness of each study and their impact on our understanding of cellular engineering in this minimal microbe. Data that have surfaced subsequent to these publications will be presented, as will directions for future research.

Before we could begin investigation of the molecular content of the *M. pneumoniae* gliding machinery and attempt to elucidate relationships between the various terminal organelle functions, we found ourselves faced with several problems. Thus, in the 40 years since *M. pneumoniae* gliding was first described, there had been no reproducible assays developed to assess quantitatively differences in gliding capability between strains. Additionally, before undertaking a large-scale attempt to identify *M. pneumoniae* proteins specifically functioning in cell gliding apart from cytoadherence, we had to verify that these properties were separable for *M. pneumoniae*. And furthermore, we understood that examination of the relationships between *M. pneumoniae* gliding and cell division would require the ability to monitor individual cells over extended time-lapse observations while tracking the location of specific gliding-associated proteins throughout the division cycle. These issues were confronted in chapter two, establishing a solid foundation upon which to layer subsequent studies. I developed two distinct motility assays enabling the rapid identification of potential *M. pneumoniae* gliding mutants based upon deficiencies in colony spreading (satellite growth) and allowing for characterization of specific gliding defects at the cellular level. I demonstrated the fidelity of each assay by examining mutants lacking or producing altered derivatives of terminal organelle adhesin P30, showing that reductions in satellite growth correlated directly with gliding deficiencies at the cellular level. In the process, I provided direct genetic evidence demonstrating the requirement for P30 in *M. pneumoniae* cell gliding. Perhaps more significantly in the context of future studies, I was able to demonstrate that, for *M. pneumoniae*, hemadsorption and gliding motility are separable properties. Finally, I demonstrated the functionality of a P30-YFP fusion, a terminal organelle reporter to be utilized extensively in future studies.

The foundations established in chapter two enabled us to engage confidently in the first large-scale genetic analysis of *M. pneumoniae* gliding motility. Additionally, the tools

were now available to characterize the properties and kinetics of *M. pneumoniae* terminal organelle development. The latter study was presented first, as it not only demonstrated the requirement for gliding motility during cell division, but also identified the first regulated cell process for *M. pneumoniae*, revealing that intricate modulations in gliding motor activation coincide with the development and displacement of nascent terminal organelles during cell division. Furthermore, via the quantification of fluctuations in focal emissions combined with analyses of terminal organelle development under conditions inducing translational arrest, the data in chapter three strongly suggest that nascent *M. pneumoniae* terminal organelles develop from *de novo* protein incorporation, in contrast to the previous hypothesis suggesting a semi-conservative mechanism of terminal organelle duplication (Boatman, 1979). Finally, I demonstrated the ability to assess the relative chronologies by which specific proteins incorporate into developing terminal organelles, showing that cytoskeletal element P65 traffics to developing terminal organelles concurrently and co-localizes with P30, whereas cytoskeletal element P41 is incorporated at sites of future terminal organelle assembly prior to P30, localizing to the base of the structure, and thus likely functions early in the hierarchy of events required for nascent terminal organelle development.

With the knowledge that gliding motility and cytodherence are separable properties, with the former appearing to be intricately associated with cell division, I conducted an extensive survey to identify *M. pneumoniae* genes required for cell gliding but dispensable for cytodherence in hopes of identifying specific components of the *M. pneumoniae* gliding motor and the mechanism of its function. Lacking means for directed gene knockout, I employed global transposon mutagenesis to identify transformants exhibiting reduced or altered satellite growth characteristics hoping that, like for P30 mutants, altered satellite growth phenotypes would correlate directly with gliding deficiencies at the cellular level. Out of over 3500 wild-type transformants examined, I identified approximately 50 transposon-

insertion mutants exhibiting satellite growth defects. Subsequent insertion mapping revealed the disruption of approximately 30 previously-uncharacterized genes that were dispensable for cytoadherence but required for normal satellite growth. Among these were ten genes encoding proteins of unknown function found only in *M. pneumoniae* and related gliding mycoplasmas. I also disrupted several genes encoding DNA or protein-modifying enzymes, including the sole *M. pneumoniae* protein phosphatase (PrpC) to suggest a role for protein phosphorylation in gliding motor function or regulation. Finally, and most significantly, I disrupted several genes producing terminal organelle and / or cytoskeletal components of unknown function, including MPN311, the gene encoding P41.

The studies in chapter four represented the first widespread genetic analysis of gliding motility in *M. pneumoniae* and put us in a position for more specific inquiry into the engineering and regulation of the gliding machinery. As disruption of MPN311 resulted in some of the most severe gliding defects among our new bank of gliding mutants, and as we had already characterized the localization and developmental patterns of its product, P41, during cell division of wild-type cells, we opted to pursue specifically its function in *M. pneumoniae* gliding and terminal organelle development.

At the beginning of chapter five, I demonstrated that MPN311 mutants failed to express protein P41, as expected, as well as the product of the gene immediately downstream, P24, which normally co-localizes with P41 at the base of the terminal organelle (Kenri *et al.*, 2004). Originally identified on the basis of their highly filamentous satellite growth, individual cells were found to exhibit an elongated morphology, typically 2-8 times the length of wild-type cells, and were commonly neighbored by smaller, detached forms which reacted intensely with antibodies against terminal organelle components P30, P1, and P65. These antibodies likewise associated with specific sites on the MPN311 mutant cells,

although reactive foci were evident at both lateral and polar positions contrary to wild-type. By DAPI staining, MPN311 mutant cells appeared to have multiple regions of chromosome condensation along their cell axis, however the detached forms lacked genetic material. Subsequent microcinematographic examination revealed that the smaller separated forms originated from the elongated MPN311 mutant cells, detaching from the leading end of motile cells when drag was induced upon the cell body. Amazingly, these minute bodies continued to glide independently after separation at near wild-type velocities, for up to 1 hr. Delivery of P30-YFP into the MPN311 mutants confirmed that the detaching structures were indeed terminal organelles, proving definitively that the *M. pneumoniae* gliding motor is harbored within the structure and suggesting a direct requirement for P41 and / or P24 in anchoring the terminal organelle to the cell body. Extended time-lapse examination of the MPN311 mutants suggested that, in addition to conferring stabilizing roles on terminal organelle architecture, P41 and / or P24 may play a regulatory role to coordinate the placement of terminal organelle assembly and the motor function of both the nascent and existing terminal organelle gliding motors. Thus, the MPN311 mutants failed to regulate properly the motor activities of existing and nascent terminal organelles during cell division, with the latter often forming at sites devoid of preexisting structures and becoming gliding competent rapidly after the incorporation of protein P30. Finally, I demonstrated that the delivery of recombinant P41 alone was sufficient to restore wild-type cell morphology, satellite growth, and stable terminal organelle linkage to the cell body. MPN311 mutants producing recombinant P24 alone retained the parental phenotypes, suggesting a separate and still undefined role for P24 by morphological examination alone.

I extended our studies of P41 and P24 in chapter six, constructing recombinant mutants lacking solely P41 or P24 to elucidate specifically the role of each protein in cell gliding and terminal organelle development. For cells expressing P24 alone, effectively P41

mutants, cell gliding velocities and gliding frequencies remained indistinguishable from the parental MPN311 mutants. Patterns of terminal organelle development likewise failed to be rescued. Thus in the absence of P41, no function was apparent for P24. However, cells expressing P41 alone, effectively P24 mutants, and which were morphologically indistinguishable from wild-type, exhibited significant (~60%) reductions in both cell gliding frequencies and rates of terminal organelle development. The data indicated a possibly related regulatory function for P24 in both processes, identifying the first *M. pneumoniae* protein functioning in such a capacity. Furthermore, this putative regulatory role appeared dependent on the presence of P41. Delivery of a YFP-P24 fusion into each MPN311 mutant verified this dependency, showing that in the absence of P41, P24 is unable to associate stably with the terminal organelle. Thus P41 was found not only to be required for physically connecting the *M. pneumoniae* terminal organelle to the cell body, but for sequestering to the structure the putative regulatory protein P24.

The current data have provided considerable new insight into the development and function of the *M. pneumoniae* terminal organelle, opening several new avenues for future study. Clearly, a major question that remains centers around the exact mechanism of the terminal organelle gliding motor. The current model proposes that conformational changes in the terminal organelle core may power gliding by an inchworm-like process provided that surface adhesins are physically connected to the core (Henderson and Jensen, 2006). In chapter two, we demonstrated definitively that P30 is required for cell gliding, although the studies were insufficient to identify the capacity in which it contributed. We now have preliminary data suggesting that P30 may be anchored to the terminal organelle core by cytoskeletal element P65. Thus, during our global survey of gliding-associated genes, three transformants exhibiting only intermediate HA capacity and which were not included in the

study were later discovered to have transposon insertions in gene MPN309 encoding P65, generating truncated P65 species which fail to localize consistently to the terminal organelle. These disruptions result in reduced levels of P30, as well as HMW2, encoded by MPN310 immediately downstream. Delivery of P30-YFP into each MPN309 mutant revealed that during cell gliding, P30 traffics from the terminal organelle to the trailing filament where it accumulates into a distinct focus at the opposite cell pole, and periodically detaches from the cell body leaving a substrate-bound protein trail (Fig. 7.1). This failure to anchor properly at the terminal organelle appears to be specific for P30. We have examined P1, P41, and P24 for similar localization patterns, but each appears unaffected by MPN309 disruption. While patterns of P30 localization return to wild-type parameters in MPN309 mutant excision revertants, the delivery of recombinant P65 alone or HMW2 alone into each MPN309 mutant is not sufficient to maintain P30 at the terminal organelle during cell gliding. Thus cytoskeletal proteins P65 and HMW2 may function together to tether P30 to the terminal organelle cytoskeleton. While the molecular identities of the terminal organelle core remain undefined, HMW2 is hypothesized to be a structural component. Interestingly, HMW2 is found to be phosphorylated in wild-type extracts. Considering the significant gliding deficiencies associated with disruption of PrpC, the sole *M. pneumoniae* protein phosphatase (chapter 4), perhaps HMW2 constitutes the conformationally-flexible core subunits identified by Henderson (2006), undergoing dynamic structural changes upon phosphorylation, and transferring force through P65 to substrate-bound P30. Further analyses of these mutants is in progress.

In addition to the promise of illuminating the mechanism of the gliding apparatus, the current studies appear to have made future investigations into the energetics of *M. pneumoniae* gliding quite feasible. Over the last few months, we have discovered that by

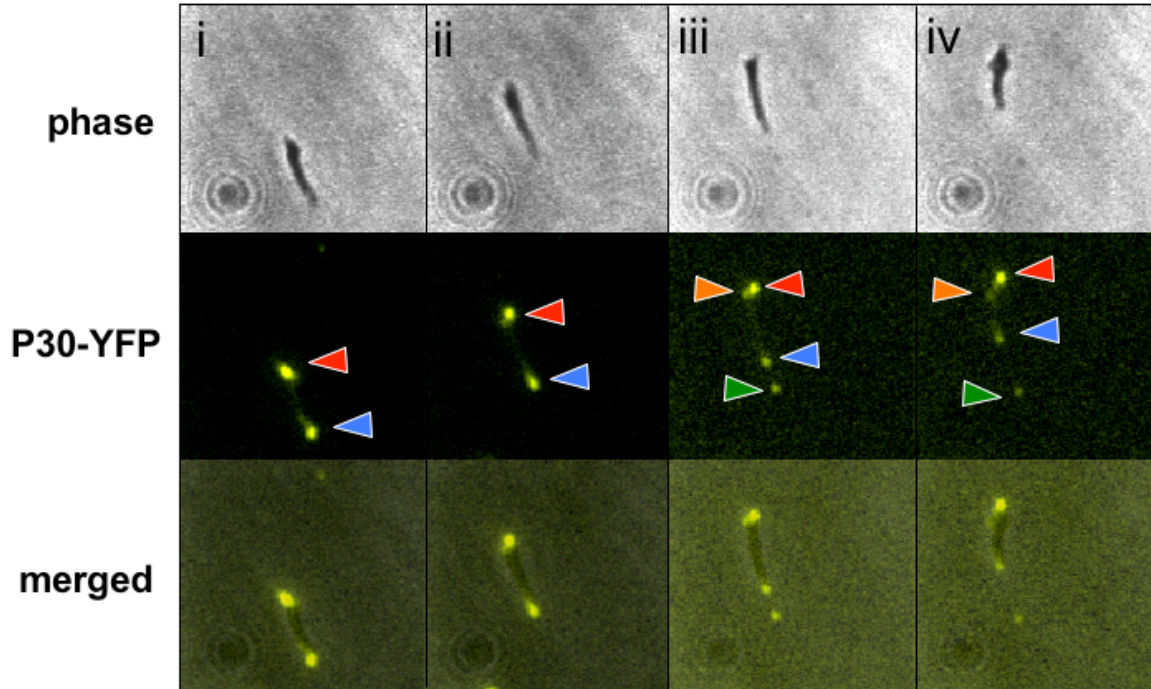


Figure 7.1. Loss of P30 from the trailing filament of gliding MPN309 mutants. MPN309 mutants expressing P30-YFP were monitored by time-lapse microcinematography. Cells possessing P30-YFP foci were typically motile, with the leading cell pole, corresponding to the terminal organelle, exhibiting greater P30 fluorescence intensity (red arrowheads). During the course of cell gliding, small amounts of P30 (orange arrowheads) became displaced to the trailing filament, accumulating at the opposite cell pole (blue foci), and then detached but remained substrate-bound (green arrowheads). After detachment from the trailing pole, the cell body typically recoiled and shortened (panel iv). Images taken at 10 min intervals. Scale bar, 1 μm .

filtering MPN311 mutant cultures through a 0.2 μm filter, terminal organelles can be isolated in the absence of other contaminating cell material. Furthermore, preliminary experiments have demonstrated that after growth to log phase in SP-4 medium (Tully *et al.*, 1977), wild-type cells will cease gliding 24-48 hr after transfer to a minimal mycoplasma medium (i.e. PBS supplemented with fetal bovine serum). Significantly, the addition of fresh SP-4 back to these apparently energy-starved cultures results in the reacquisition of cell motility. Thus, it may be possible to conduct similar re-constitution studies with isolated terminal organelles, identifying the precise energy source utilized by the gliding motor. Furthermore, the ability to isolate intact terminal organelles holds promise for investigating the ultrastructure of the gliding motor by electron tomography to determine the subunits present in detached terminal organelles.

Finally, a major question that remains regards the means by which terminal organelle assembly is regulated temporally with chromosome segregation and spatially so that nascent structures always assemble at the cell pole of wild-type cells. The aberrant locations of terminal organelle assembly in the MPN311 mutants may make these inquiries possible. The data in chapters three and five suggest that nascent terminal organelles develop *de novo* and have clearly demonstrated that the development of adherence and gliding-competent terminal organelles does not require spatial association with the existing terminal organelle, raising the question as to why wild-type *M. pneumoniae* cells consistently assemble nascent structures at the cell pole. We speculated in chapter 5 that a specific chromosomal locus oriented towards the terminal organelle may serve as a marker directing the assembly of wild-type terminal organelles to the cell pole, the duplication of which during chromosome replication could initiate terminal organelle assembly. Fluorescence *in situ* hybridization approaches utilizing both wild-type and MPN311 mutants appear feasible to substantiate this hypothesis. Thus, in the absence of P41, terminal organelles commonly

form at lateral sites along the elongated, seemingly multinucleated cell body of the MPN311 mutants. By labeling the origin of replication and other specific chromosomal sites, we may be able to determine if these lateral locations of terminal organelle development correlate with specific chromosomal loci.

In summary, the current collection of data have provided considerable insight into the location, components, architecture, and regulation of the *M. pneumoniae* gliding motor. I have demonstrated the mode and kinetics of terminal organelle assembly and have investigated the relationships between the various terminal organelle functions, showing that cytodherence and gliding are separable properties and that modulations in gliding motor activation are intricately involved in cell division. Significantly, I have identified two terminal organelle components which appear functionally distinct but intricately associated in governing the assembly, activation, and anchoring of the *M. pneumoniae* gliding motor, and have generated a collection of over 30 gliding mutants, the future characterization of which should provide years of research opportunity and further insight into the remarkable level of cellular complexity exhibited by this extraordinary bacterium.

References

- Boatman, E.S. (1979) Morphology and Ultrastructure of the *Mycoplasmatales*. In *The Mycoplasmas: Cell Biology*. Vol. 1. Barile, M.F. and Razin, S. (eds): Academic Press, pp. 63-102.
- Chanock, R.M., Hayflick, L., and Barile, M.F. (1962) Growth on artificial medium of an agent associated with atypical pneumonia and its identification as a PPLO. *Proc Natl Acad Sci U S A* **48**: 41-49.

- Henderson, G.P., and Jensen, G.J. (2006) Three-dimensional structure of *Mycoplasma pneumoniae's* attachment organelle and a model for its role in gliding motility. *Mol Microbiol* **60**: 376-385.
- Kenri, T., Seto, S., Horino, A., Sasaki, Y., Sasaki, T., and Miyata, M. (2004) Use of fluorescent-protein tagging to determine the subcellular localization of *Mycoplasma pneumoniae* proteins encoded by the cytoadherence regulatory locus. *J Bacteriol* **186**: 6944-6955.
- Krause, D.C., and Baseman, J.B. (1982) *Mycoplasma pneumoniae* proteins that selectively bind to host cells. *Infect Immun* **37**: 382-386.
- Krause, D.C., Leith, D.K., Wilson, R.M., and Baseman, J.B. (1982) Identification of *Mycoplasma pneumoniae* proteins associated with hemadsorption and virulence. *Infect Immun* **35**: 809-817.
- Krause, D.C., and Balish, M.F. (2004) Cellular engineering in a minimal microbe: structure and assembly of the terminal organelle of *Mycoplasma pneumoniae*. *Mol Microbiol* **51**: 917-924.
- Seto, S., Layh-Schmitt, G., Kenri, T., and Miyata, M. (2001) Visualization of the attachment organelle and cytoadherence proteins of *Mycoplasma pneumoniae* by immunofluorescence microscopy. *J Bacteriol* **183**: 1621-1630.
- Tully, J.G., Whitcomb, R.F., Clark, H.F., and Williamson, D.L. (1977) Pathogenic mycoplasmas: cultivation and vertebrate pathogenicity of a new spiroplasma. *Science* **195**: 892-894.